Department of Hydrology
Albert-Ludwigs-University Freiburg i.Br.

Master Thesis

Monitoring root water uptake of Centaurea jacea using water stable isotopes

Advisor: Dr. Maren Dubbert
Co-Advisor: Prof. Dr. Markus Weiler
Research Supervisor: Prof. Dr. Youri Rothfuss

Kathrin Kühnhammer - 3302812
Freiburg i.Br., 22.05.2018

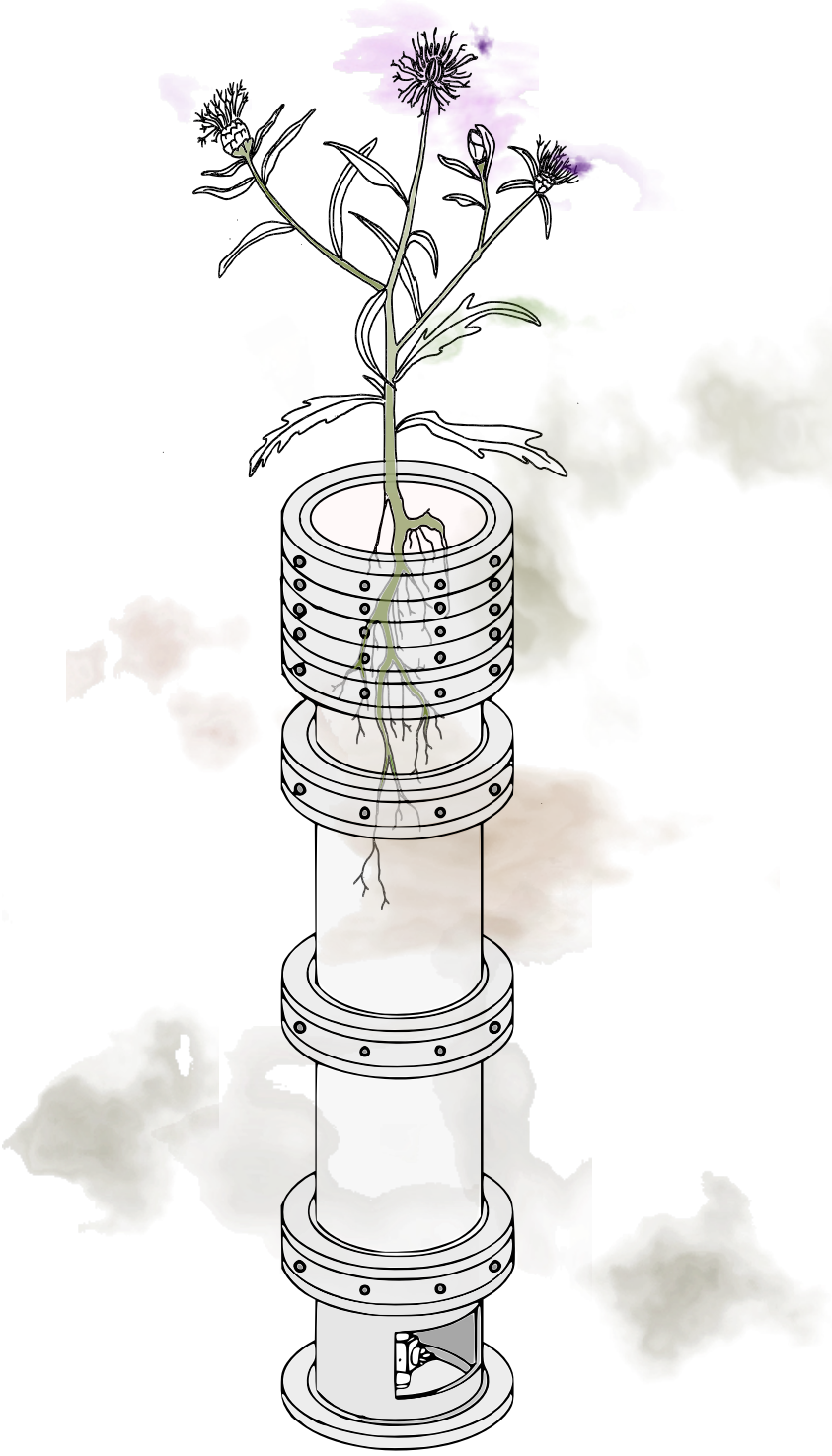

Danksagung

An erster Stelle möchte ich Prof. Dr. Youri Rothfuss danken, für seine umfangreiche Betreuung während des Laborversuchs am Forschungszentrum Jülich. Für seine Geduld und Freude daran, mir den experimentellen Aufbau näher zu bringen und die Zeit, die er sich genommen hat für ausgedehnte Diskussionen über neue Ergebnisse und gelegentlich auftauchende Hindernisse. Für die gute Laune und dafür, dass ich meine eigenen Ideen und Vorschläge einbringen konnte und er mich darin bestärkt hat.

Vom Forschungszentrum danke ich außerdem:

- Holger Wissel, Franz Leistner und Dr. Andreas Lücke für ihre Unterstützung bei der Laborarbeit und bei der Suche nach kleineren und größeren Dingen zur Optimierung des Setups
- Normen Hermes für seine unentbehrliche Hilfe bei allen technischen Fragen und diversen LabView Problemen
- PD Dr. Lutz Weihermüller für die Analyse der Bodenproben
- Dr. Steffen Merz für die Hilfe beim Füllen und Aufsättigen der Säulen

Und vielen anderen Menschen, für allerlei Anmerkungen und Denkanstöße oder einfach nur ein ablenkendes Gespräch in der Kaffeepause.

Meiner Betreuerin Dr. Maren Dubbert danke ich für die Vergabe des spannenden Themas, ihre Entscheidungshilfen bei der finalen Datenauswertung und die Bestärkung während der stressigen Endphase.

Prof. Dr. Markus Weiler danke ich für die unkomplizierte Übernahme der Zweitkorrektur.

Ein großes Dankeschön geht an Charlie, Matthias und Samuel für die finale Korrektur der Arbeit und an alle meine Freunde und Bürokollege in Freiburg und Jülich für die Unterstützung in diversen Lebenslagen der letzten Monate.

Mein größter Dank gilt meinen Eltern, die mich während meines Studiums immer bedingungslos unterstützt haben und mir ermöglichen, dass ich meinen eigenen Weg gehen kann.

Danke.

Contents

List of Figures

List of Tables

Extended Summary

Root water uptake plays a crucial role in the water cycle, as it is the largest flux on land surfaces returning water to the atmosphere. Its complex dynamics and ecosystem feedbacks are however still not well understood and can therefore not be adequately accounted for in models simulating water transport in the soil-plant-atmosphere interface. Especially on short time scales, high uncertainty exists with regards to the plasticity of water uptake and its associated driving forces. In view of an increase in hydrological extremes and a changing climate, a more mechanistic understanding is however crucial.

For five decades, water stable isotopes substantially improved our knowledge about this hard to observe belowground process. However, monitoring short-term variations was restricted, due to the necessity for destructive sampling and laborious sample analysis. Recent methodological advances now offer new possibilities to overcome these constraints and triggered the development of new approaches, which enable an in-situ monitoring of water stable isotopes in soil water and water taken up by plants. First combined in-situ measurements were already conducted in trees, but have not yet been applied to the examination of root water uptake in herbaceous species.

In the presented work, a new method is tested that allows for long-term in-situ sampling of water stable isotopes across a soil column and in plant transpiration under controlled conditions in the laboratory, using Cavity Ring-Down Spectroscopy. For this purpose, an existing soil column setup is further developed and expanded by a plant component. Dual isotope data in daily and sub-daily temporal resolution is collected across soil isotopic profiles and transpiration of *Centaurea jacea*, respectively. It will be shown that measured transpiration values reflect a mixture of soil water differing in its isotopic composition across the profile throughout a period of six weeks, despite pronounced dynamic changes in both systems. Derived measurement precision is comparable to that of established and also other newly developed in-situ methods.

The setup proved to be an adequate tool for capturing short-term variations in root water uptake in response to differences of water availability in daily resolution. To visualize water uptake profiles, data sets of the isotopic composition in plant transpiration and soil profiles are combined in a statistical multi-source mixing model. Observed trends can logically be interpreted with existing knowledge on water uptake dynamics and plasticity, while highlighting knowledge gaps in the mechanistic understanding of contributions of underlying processes. Prospectively, the implementation of data sets, obtained with the tested method, in mechanistic state-of-the-art

models could help to further disentangle complex interactions between soils and root systems. On the other hand modeling approaches across scales that now more commonly include water stable isotopes, will potentially benefit from recorded time series. Therefore temporally highly resoluted data sets should be collected for a range of plant species, soil types and scenarios in the future.

Keywords: water stable isotopes, dual isotope approach, Cavity-Ring Down Spectroscopy (CRDS), root water uptake (RWU), plant-water relation, ecohydrology, mixing model, transpiration, laboratory experiment

Zusammenfassung

Wurzelwasseraufnahme ist der größte terrestrische Fluss, welcher flüssiges Wasser in Dampfform an die Atmosphäre recycelt und stellt deswegen eine zentrale Komponente des Wasserkreislaufs dar. Seine komplexe Dynamik und Interaktionen innerhalb des Ökosystems sind jedoch bis heute wenig verstanden und können daher in ökohydrologischen Modellen nicht angemessen repräsentiert werden. Hohe Unsicherheiten gibt es vor allem im Wissen über die kurzfristige Plastizität der Pflanzenwasseraufnahme und ihrer zugrunde liegenden Antriebskräfte. Vor allem in Anbetracht einer Häufung hydrologischer Extreme und einem sich schnell verändernden Klima, ist ein besseres mechanistisches Verständnis jedoch unerlässlich.

Die Untersuchung stabiler Wasserisotope hat in den letzten fünf Jahrzehnten wichtige Beiträge zum Verständnis von Wasserflüssen beigetragen. Dies trifft vor allem für die Interaktion zwischen Boden und Wurzeln, welche wegen ihrer schlechten Zugänglichkeit schwer zu beobachten sind, zu. Insbesondere kurzfristige Dynamiken konnten aufgrund von methodischen Restriktionen nur unzureichend beobachtet werden. Technische Fortschritte in der Analyse stabiler Wasserisotope führten in letzter Zeit zur Entwicklung neuer in-situ Methoden, welche die destruktive Probenahme und aufwendige Probenanalyse umgehen. Ansätze für die gleichzeitige, zeitlich hoch aufgelöste in-situ Messung von stabilen Wasserisotopen in Bodenprofilen und in von Pflanzen aufgenommenem Wasser, wurden jüngst für Bäume getestet, jedoch ist kein Ansatz für die Untersuchung krautiger Pflanzen bekannt.

Die vorliegende Arbeit testet einen neuen Laboraufbau, welcher die simultane Aufzeichnung stabiler Wasserisotope in einer Bodensäule und Pflanzentranspiration unter kontrollierten Bedingungen mittels Cavity Ring-Down Spectroscopy ermöglicht. Hierfür wird ein bestehendes Bodensetup weiterentiwckelt und um eine Pflanzenkomponente erweitert. Zeitliche Verläufe der Verhaltnisse stabiler Sauerstoff- und Wasserstoffisotope werden für Bodenprofile in täglicher Auflösung aufgenommen. Die Zusammensetzung der Transpiration eines Individuums der Pflanzenart *Centaurea jacea* wird mehrmals täglich gemessen. Es wird gezeigt, dass die gemessenen Transpirationswerte auf die über die Bodentiefe variable Zusammensetzung des Bodenwassers zurückgeführt werden können. Dies war möglich über eine Zeitspanne von sechs Wochen, trotz deutlicher und schneller isotopischer Veränderungen in beiden Systemen und stark variierender Wasserverfügbarkeit. Die Präzision durchgeführter Messungen, beeinflusst durch die Datenanalyse, ist vergleichbar mit etablierten Methoden und neu entwickelten in-situ Ansätzen.

Das Setup hat sich als ein angemessenes Werkzeug zur Beobachtung kurzfristiger Veränderungen in der Wurzelwasseraufnahme bewährt. Um die tägliche Änderung des Wasseraufnahmeprofils zu veranschaulichen, werden Datensätze der Isotopenzusammensetzung in Transpiration und in den Bodenprofilen in einem statistischen multi-source mixing model kombiniert. Hiermit beobachtete Trends können logisch mit bekannten Kenntnissen über Wurzelwasseraufnahmedynamik und -plastizität erklärt werden und heben gleichzeitig Wissenslücken im mechanistischen Verständnis zugrunde liegender Prozesse hervor. Zukünftig könnte die Implementierung von mit der neuen Methode gewonnenen Datensätzen in mechanistischen Modellen dabei helfen, die komplexen Interaktionen zwischen dem Boden und Wurzelsystemen besser zu verstehen. Andererseits können ökohydrologische Modelle auf diversen Skalen, welche immer häufiger die Modellierung stabiler Wasserisotope implementieren, von den aufgezeichneten Zeitreihen profitieren. Hierfür sollten zukünftig zeitlich hoch aufgelöste Datensätze für eine Bandbreite an Pflanzen- und Bodenarten als auch für unterschiedliche Szenarios aufgenommen werden.

1 Introduction

1.1 Motivation

Precipitation reaching the land surface can essentially take three different paths: either it contributes to runoff, groundwater recharge or is returned to the atmosphere in vapor form. The latter is termed evapotranspiration, a combination of water evaporating from bare soil or other surfaces and plant transpiration. While, on the global scale, most water vapor in the atmosphere is provided by evaporation from the ocean, plant transpiration plays a crucial role in the terrestrial water cycle (D'Odorico et al., 2010). For a long time the contribution of transpiration to terrestrial evapotranspiration was estimated from climate models with highly uncertain predictions ranging from 20 to 65 % (Jasechko et al., 2013). Conducting a meta analysis in partitioning evapotranspiration using water stable isotope data from across the world, Jasechko et al. (2013) state that transpiration is by far the largest flux returning water from land surfaces to the atmosphere, with a proportion of 80 % to 90 %. While Coenders-Gerrits et al. (2014) calculated a contribution of 35 % to 80 % using different input data and more conservative uncertainty estimates, it is clear that transpiration plays a major role in the terrestrial water cycle, which was underestimated in the past. Difficulties in the quantification of this flux also arise from its pronounced variability on different scales in space and time (see e.g. Dubbert et al. (2014)).

By returning water to the atmosphere, plants have an important influence on climate conditions. They affect atmospheric moisture content and temperature as well as wind and rainfall patterns on a local to global scale (Sheil, 2014). Furthermore, the quantity of water they take up in space and time and their effect on soil conductivity changes runoff processes and infiltration (Thompson et al., 2010) and consequently impacts water resource availability and the occurence of floods, droughts and soil erosion (Schlesinger & Jasechko, 2014).

In addition, water availability is the main driver of plant productivity in most ecosystems (Werner & Dubbert, 2016). Because water supply and environmental conditions, like relative humidity (rh), temperature and solar irradiation, are not constant over time, the amount of plant transpiration and depth of root water uptake can be highly dynamic (Volkmann et al., 2016a). This contradicts with most ecological, hydrological and climate models simplifying driving forces behind root water uptake by assuming a direct link between root density and water uptake distribution (Werner & Dubbert, 2016).

Along with an increase in temperature, climate change in large parts of the world will likely lead to an increase of hydrological extremes with heavy precipitation events happening in higher frequency and magnitude as well as to the occurrence of more intense and longer periods of drought (IPCC, 2013). Research suggests that an increase in temperature and length of growing season could increase transpiration, thus intensifying the water cycle (Huntington, 2006). On the other hand, an increase in atmospheric CO_2 enhances plant water-use efficiency, therefore decreasing transpiration. Similar to observed changes in runoff and soil erosion due to loss of vegetation in the geological past, this could result in greater runoff and alter vegetation compositions (Schlesinger & Jasechko, 2014). Additionally, the increase in extreme events causes a higher temporal variability, thus influencing the annual water budget.

In view of these changes, a better understanding of the dynamics and mechanisms of root water uptake (RWU) is needed to increase the accuracy in predicting effects on plant cover, plant productivity, associated water fluxes and feedbacks on climate conditions. This is especially true for ecosystems like grassland communities dominated by plants with shallow root systems. Since plants in these communities are commonly not connected to groundwater, but rely on water being available in the upper soil (Jobbagy & Jackson, 2004), they could be more vulnerable towards changes in precipitation patterns and extended periods of drought.

Despite of its importance, the complex dynamics and feedbacks of water transport in the soil-plant-atmosphere interface are hard to observe and can not yet be quantified adequately (Werner & Dubbert, 2016; Schymanski et al., 2008). Therefore, measuring in high time resolution, which soil water resources are actively taken up by roots poses one of the biggest challenges in ecohydrology (Beyer et al., 2016; Kulmatiski et al., 2010). Promising advances arise from new methodological approaches, which sample water stable isotope ratios in real time (McDonnell, 2014). This could facilitate a better understanding of the physical mechanisms and the dynamics associated with transpiration and root water uptake.

1.2 Methodological state of the art

Oxygen and hydrogen isotopes are an integral part of the water molecule and therefore often considered as ideal tracers (Sprenger et al., 2017). Well-understood fractionation processes, for example during evaporation, lead to distinguishable water pools (compare chapter 2.2 and 2.4). This allows for following water movement along the water cycle on a broad variety of spatial and temporal scales. In cases where differences in stable isotopic compositions are not pronounced enough or a specific path of water flow is to be traced, waters artificially enriched or depleted in heavy isotopes are also added to environmental systems as tracers (see for example Piayda et al. (2017); Volkmann et al. (2016a); Stahl et al. (2013); Moreira et al. (2000)).

Over 50 years ago, Zimmermann et al. (1966) introduced the use of water stable isotopes as a tracer for water movement in soils and evapotranspiration. Since then, water stable isotopes provided important insights in multiple fields of hydrological research. In watershed hydrology, for instance, they were applied to determine evaporation rates, quantify surface and subsurface runoff and groundwater recharge, perform hydrograph separation and estimate streamflow response as well as residence times of water in different water pools (McGuire & McDonnell, 2008).

Wershaw et al. (1966) found that, in contrast to evaporation, plant root water uptake does not alter the ratios between heavy and light isotopes of neither oxygen nor hydrogen. In the following, these ratios are referred to as water stable isotopic composition. Since this discovery, water stable isotopes are extensively used to investigate plant-water relations. As opposed to destructive sampling of the root system via excavation, this approach can be applied to living plants, having the additional advantage of only including the active uptake of soil water resources by roots (Ehleringer & Dawson, 1992).

Water uptake by plants can be studied by comparing the isotopic composition of water in plant tissues to that of potential contributing sources. A multitude of studies assessed the utilization of few sources that can be clearly separated by their isotopic compositions. Researchers examined, for example, the seasonal use of surface versus deep soil water (White et al., 1985) and groundwater versus stream water in riparian ecosystem (Ehleringer et al., 1991).

Furthermore, water stable isotopes were used to study resource partitioning and competition between different plant species (Meinzer et al., 1999) also in relation to hydraulic lift (Meunier et al., 2017; Sun et al., 2014), as well as rooting depths and depth-dependent uptake dynamics (Beyer et al., 2016). Studies were conducted in a wide range of ecosystems. Further examples and applications can be found

in the reviews of Ehleringer and Dawson (1992) and Dawson et al. (2002). In their supplements Rothfuss and Javaux (2017) provide an overview of publications applying water stable isotopes for examining root water uptake. They list 160 studies from 1985 to 2016, also showing soil information provided, plant cover and method used for estimating source contributions.

The isotopic composition of plant transpiration represents a mixture of all water sources absorbed from the soil during a specific time step. With the two isotope ratios of oxygen and hydrogen measured, a unique solution of source contributions can be obtained for a maximum number of three isotopically distinct water sources (Phillips & Gregg, 2003). However, the isotopic variance across a soil profile does usually not feature water sources that are clearly distinguishable, but isotopic compositions rather change gradually. To still allow for an estimation of water uptake under these circumstances, bayesian multi-source mixing models are often utilized as an easy to use statistical approach. For instance, Parnell et al. (2010) developed a package for stable isotope analysis in R in underdetermined systems. Even though the package was primarily aiming at the analysis of animal tissues, in order to calculate contributions of different food sources, it can also be used to model water uptake patterns. To enhance the explanatory power of the model, gradients across the soil profile should be pronounced and preferably monotonic. Additionally, differing profiles for oxygen and hydrogen isotope ratios that would naturally fall onto one evaporation line in the dual isotope space, would be favorable, to make isotopologues less strongly correlated and therefore add information to improve (statistical) root water uptake modeling.

Based on catchment-scale field observations of differences in the isotopic composition of water in streams and transpired by trees, McDonnell (2014) proposed his hypothesis on two separated water worlds. Essentially, the theory proposes that in certain catchments plants use a different, more tightly bound water pool, while groundwater recharge and streamflow are fed by a more mobile water pool. This challenged long-standing concepts on displacement of water via translatory flow and mixing of waters in soils. Analyzing water stable isotope data from around the world, Evaristo et al. (2015) even conclude that ecohydrological separation is a widespread global phenomenon, taking place in a variety of biomes. Even though this hypothesis is the subject of ongoing debates (see e.g. Berry et al. (2018); McCutcheon et al. (2017); Sprenger et al. (2016)), it puts emphasis on a lack of process-based understanding of the mechanisms controlling water flow in the soil-plant-atmosphere interface (Beyer et al., 2016).

In the past the isotopic composition of water in soils and plants could only be sampled destructively, followed by water extraction and analysis of extracted water in the laboratory. This laborious procedure on the one hand greatly limited temporal and spatial resolution, while it only allowed for a retrospective identification of source water utilization on the other hand (Vereecken et al., 2015). Over the last decades multiple methods for extracting water contained in soil and plant samples were invented and tested, with cryogenic vacuum extraction being one of the most prevalent methods (Orlowski et al., 2013). Even though extraction methods were extensively used in the past, a systematic evaluation of differences between methods was only conducted recently for soil samples, revealing significant deviations of all tested methods from spiked reference water (Orlowski et al., 2016a). Current results from a worldwide inter-laboratory comparison of cryogenic water extraction systems also exposed significantly large differences between participating laboratories, questioning the use of the method as a standard for analyzing the isotopic composition in soil and plant samples (Orlowski et al., 2018).

The recent development of instruments measuring isotope ratios by means of laser spectroscopy, led to a new type of sampling methods that are independent from extracting water from samples prior to analysis (McDonnell, 2014). Instruments are able to measure the isotopic composition of water vapor on-line with high precision, while also being field deployable (Gupta et al., 2009). Therefore, they enable a new dimension in the temporal resolution of acquired data sets (Werner et al., 2012). Taking advantage of this technical innovation, Wassenaar et al. (2008) introduced a new method to measure pore water stable isotopes in soils, based on isotopic equilibration between liquid water and the sampled vapor phase. In recent years, multiple new in-situ methods for monitoring isotopic composition in soil profiles (Rothfuss et al., 2015; Volkmann & Weiler, 2014; Rothfuss et al., 2013) and tree xylem (Volkmann et al., 2016b) were developed.

Additionally, the possibility to measure water vapor allows for the direct determination of the isotopic composition of evaporation and transpiration fluxes. New in-situ methods to monitor plant transpiration in high temporal resolution (Dubbert et al., 2014, 2013; L. Wang et al., 2012) reinforced the potential of this approach in gaining insights into water uptake dynamics and for partitioning evapotranspiration (Piayda et al., 2017).

An experiment combining in-situ measurements of water stable isotopic compositions in soil profiles and transpiration was conducted by Volkmann et al. (2016a). In a field trial, they followed the uptake of a rain pulse enriched in ^2H after four weeks of artificial drought in two different tree species. While both oak and beech showed

a quick reaction in transpiration hydrogen isotopic composition, the authors found clear differences between species. For oak and the mixed stand, the change in the water uptake pattern could neither be explained with the root distribution nor with the modified soil water availability. This highlights knowledge gaps in the plasticity and physical mechanisms of root water uptake.

In their literature review Rothfuss and Javaux (2017) identified an increase in publications addressing root water uptake questions with water stable isotopes in both 2015 and 2016. In their listing it becomes obvious that trees are the most studied plant functional group accounting for around 50 % of research. Technical innovations on one side and controversially discussed publications on the underestimation of transpiration fluxes (Jasechko et al., 2013) and missing explanations for isotopic differences of water returned to the hydrosphere by plants and streams (McDonnell, 2014) on the other side are certainly some of the reasons for a growing interest in ecohydrological research and, more specifically, a better understanding of root water uptake.

1.3 Research questions and objectives

For a long time, water stable isotopes were utilized to gain insight into water uptake by plants. New technical developments now enable in-situ measurements of isotopic composition in both soil profiles and plant transpiration, omitting laborious and destructive sampling of water for the analysis of its isotopic composition. The accompanied increase in temporal resolution offers a new possibility to examine the dynamics and plasticity of plant water uptake that could not be observed with established methods.

The primary objective of this thesis is to test a new laboratory method, combining online measurements of water stable isotopes in a soil column and in plant transpiration, to follow root water uptake in high temporal resolution. For this purpose, the soil column setup of Rothfuss et al. (2015) that allows for sampling water stable isotopes in various soil depths, is further developed.

So far, measurements of soil isotopic composition with this setup were only conducted with standardized sand. Therefore a preliminary experiment monitoring bare soil evaporation in a natural soil is performed. Additionally, this allows for the development of an isotopic gradient across the soil profile. To further enhance the soil isotopic depth gradient, the profile is manipulated by adding different waters, depleted and enriched in heavy isotopes. The main goal thereof is the creation of a monotonic, isotopically heterogeneous soil profile, thus setting the prerequisites in

soil water for optimizing root water uptake estimations in the laboratory.

For soil measurements it is hypothesized that the measured isotopic composition

- is in line with water added to the soil column
- measured values are reproducible
- observed isotopic shifts can be explained with existing knowledge on water movement and soil physics

To incorporate plant transpiration measurements into the existing setup, one single *Centaurea jacea* is planted into the soil column. Its transpiration rate and corresponding isotopic composition is monitored in a steady-state plant chamber with constant flow rate in the second experimental section.

The focus is hereby on the following assumptions:

- plant chamber measurements allow for monitoring dynamic changes in transpiration isotopic composition
- sampled transpiration water can be traced back to water in the soil column, thus plant water uptake can be estimated by combining both data sets

Finally, both data sets are utilized in a statistic multi-source mixing model to estimate contributions of soil water in measured depths to plant water uptake. With modeling of water uptake using two highly temporally resolved data sets, isotopic changes in soil profiles can be accounted for. Calculated water uptake profiles therefore illustrate actual changes in the plants uptake dynamics. Potential ecohydrological causes for modeled shifts are discussed with a focus on heterogenities in soil water availability and plasticity of root system properties. Specifically, it is assumed that the presence of roots alone fails to explain recorded time series, as often assumed in ecohydrological modeling.

2 Water stable isotopes and plant water uptake

2.1 Definitions and δ-notation

Isotopes are atoms of the same element that differ in their amount of neutrons and therefore have different atomic masses. If the respective isotope is not subject to radioactive decay, it is called stable. For oxygen three stable isotopes ^{16}O, ^{17}O and ^{18}O exist, hydrogen occurs as ^{1}H and ^{2}H. While there are other possible combinations for one water molecule, it is mostly found in the three configurations $^{1}H_2^{16}O$, $^{2}H_2^{16}O$ and $^{1}H_2^{18}O$. For both elements the lightest isotope is by far the most abundant in nature (see table 2.1). In environmental applications isotope occurrence is usually expressed as the ratio of light to heavy isotope in the sample (R_{sample}) in reference to a standard ($R_{standard}$). The calculation of the so-called δ-Notation is shown in equation 2.1 (Sulzman, 2008).

$$\delta = (\frac{R_{sample} - R_{standard}}{R_{standard}}) \tag{2.1}$$

Because differences in natural abundances are rather small, the dimensionless measurand is mostly expressed in per mil (‰).

For oxygen and hydrogen as part of the water molecule Vienna Standard Mean Ocean Water (VSMOW) has been the internationally accepted standard for half a decade. It has an isotopic signature in the range of seawater as the basis of the meteorological cycle with isotope ratios $R_{standard}$ of $2005.2 \pm 0.45 \cdot 10^{-6}$ and $155.76 \pm 0.05 \cdot 10^{-6}$ for oxygen and hydrogen respectively (Clark & Fritz, 1997).

The experiment followed a dual isotope approach using the ratios between ^{18}O and ^{16}O as well as ^{1}H and ^{2}H. Hereafter the expressions $\delta^{18}O$ and $\delta^{2}H$ refer to the isotope ratios in reference to VSMOW as defined in equation 2.2 and 2.3 respectively. The higher the value for a specific water sample is, the more heavy isotopes it contains. Samples with positive values are enriched in the respective heavy isotope in comparison to the standard, negative values indicate a depletion.

$$\delta^{18}O_{sample} = \left(\frac{\frac{^{18}O}{^{16}O}_{sample}}{\frac{^{18}O}{^{16}O}_{VSMOW}} - 1 \right) * 1000 \text{ [‰]} \tag{2.2}$$

$$\delta^{2}H_{sample} = \left(\frac{\frac{^{2}H}{^{1}H}_{sample}}{\frac{^{2}H}{^{1}H}_{VSMOW}} - 1 \right) * 1000 \text{ [‰]} \tag{2.3}$$

Table 2.1: Stable isotopes of oxygen and hydrogen and their natural abundances (adapted from Sulzman (2008)).

Element	Isotope	Natural abundance [%]
hydrogen	^{1}H	99.985
	^{2}H	0.0155
oxygen	^{16}O	99.759
	^{17}O	0.037
	^{18}O	0.204

2.2 Fractionation processes

Due to the differing amount of neutrons, any thermodynamic reaction that involves different molecular species, leads to a shift in isotope ratios towards one side of the reaction (Clark & Fritz, 1997). This process is called isotope fractionation. The change in the isotope ratio between reactant and product can be expressed with the theoretical fractionation factor α. As the fractionation during the transition of water from liquid to vapor phase and vice versa is elementary for understanding natural isotope variations and a key process in this experiment, its dynamics and controlling factors will be discussed hereafter. Equation 2.4 shows the definition of α for oxygen during the phase transition of water from liquid to vapor phase (Clark & Fritz, 1997). For hydrogen α is calculated analogously.

$$\alpha = \frac{\frac{^{18}O}{^{16}O}_{water}}{\frac{^{18}O}{^{16}O}_{vapor}} \tag{2.4}$$

The main reasons for the different physical behavior of isotopes are differences in velocity and bond strength between molecules. In the same physical environment, a water molecule containing heavy isotopes will travel with a slower velocity than a lighter one. It also vibrates more slowly, resulting in lower energy and therefore formation of stronger hydrogen bonds (Sulzman, 2008). For the transition of water between liquid and vapor phase, this produces a lighter, depleted isotopic composition in the vapor phase and enrichment in the liquid phase.

As hydrogen and oxygen are both light elements, their isotopes show a pronounced disparity in mass. Comparing the examined isotopes, a relative mass difference of 100 % and 12.5 % exists for hydrogen and oxygen respectively (Sulzman, 2008). This makes both elements suitable environmental tracers with pronounced fractionation processes due to phase changes and diffusion processes along the water cycle, leading to naturally distinguishable waters (Marshall et al., 2008).

2.2.1 Equilibrium fractionation

In a closed system an isotopic equilibrium between liquid and vapor phase is reached when the rates of forward and backward reaction are equal and the system is well mixed (Clark & Fritz, 1997). As mentioned before, the higher bond strength between molecules containing heavy isotopes, results overall in an isotopic enrichment in the liquid phase. The differences in the stability of hydrogen bonds is also expressed with deviations in vapor pressure when comparing molecules of different isotopic compositions (Sulzman, 2008). The vapor pressure of $^{2}H_{2}^{16}O$ for example is about 13 % lower than that of $^{1}H_{2}^{16}O$ at 23 °C (Wahl & Urey, 1935).

The extent of the fractionation under equilibrium conditions is strongly dependent on temperature. An empirical correlation, first proposed by Majoube (1971) and confirmed by multiple investigations over the last decades, approximates the relationship between the theoretical value α and the reaction temperature. Equation 2.5 shows the basic formula applicable to isotope fractionation in various reactions (Clark & Fritz, 1997). The coefficients for oxygen and hydrogen during the phase transition from water to vapor, introduced by Majoube (1971) for a range of 0 - 100 °C, are listed in table 2.2.

$$10^3 \, ln \, \alpha_{eq} = a \, \frac{10^6}{T^2} + b \, \frac{10^3}{T} + c \tag{2.5}$$

T is the reaction temperature in Kelvin. A, b and c are coefficients with differing empirical values depending on the considered reaction and its components.

Table 2.2: Coefficients for the calculation of α during phase transition from liquid water to water vapor using equation 2.5 (Majoube, 1971).

Element	a	b	c
hydrogen	24.844	-76.248	52.612
oxygen	1.137	-0.4156	-2.0667

With alpha representing the ratio between the isotopic compositions of both phases, the isotopic composition in delta-Notation of liquid water (δ_{water}) can be derived from the vapor phase composition (δ_{vapor}) with equation 2.6 (Clark & Fritz, 1997). Because isotope effects are mostly small and research investigates the differences in isotopic composition between samples or changes over time, those deviations are often reported as enrichment ($\epsilon > 0$) or depletion ($\epsilon < 0$) factor (Sulzman, 2008). ϵ expresses the difference of the isotopic composition between two samples in δ-notation and can be approximated by equation 2.7. As this relation is only suitable for reactions where fractionation and isotope separations are small (Clark & Fritz,

1997), equation 2.6 was used in the presented study.

$$\delta_{water} = \alpha\,(1000 + \delta_{vapor}) - 1000 \tag{2.6}$$

$$\epsilon = 10^3\,\ln\alpha \tag{2.7}$$

2.2.2 Kinetic fractionation

Kinetic fractionation takes place in a reaction, where the forward exceeds the backward reaction and therefore no isotopic equilibrium is reached (Clark & Fritz, 1997). This is the case for water evaporating in an open system, with water vapor moving away from the liquid. Because molecules which contain lighter isotopes show higher diffusion rates (Marshall et al., 2008), the remaining water is subsequently enriched in heavy isotopes. This in return also leads to an increase of heavy isotopes in water vapor with proceeding evaporation. The effect occurs if ambient air is not fully saturated and is more pronounced with lower values for relative humidity (Clark & Fritz, 1997).

Total isotope fractionation in an open system can be estimated by adding enrichment or depletion factors for equilibrium and kinetic fractionation. See equation 2.8 for the calculation of the difference between liquid and vapor isotopic composition for oxygen isotopes, considering enrichment for both kinetic (ϵ_{kin}) and equilibrium fractionation (ϵ_{eq}) (Clark & Fritz, 1997). In the presented experiment, it can be applied to evaporation from the soil column leading to subsequent enrichment in heavy isotopes at the top and therefore explains the shaping of the monitored isotope profile.

$$\delta^{18}O_{water} - \delta^{18}O_{vapor} = \epsilon_{eq}\,{}^{18}O + \epsilon_{kin}\,{}^{18}O \tag{2.8}$$

2.2.3 Global Meteoric Water Line

Craig (1961) compared the isotopic compositions in water samples from rivers, lakes and precipitation across the world and found a strong linear correlation between samples when plotting their respective $\delta^{18}O$ against $\delta^{2}H$. His key finding that globally meteoric waters behave predictably, set a fundamental basis for the widespread use of water stable isotopes in the evaluation of water movement through the environment. If waters have not undergone strong evaporation, enrichment in heavy isotopes in warmer regions and depletion in colder parts of the world can be observed. Equation 2.9 defines this relationship, which is known as the Global Meteoric Water Line (GMWL).

$$\delta^{2}H = 8 \cdot \delta^{18}O + 10\,‰ \tag{2.9}$$

With the establishment of the Global Network of Isotopes in Precipitation by the International Atomic Energy Agency and the World Meteorological Organization the correlation was refined and evaluated for precision of measurements. The analysis of long-term averages of $\delta^{18}O$ and $\delta^{2}H$ in precipitation from 219 meteorological stations across the world resulted in equation 2.10 (Clark & Fritz, 1997).

$$\delta^{2}H = 8.17\,(\pm 0.07) \cdot \delta^{18}O + 11.27\,(\pm 0.65)\,‰ \tag{2.10}$$

On a local scale the correlation between $\delta^{18}O$ and $\delta^{2}H$ will deviate from the GMWL in slope and intercept, due to particular climatic factors, like origin of water vapor masses and extent of evaporation after condensation. Another determinant is the degree of recycling of precipitation by means of evapotranspiration along the trajectory of water vapor masses from the ocean over the continents. The GMWL can therefore be comprehended as a global average of Local Meteoric Water Lines (LMWL) (Clark & Fritz, 1997).

Because condensation only occurs in air with a rh close to 100 % (air is saturated), isotope separation hereby can mostly be explained with the concept of equilibrium fractionation. The slope of the GMWL is theoretically determined as the ratio of α_{eq} (^{2}H) and α_{eq} (^{18}O) at a specific temperature. It changes linearly according to the average temperature of condensation and has theoretical values of 9.15 at $0\,°C$ and 8 at $30\,°C$ (Clark & Fritz, 1997).

Water vapor masses form through evaporation, which increases fractionation for both

isotopes in comparison to equilibrium conditions. Because in water kinetic fractionation of oxygen is higher than of hydrogen, the GMWL has a positive y-axis intercept, which is referred to as the 'deuterium-excess'. On a global scale it averages around 10 (Clark & Fritz, 1997).

When water is subject to excessive evaporation, the bigger effect of kinetic fractionation of oxygen leads to a deviation of data points from the global or local meteoric water line (MWL) with slopes lower than 8. For evaporation taking place at 90 % rh the slope approaches a value of 8. For a rh of 75 %, theoretically the slope would be bigger than 5, 25 % produces a slope of 4 (Clark & Fritz, 1997). When plotting $\delta^{18}O$ of obtained measurements against their respective $\delta^{2}H$ and comparing the cloud of points with the MWL, the existence of evaporative effects can be investigated.

2.3 Factors controlling root water uptake

Plants necessarily need water as universal solvent for the transport of nutrients and assimilates and for stability, especially in herbaceous species. The water taken up by plants highly exceeds the dry mass accumulated. Sunflowers for example need on average 1 kg of water to produce 1.7 g of dry mass (Schopfer & Brennicke, 2016).

Apart from few exceptions, like foliar uptake of redwood forest species in California (Limm, Simonin, Bothman, & Dawson, 2009), plants obtain all the water needed from soils, causing the necessity to transport it against gravity. The amount of water taken up by the entire root system from the soil during a defined time step is called RWU (Rothfuss & Javaux, 2017). In all higher plants this passive transport takes place in special vessels, called xylem, customized for this purpose and is driven by the gradient of water potential from soil through plants to the atmosphere. Along this pathway, the water potential becomes increasingly negative. The highest pressure gradient usually exists on the interface between plant and atmosphere. Therefore the transpiration suction is pulling water up the plant. This can be explained with a continuous water column under tension, held together by cohesion of water molecules to each other and adhesion to surrounding vessel walls due to the polarity of the water molecule (Schopfer & Brennicke, 2016). This concept, called cohesion-tension theory, is widely accepted as a physically based explanation of water transport through plants (Steudle, 2001).

To a smaller extent, water can also be pushed upwards by root pressure, caused by an osmotic potential due to active accumulation of ions in root vessels. Even though quantitatively this can often be neglected when transpiration takes place, it can be of importance especially in herbaceous plants and under conditions of high relative humidity or during the night (Schopfer & Brennicke, 2016).

Despite the fact that water is mostly transported passively, plants regulate this transport by permanent adaptions to climate and more flexible reactions to short-term changes of environmental conditions. Within the soil-plant-atmosphere continuum, the amount and velocity of transported water depend on resistances along its pathway, namely root, stem, leaf, stomata and cuticular hydraulic resistance (Blum, 2011).

As the gradient in water potential is highest at the interface of plant and atmosphere, controlling water loss from leaves is crucial for plants. Besides permanent adaptions, like leaf morphology, thickness of cuticular layer or trichomes, water loss can be regulated by means of stomatal opening and closing as a much faster reaction to changing environmental factors. Because CO_2 for photosynthesis is also taken up via stomata, their extent of aperture is a complex trade-off between rate of photosynthesis and excessive water loss (Blum, 2011).

At the interface between soil and plant, water uptake is governed by both soil and root spatial organization and hydraulic properties. Water uptake from soil is naturally restricted to areas containing roots. The spatial extent of the root system sets an upper boundary limiting water extraction and is therefore a major factor influencing water availability (Lobet et al., 2014). Hereby the root density in different soil areas is of special importance, because it governs the size of the rhizosphere and therefore the contact area between soil and plant roots. Many plants increase this contact area and therefore water and nutrient uptake by means of mycorrhiza, a symbiosis between plant roots and fungi (Blum, 2011).

Ecohydrological and climate models often assume that RWU is directly linked to the root density distribution (Varado et al., 2006). Because presence of roots is not static in time, especially in ecosystems with pronounced seasonality or irregularity of water availability, a dynamic adjustment of their vertical density improved modeling results (Schymanski et al., 2008). Nevertheless, the dynamics of water uptake both in space and time can often still not be reproduced. Recent findings suggest that depending on species and history of soil water status, the root density distribution alone fails to provide an estimation of water uptake patterns (Volkmann et al., 2016a). On the one hand, this can be explained by the fact that individual root segments vary in their hydraulic conductivity and connection to the shoot base (Lobet et al., 2014). On

the other hand, the determination of root length density is difficult, either comprising destructive laborious sampling in the field or associated with high uncertainties. This also decreases the ability of the property root length density for an accurate estimation of RWU.

On its way from the soil into the root xylem, water needs to pass through multiple cell layers. For this radial transport three parallel pathways exist: the transcellular path crosses cell membranes, while the symplastic path uses the plasmodesma and the apoplastic path in between cells. The continuity of the latter allows for bulk flow of water, but transport is limited by the casparian strip controlling both nutrient uptake into plants and preventing water loss from roots into the soil (Blum, 2011). Such hydrophobic structures as well as the tissular structure of root segments were shown to be influenced over the long term by the growing medium and to develop in response to the history of environmental conditions like water availability (Lobet et al., 2014).

With increasing suberisation of roots for example with aging, the apoplastic transport is more and more limited and cell-to-cell transport becomes more important (Vetterlein & Doussan, 2016). The transport across cell membranes is facilitated by specific water channel proteins called aquaporins which contribute between 30 % and 90 % to plant water uptake (Javot & Maurel, 2002).

Root hydraulic conductivity also changes on shorter timescales and is therefore not only a property of its morphology. This was observed as a reaction to a variety of environmental stimuli like diurnal cycles or nutrient and water availability (Javot & Maurel, 2002). While high uncertainty in the controlling mechanisms and underlying causes still exists, aquaporins, which are presumably influenced by plant hormones, could hereby play a central role (Blum, 2011).

Because water flows from higher to lower water potential, water uptake generally decreases with subsequent drying of soil material. In addition, water redistribution to areas where RWU takes place is increasingly limited with advancing drying of the soil (Lobet et al., 2014). This illustrates that soil hydraulic conductivity also has a big impact on water resources available to plants. Lobet et al. (2014) pointed out that root distribution often becomes a poor indicator of the RWU profile, when soil water content is heterogeneous. A strong influence of soil water status on water acquisition was for example observed by Kulmatiski et al. (2017). Tracing injections of deuterated water, they found that RWU in a sagebush-steppe-ecosystem could be better linked to resource availability than root biomass distribution.

To deal with the heterogeneous distribution of soil water, plants alter their water uptake patterns by adaptive root growth and root conductivity as well as changes in exudations like root mucillage (Rothfuss & Javaux, 2017). While the spatial distribution of water in soils influences root water uptake, plants are able to actively alter soil moisture contents by hydraulic lift, redistributing water from deeper and wetter to shallower and drier soil regions with usually higher amounts of nutrients (Blum, 2011).

As shown, RWU is a complex process governed by multiple codependent factors and is additionally highly variable in space and time. This highlights the necessity of combined measurements of soil properties and transpiration in high temporal and spatial resolution, in order to improve the understanding of RWU.

2.4 Water stable isotope composition in the soil-plant-atmosphere continuum

Water stable isotopes have been used to investigate plant-water relations for the last five decades (Rothfuss & Javaux, 2017). The pivotal assumption for these studies is that investigated plants do not fractionate the isotopes of water during uptake (Wershaw et al., 1966; Dawson et al., 2002). Therefore, analogously to the quantity of water acquired by roots, the isotopic composition in the xylem reflects the integrated composition of RWU. Discrimination against ^{2}H but not ^{18}O was only observed in halophytic and xerophytic species (Ellsworth & Williams, 2007). Consequently, xylem water is extensively used to study water uptake patterns in space and time, where ecosystem water pools are isotopically distinguishable.

Natural variations of isotope abundances are the result of fractionation due to phase transition and diffusion processes (Marshall et al., 2008). While this has effects on the isotopic composition of precipitation on a global and regional scale, at one specific location precipitation values will also vary with seasons and to a smaller extent for each event. Groundwater and deep soil water are therefore a mixture of all waters recharging it. Its value often lies close to the mean isotopic composition of annual precipitation. Soil profiles frequently show unique patterns that originate from water infiltration, movement and isotopic enrichment at the surface due to evaporation (Marshall et al., 2008).

When it reaches the leaves, water evaporates through stomata, leading to enrichment of the remaining water in both isotopologues. This enrichment depends on leaf temperature (equilibrium fractionation), relative humidity of the surrounding atmosphere (kinetic fractionation) as well as evaporative flux and the specific turnover time of leaf water (Dubbert et al., 2017). Bulk leaf water is therefore a mixture of waters differing in isotopic enrichment, from highly enriched water at the evaporation site to unfractionated xylem water following (Cuntz et al., 2007). As a result of both convection of xylem water towards the evaporation front and backward diffusion of enriched water, gradients of enrichment exist across the leaf (Marshall et al., 2008; Cuntz et al., 2007).

Under constant ambient conditions, e.g. relative humidity, temperature and stomatal conductance, plant transpiration approaches or reaches a steady-state, for which transpired water vapor reflects the isotopic composition of xylem water and therefore water taken up across the soil profile (Marshall et al., 2008). The isotopic composition is then not or only marginally influenced by the isotopic enrichment in the bulk leaf water (X.-F. Wang & Yakir, 2000).

If steady-state is not reached yet, the isotopic composition of transpired water deviates from that of source water. While the mechanisms of non-steady-state are better known for leaf water itself, short-term changes in the isotopic composition of transpired water vapor were only monitored recently (Dubbert et al., 2014). Obtained results challenge the steady-state assumption.

In reaction to increased CO_2 concentrations and therefore decrease of stomatal conductance, Simonin et al. (2013) observed that it took about 30 min for the transpiration of tobacco leaves to return to values close to steady-state. Dubbert et al. (2017) followed the response of the oxygen isotopic composition in transpiration with step changes in relative humidity across a range of species. They found that for all species transpiration isotopic composition values changed in a similar magnitude after the step change, but showed pronounced differences in the time needed to return to steady-state values. In an open cork-oak woodland in Portugal Dubbert et al. (2014) observed that the isotopic composition of transpiration was always lower compared to xylem water during daytime over the whole vegetation period and therefore never reached the steady-state. A modeling approach including non steady-state conditions suggested that during the night, transpiration was in contrast enriched in heavy isotopes. This diurnal pattern matches well with diurnal patterns of the isotopic composition of bulk leaf water, which shows an inverse diurnal rhythm, with highest enrichment midday and lowest values during the night (Cernusak et al., 2016).

Under field conditions steady-state might therefore rarely be reached, because the variation in environmental parameters happens faster than the approximation in leaves towards steady-state (Dubbert et al., 2014). Due to stable ambient conditions in the laboratory though, transpiration is expected to be at or close to steady-state for most time of the day in the presented experiment.

3 Materials and Methods

This chapter describes the different parts of the setup, their combination to an integrated system and the processing for all data collected. Experiments were conducted in the Institute of Biogeosciences - Agrosphere (IBG-3), biosphere-atmosphere exchange group at Forschungszentrum Jülich in the period from 14.11.2017 until 28.03.2018. All mean values are reported with standard deviation (sd). $\delta^{18}O$ and $\delta^{2}H$ refers to the isotope ratios of oxygen and hydrogen, respectively, that are expressed in per mil (‰) as relative deviation from the VSMOW standard as described in chapter 2.1 and will be referred to as isotopic compositions.

3.1 Cavity Ring Down Spectroscopy

A wavelength-scanned cavity ring-down spectrometer (CRDS, L2130-i Isotopic H_2O, Picarro Inc., Santa Clara, USA) was used to analyze the isotopic compositions of water vapor samples. Subsequent descriptions of measurement principles are based on Crosson (2008). The measurement technique depends on the unique optical absorbance of different small gas phase molecules. The central element of the instrument is a cavity with constant sub-atmospheric pressure and highly reflective mirrors. Therein the light from a single frequency laser is introduced, until a certain threshold in intensity is reached. When switching off the laser, light stays in the cavity, traveling between the mirrors on an effective path length of tens of kilometers. Meanwhile light intensity decreases due to losses through cavity mirrors and absorption of molecule mixture by the gas sample introduced. The exponentially shaped so-called ring-down of light intensity is monitored by a photo-detector outside the cavity. The course of this decay is shaped by the different optical absorbance of gas phase molecules. Using light in different wave-lengths hence allows for determining concentrations of different gas species inside the sample. The device used is equipped to measure ratios of $^{18}\mathrm{O}\,/^{16}\mathrm{O}$ as well as $^{2}\mathrm{H}\,/^{1}\mathrm{H}$ and provides raw values as isotope ratios in δ -notation in a resolution of 1 Hz.

3.2 Soil columns

3.2.1 Setup and equipment

For the experiment three custom made acrylic glass columns with an inside diameter, height and volume of 0.11 m, 0.60 m, 0.0057 m^3 respectively were used. See Rothfuss et al. (2015) for a detailed description and an evaluation of an evaporation experiment

using sand. Hereafter, lower soil depth refers to the column top, high soil depths indicate the column bottom. For each column a porous glass plate (Robu® GmbH, Hattert, Germany, pore size diameter between 10x10^{-6} m and 16x10^{-6} m), which is in contact with soil material, can be found at the bottom. It is connected to a two-way manual valve (SMC Pneumatik GmbH, Germany) allowing for saturation of the soil column from the bottom up.

Water vapor mixing ratio (*wvmr*) and isotopic composition of soil water vapor could be derived using two ports, one providing synthetic air (20.5 % O_2 and 79.5 % N_2, 20-30 ppmv water vapor, Air Liquid, Germany), the other being used as sample air outlet in eight different depth at 1, 3, 5, 7, 10, 20, 40 and 60 cm. In each depth the two ports were connected with a microporous polypropylene tube (Accurel® PP V8/2 HF, Membrana GmbH, Germany) of approximately 17.5 cm length and 8.6 x 10^{-3} m, 5.5 x 10^{-3} m and 1.55 x 10^{-3} m in outside diameter, inside diameter and wall thickness respectively describing a horizontal semicircle inside the soil column. While the material of the tubing has strong hydrophobic properties prohibiting liquid water to intrude its vicinity, it allows the collection of water vapor through its $0.2\,x\,10^{-6}\,m$ diameter pores. Assuming thermodynamic equilibrium the isotopic composition of liquid soil water can be derived from the values of sampled water vapor (see chapter 2.2.1). Figure 3.1 shows a scheme of the column used in the experiment published by Rothfuss et al. (2015).

For an accurate calculation of equilibrium fractionation factors, soil temperature sensors (type K thermocouple, Greisinger electronic GmbH, Regenstauf, Germany, precision: 0.1 °C) were installed in columns I and II using separate ports at the investigated depths. While column II provided measurements at all available ports, column I recorded soil temperature at 3, 10, 20, 40 and 60 cm depth. In column I volumetric water content was measured at 1, 5, 10, 20, 40 and 60 cm depth using a frequency domain sensor (EC-5, Decagon Devices, USA, precision: $0.02\,m^3\,m^{-3}$). Soil moisture sensors were installed with the probes plane orientated vertically, reducing the risk of changing vertical water movement due to water retention on top of the sensor prongs. As column III was designed to also conduct measurements with Magnetic Resonance Imaging (MRI), no additional measurement sensors were installed.

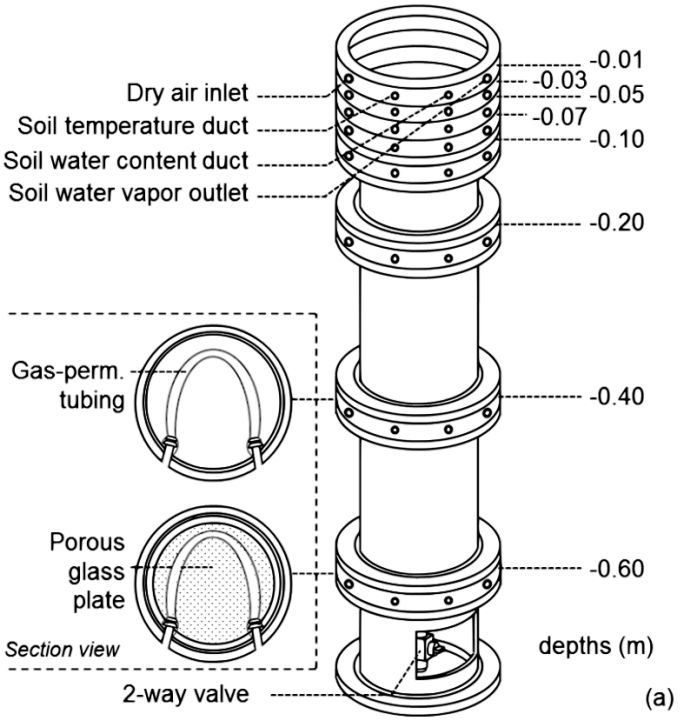

Figure 3.1: Scheme of the acrylic soil column used in the experiment with sampling depths, measurement ports and a cross section showing the placement of the polypropylene tubing (adapted from Rothfuss et al. (2015)).

3.2.2 Filling with soil and saturation

Soil used in the experiment was collected from the Institute of Ecosystem Physiologies experimental field site "Flugplatz" in Freiburg (coordinates: N48°01′13″ E7°49′36″, EPSG 3857) in a depth of approximately 0 to 40 cm. This specific location was picked for soil extraction to facilitate comparison between the presented laboratory experiment and a parallel field trial at the sampling location, associated with the corporate DFG project. Fine soil was separated from the skeleton-rich Anthrosol using a screen with a mesh size of 2 mm. Subsequently, the resulting soil material was dried at 105 °C for 24 h. The results of a particle size analysis conducted at Forschungszentrum Jülich are summarized in table 3.1. To determine textural properties, a combination of wet sieving for sand (grain diameter > 63 μm) and the pipett method to separate silt and clay particles (Sedimat 4-12, Umwelt Geräte Technik GmbH, Müncheberg, Germany) was applied. With the analyzed soil texture the soil is classified at the border between loam and silty loam according to the WRB (World Reference Base for Soil Resources) soil classification (Working Group WRB, 2015).

Table 3.1: Particle size distribution of the soil used in the soil columns.

Fraction		Percentage [%]	
sand		37.76	
silt	coarse	48.59	18.95
	middle		18.07
	fine		11.57
clay		13.65	

The relationship between soil water content and soil water potential (retention curve) was characterized for a sampling ring containing the soil used in the experiment with the associated bulk density of 1.11 g cm^{-3}. Hydraulic properties were estimated using the HYPROP®(UMS, Germany) method (Schindler et al., 2010) in combination with the WP4®Dewpoint Potentiometer (Decagon Devices, WA, USA) for soil water potentials with values higher than pF 3.

The resulting retention curve for soil dehydration and the corresponding shape parameters (α_{vG} and n) of the van-Genuchten equation are shown in figure 3.2. Also provided are values for residual soil moisture content and volumetric soil moisture at saturation. K_s is the determined saturated hydraulic conductivity.

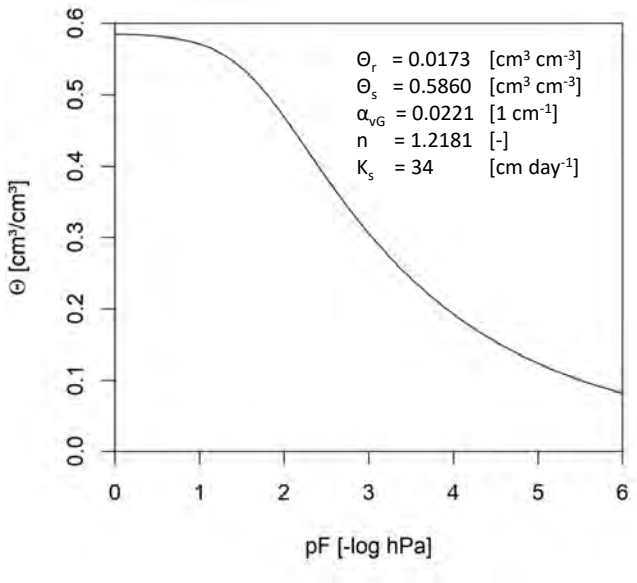

Figure 3.2: Retention curve and shape parameters of the van-Genuchten equation for the soil used in the soil column at a bulk density of 1.11 g cm^{-3}.

After the columns were assembled and tested for impermeability, they were filled with soil from the top in one go to reduce partitioning of soil textures. Repeated shaking of filled columns increased the bulk density of the soil finally reaching a value around $1.11\,g\,cm^{-3}$, while also reducing the risk of gaps around the instrumentation.

All columns were saturated concurrently with deionized water of known isotopic composition ($-7.97 \pm 0.05\,‰\,\delta^{18}O$ and $-53.5 \pm 0.37\,‰\,\delta^{2}H$) from the bottom on 14.11.2017 using the two-way manual valves. Saturation was driven by the difference of hydraulic heads between the water level in the column and the water tank and took up to five and a half hours. When the water level reached the top of one column, it was closed with a lid to minimize evaporation before the first measurement. All lids were opened the subsequent day and columns were allowed to evaporate freely for more than ten weeks until 26.01.2018.

To monitor evaporative losses, columns were placed on balances. The weight of the continuously measured column I was logged automatically with a time resolution of ten seconds by connecting the balance (Plattformwaage DS, Kern & Sohn GmbH, Germany, accuracy 0.2 g) to a LabView program. The weights of columns II and III were recorded manually from a different balance (Miras2-60 EDL, Sartorius, USA, accuracy 1 g).

3.3 Isotope standards

Standardization of obtained water stable isotope measurements was realized with two laboratory standards using airtight acrylic glass cylinders with 12 cm, 22 cm and 2,5 l of inner diameter, height and volume respectively, tested in detail in Rothfuss et al. (2013). The lid of each vessel offered a port for dry air inlet and sample air outlet that were connected with a 30 cm piece of the polypropylene tubing also used in the soil columns. After being checked for air tightness, a third sealable inlet was used to fill the cylinder with soil. As soil physiochemical properties, in particular the amount of clay, could have an influence on the measured isotopic composition (Gaj et al., 2017), the same batch of soil was used in columns and standards. Standards were also shaken to increase bulk density, reaching values of 1.18 and $1.19\,g/cm^3$, before being saturated with waters of distinct isotopic composition from the bottom until the soil was fully saturated.

Hereafter St_{heavy} refers to the enriched standard with $\delta^{18}O = 16.84 \pm 0.10\,‰$ and $\delta^{2}H = 34.80 \pm 0.67\,‰$, St_{light} indicates the depleted standard with $\delta^{18}O = -19.60 \pm 0.20\,‰$ and $\delta^{2}H = -83.09 \pm 1.20\,‰$. Analogously to the soil columns, measurements of water stable isotopes in standards were carried out in vapor phase assuming thermodynamic equilibrium. To reduce temperature fluctuations and therefore changes in isotope equilibrium fractionation, they were placed in a box lined with insulation material (Armaflex, armacell engineered foams, Germany). Temperature was recorded inside the box between the standard vessels using the same sensor type as those installed in the soil columns.

3.4 Measuring the transpiration flux and isotopic composition

3.4.1 *Centaurea jacea* - characteristics and transplantation

The investigated plant species *Centaurea jacea* is one of the dominant species being monitored in the parallel field trial in Freiburg. With a pronounced lignification of its stem in comparison to other herbaceous plants and a tendency to develop a deep tap root, it also met favorable preconditions for a successful first trial of the new method. The perennial plant can survive on a broad range of soil types, pH values and under nutrient-poor conditions but requires exposure to direct sunlight and prefers soils that are well drained (PFAF, 2012).

Plant individuals were grown in the laboratory under the LED lights also used in the final setup. One of them was transferred into column I on 26.01.2018. Therefore a hole of 17 cm depth was predrilled into the soil. To decrease manipulation of the isotopic composition along the soil profile, plant roots were cautiously freed from soil material and dried before insertion into the soil column. A picture of the plant individual right before insertion into column I is displayed in figure 3.3. Because the contact area between roots and soil was initially low, plants were irrigated with water from the top from that day on. In order to maintain a monotonic soil profile and even enhance the isotopic gradient that developed in the course of bare soil evaporation, this was done using enriched water with $9.57 \pm 0.07\,‰ \delta^{18}$O and $6.5 \pm 0.2\,‰ \delta^{2}$H.

Figure 3.3: Picture of the *Centaurea jacea* individual planted in column I with cleaned root system right before insertion.

3.4.2 Measuring plant transpiration

A plant chamber with $0.30\,m$, $0.32\,m$ and $0.0226\,m^3$ in inside diameter, height and volume respectively was installed to measure quantity and isotopic composition of transpiration flux. The chamber consists of acrylic glass and has three ports: one air inlet, one sample air outlet and a third access port for a sensor measuring air temperature and rh (RFT-2, UMS GmbH, Germany, precision: $rh\,2\,\%$, $T\,0.1\,°C$). To prevent an isotope exchange between chamber air and walls, the latter was covered with transparent teflon foil. The bottom, made out of two semicircles, has a small hole for the plant stem so that the plant transpiration signal can be isolated from soil evaporation and contamination with ambient air. To fill up the hole completely, the plant stalk was wrapped with teflon tape. The slot in the base plate was closed with sealing rubber.

A Membrane pump provided air from the laboratory at a constant flow rate. The input air flow rate value was set in order to observe a positive excess at the outlet of the plant chamber. Furthermore, this excess had to be greater than the amount of air needed by the laser spectrometer to perform isotopic measurements to avoid contamination with laboratory air. The amount of air flow was set in a manner that, despite some air leakage from the chamber, outflow was still sufficiently high to exclude the risk of ambient air intruding, hence distorting the results. Five axial fans ensured thorough mixing of the air inside the chamber. A schematic drawing of the plant chamber can be found in figure 3.4.

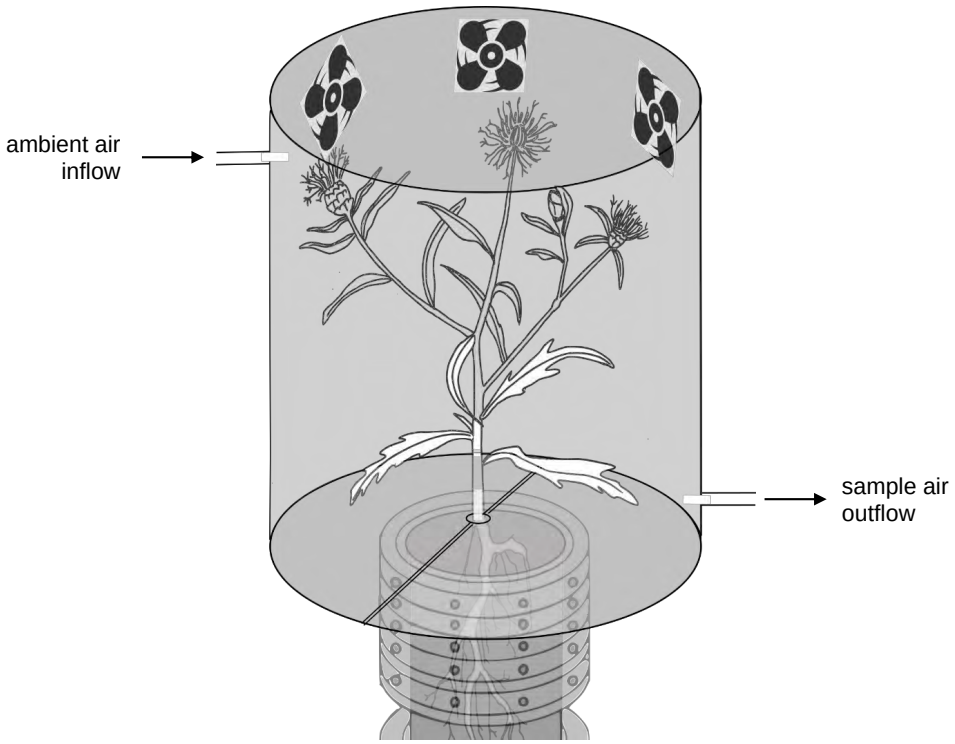

Figure 3.4: Schematic drawing of the plant chamber with ports for inflow of ambient air and outflow of sample air. Five fans ensured mixing of air inside the chamber. Sensor measuring temperature and rh is not displayed.

A comparison of the water vapor mixing ratio and isotopic composition between laboratory air and air provided by the pump was carried out prior to the experiment and revealed no significant differences. LED daylight bulbs (V600 Reflector Series, VIPARSPECTRA, China) were placed 30 cm above the plant chambers. They were set to vegetative mode in a day/night cycle of 16/8 h, automatically switching on at 09:15 every morning. Glass bowls filled with water were placed on top of the chamber, keeping heating inside to a minimum.

Transpiration is dependent on the vapor pressure deficit (vpd) between the leaf and the air surrounding it. Saturation vapor pressure (e_s in kPa) for a specific temperature (T in $°C$) can be calculated with equation 3.1 (Murray, 1966). Assuming that leaf temperature is comparable to the temperature measured inside the plant chamber and the air inside the leaf is fully saturated, the vpd can be calculated from e_s and rh in the plant chamber using equation 3.2.

$$e_s = 0.61078 e^{\frac{17.27T}{T+237.3}} \tag{3.1}$$

$$vpd = \frac{100 - rh}{100} e_s \tag{3.2}$$

The chamber measurements provide water vapor mixing ratio and isotopic composition of the inflow into the chamber (background) and the outflow from the chamber containing the transpiration signal. The transpiration rate (E in $mmol\, sec^{-1}\, m^{-2}$) is calculated from the value of the difference between inflow (w_{in}) and outflow (w_{out}) water vapor mixing ratios. Considering mass preservation, it can be calculated with equation 3.3, using the air flux into the chamber u in $mol\, sec^{-1}$ (Von Caemmerer & Farquhar, 1981). Usually the transpiration rate is related to the leaf surface area. As an acurate determination was not possible, especially due to the pronounced increase in aboveground biomass during plant chamber measurements, transpiration rate was standardized to the columns cross-sectional soil area ($A = 0.0095\, m^2$).

$$E = \frac{u\,(w_{out} - w_{in})}{A} \tag{3.3}$$

The isotopic composition of transpiration was calculated with a mass balance approach analogously for both isotopes with equation 3.4 (Dubbert et al., 2014; Simonin et al., 2013). Therefore, the $wvmr$ of air flow into and out of the chamber w_{in} and w_{out} and their respective isotopic ratios δ_{in} and δ_{out} are used. The transpiration adds water that increases the air flow from the chamber compared to the air inflow. This is corrected by the second term of equation 3.3 (Dubbert et al., 2014).

$$\delta_E = \frac{w_{out}\,\delta_{out} - w_{in}\,\delta_{in}}{w_{out} - w_{in}} - \frac{w_{in}\,w_{out}\,(\delta_{out} - \delta_{in})}{w_{out} - w_{in}} \tag{3.4}$$

With data from the sensor registering rh and T inside the plant chamber, $wvmr$ inside the chamber was calculated to verify $wvmr$ measured with CRDS. Assuming instantaneous mixing of inflow air and plant transpiration, equation 3.5 with atmospheric standard pressure $p_{tot} = 101.325\,kPa$ was used (Vaisala, 2013). In the beginning measured $wvmr$ deviated systematically from calculated values as can be seen in figure A.4 in appendix A.7. Possible reasons will be discussed in chapter 5.1.2. For obtaining E and δ_E, $wvmr$ calculated from rh and the temperature measured inside the plant chamber were used.

$$wvmr = \frac{e_s \frac{rh}{100}}{p_{tot} - e_s \frac{rh}{100}} 10^6 \tag{3.5}$$

3.5 Combined setup and measurement protocol

3.5.1 Integrated measurement system

The soil column, plant chamber and standards were connected to the CRDS instrument in one single system using PTFE (Polytetrafluorethylen) tubing with $1/8\,in$ in diameter and tube fittings (Swagelok, USA). Switching between subsequent measurements of isotopic composition in ambient air, different soil depth, standards and the plant chamber was realized with a LabView program controlling solenoid magnetic valves (type 6011, Bürkert Werke GmbH, Germany) and two mass flow controllers (MFC, EL-FLOW, Bronkhorst High Tech, the Netherlands). The first MFC provided $52\,ml\,min^{-1}$ of dry synthetic air to the gas permeable tubing in soil columns and standards. To prevent condensation of sample water vapor on its way to the laser spectrometer, the second MFC was used to dilute all samples apart from laboratory air with a dry air stream of 28 ml/Min.

The ratio of flow rates for sample and dilution line resulted in a water vapor mixing ratio measured in the range of 10000 to 23000 ppmv for all soil and standard measurements. Combined flow was high enough to exclude contamination of sample air with ambient air. Excess flow was regularly controlled with a flow meter (ADM3000, Agilent Technologies, Santa Clara, California). Taking into account the gas volume needed by the laser spectrometer for measuring isotopic compositions, excess flow at the entire systems outlet was at least 20 ml/min at all times.

Ambient air was sampled passively next to the soil columns using stainless steel tubing (diameter $1/8\,in$). Air temperature and rh were recorded with one sensor (RFT-2, UMS GmbH, Germany). During this section of the experiment each soil depth was sampled twice a day. Figure 3.5 shows the experimental setup for the different components integrated.

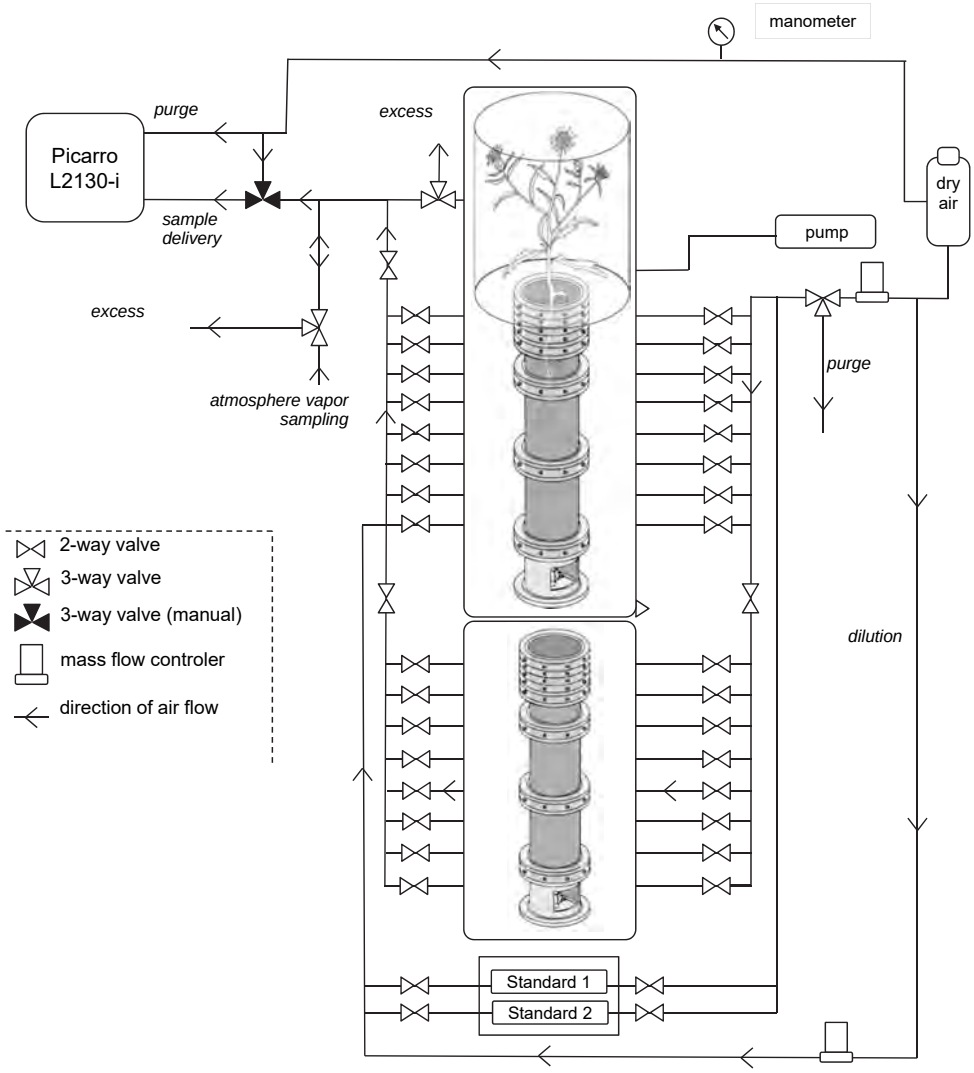

Figure 3.5: Experimental setup for automatized measurement of water stable isotopes in two soil columns and in plant transpiration, developed on the basis of Rothfuss et al. (2015).

3.5.2 Measurement protocol

From 15.11.2017 to 25.01.2018 the change of the isotope profile due to evaporation in bare soil columns was observed in daily resolution. Following the findings of Rothfuss et al. (2013), measurement duration for each sample point was at least 30 min to remove the memory of the previous measurement and to allow for the establishment of a steady plateau in water vapor and isotopic composition. Standards were each sampled four times a day subsequently. Because of higher differences in isotope ratios, sampling time was hereby extended to 45 min for standards and the following measurement. Ambient air was sampled at least two times per day for 45 min during bare soil evaporation.

The setups capacity only allowed for measuring two of the three soil columns at a time. While column I was measured in daily time resolution throughout the experiment, columns II and III were measured alternately during bare soil evaporation. While a column was not installed in the system, the respective tubings were sealed with Parafilm to prevent evaporation.

For a total of six weeks, in the period from 14.02.2018 until 28.03.2018, measurements across the soil profile were complemented by transpiration measurements in the plant chamber three times a day, when lights were switched on, for 60 min each. Each day, the 60 min measurements of plant chamber outflow ended at 12:00, 17:45 and 23:30. Because laboratory air provides the baseline conditions for the plant chamber, measurement frequency was increased during this phase of the experiment and ambient air was sampled before and after each transpiration measurement for 30 min.

In the end, combined measurements in the plant chamber and in the soil were only carried out in column I. During this section, the light cycle of the LED lights induced temperature changes of around $4\,°C$ that led to condensation of water vapor at the outlet of each gas-permeable tubing section. Therefore, the PTFE outlet tubings of the column were flushed every morning with 500 ml of dry air for one minute in each depth. The column was covered with aluminium foil to reduce bare soil evaporation.

Figure 3.6 shows the timeline for the two different sections bare soil evaporation (section 1) and combined measurements in the plant chamber and soil column (section 2). The six weeks in section 2 are defined as day of experiment (DoE) 1 to 42. For section 2, the figure also provides information on times when water was added and its respective amount and isotopic composition. In the beginning of section 2 the plant was irrigated from the top with 30 ml enriched water in the morning around 10:00 for three days (DoE 1-3). From 17.02.2018 (DoE 4) onwards no water was added to the top. The root system rapidly reached a depth of at least 40 cm, which was observable

through the transparent acrylic glass wall of the column. For this reason, the soil isotopic composition in the bottom cm of the profile were altered by means of slow saturation with depleted water (in total about 0.5 l) from 20.02.2018 till including 23.02.2018 (DoE 7-10). Meanwhile the top of the soil column subsequently dried. From 20.03.2018 to 23.03.2018 (DoE 35-38) plants were again irrigated from the top with enriched water, adding a total of 150 ml per day divided in three parts of 50 ml at 09:00, 12:00 and 16:00 for better infiltration.

In order to avoid condensation problems linked to plant growth that increases the transpiration, the plant chamber inlet air flow was increased from $1.7\,lmin^{-1}$ to $2.1\,lmin^{-1}$ at 10:00 on 19.02.2018, to $2.6\,lmin^{-1}$ at 17:30 on 16.03.2018 and to $4.5\,lmin^{-1}$ at 17:30 on 19.03.2018.

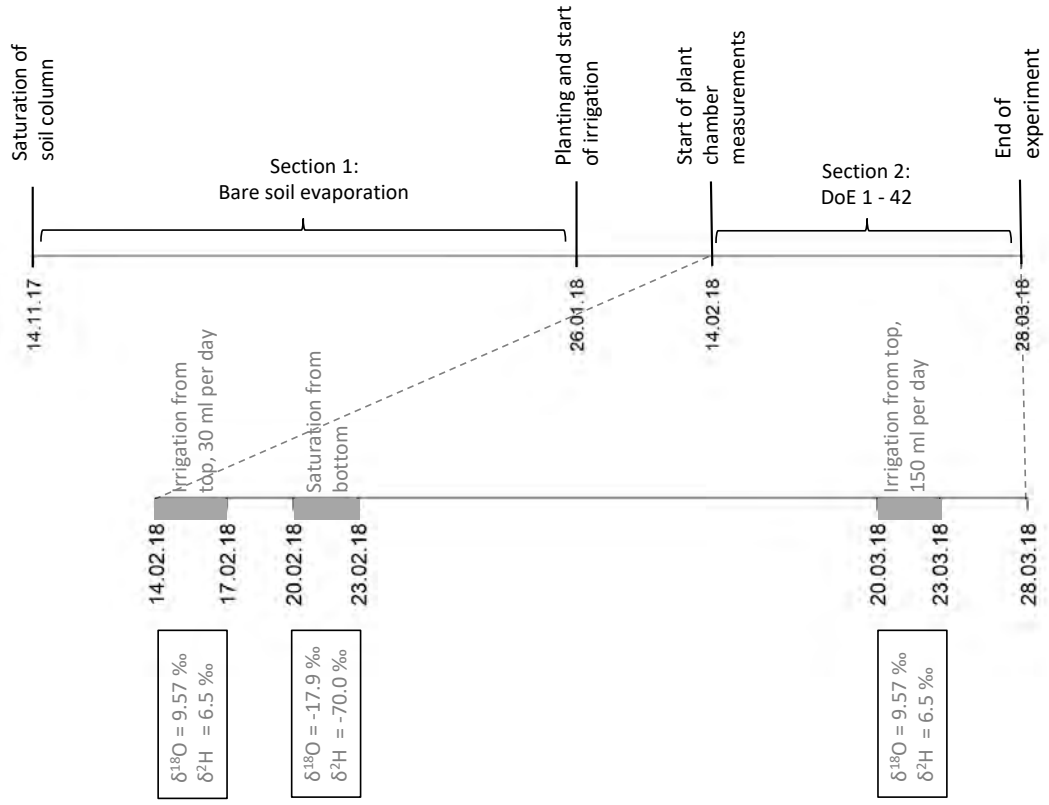

Figure 3.6: Timeline of the experiment with the two sections bare soil evaporation and plant chamber measurements. For the second section, information is also provided for amounts, isotopic composition and timing of water added to the column.

3.6 Data processing

The following chapter describes data selection and processing for soil moisture and temperature sensors as well as isotopic compositions in soil columns, ambient air and plant transpiration. Data processing and analysis was carried out using the programming and statistics language R Version 3.4.1 (R Core Team, 2017).

3.6.1 Calibration of soil moisture and temperature sensors

For each temperature sensor installed in the soil columns a one-point calibration was performed. This was carried out with measurements recorded 7 h after complete saturation, assuming water in the columns adjusted to the ambient temperature by that time. Sensors were calibrated against the temperature sensor monitoring laboratory air using mean values over one hour.

Soil moisture sensors output does not give volumetric soil water content directly but provides a voltage. This output is affected not only by soil moisture but also excitation voltage. As the latter was not constant over time, it was also monitored and calibration was carried out using the ratio of output compared to input voltage. For each soil moisture sensor an individual linear regression was calculated using 1 h averages under dry conditions e.g. before saturation and values obtained at full saturation. Volumetric water content at saturation ($\Theta_s = 0.52$) was calculated using equation 3.6 with weight of water added to the column (m_{water}), weight of dry soil (m_{dry}), bulk density (ρ_{soil}). Density of water (ρ_{water}) was assumed to be $1\,g/cm^3$. The residual water content in the dry soil column $\Theta_r = 0.017$ was taken from the retention curve analysis. Linear regressions between input voltage fraction and volumetric soil moisture content for the calibration of all six soil moisture sensors installed in column 1 are displayed in figure A.1 in appendix A.3

$$\Theta = \frac{m_{water}}{m_{dry}} * \frac{\rho_{soil}}{\rho_{water}} \tag{3.6}$$

3.6.2 Water stable isotopes in soil and transpiration

Figure 3.7 shows the schematics of the whole data processing for soil measurements from raw isotopic composition in vapor phase to liquid values at one specific time each day. The process is being explained in detail hereafter. As for plant chamber and ambient air measurements, water vapor is sampled directly, the step calculating liquid isotopic composition from vapor values is skipped in the data processing of

these measurements.

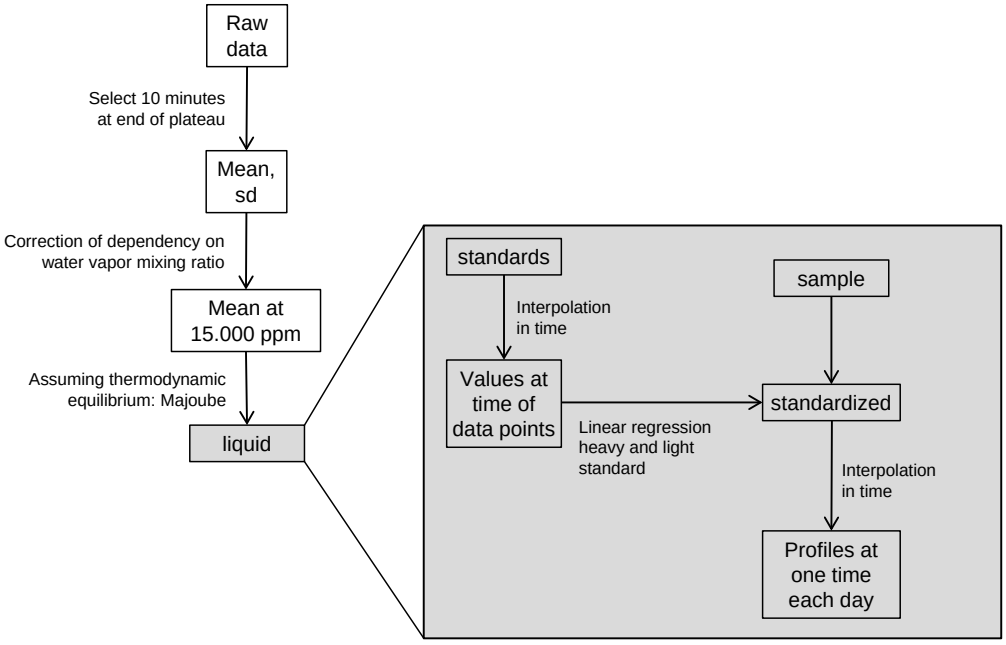

Figure 3.7: Schematics showing applied data processing to derive isotopic composition of liquid water out of vapor measurements.

For each individual measurement, the last 600 data points (equals approximately 10 min) were averaged. Graphic analysis of raw data was carried out and measurements, for which steady state due to condensation of water in the tubing or leaks at the tube fittings was not reached, were discarded. Additionally, data points with a *sd* higher than 0.35 ‰ and 0.9 ‰ for $\delta^{18}O$ and $\delta^{2}H$ respectively were discarded to ensure all measurements were stable.

Isotopic compositions measured with CRDS instruments are influenced by their water vapor mixing ratio (Schmidt et al., 2010). This device-specific dependency can also be impacted by the isotopic composition of source water and was therefore evaluated prior to the experiment using the standard vessels described in chapter 3.3. Additionally a third vessel was prepared in the same manner and saturated with isotopically intermediate laboratory water ($-7.92 \pm 0.14\,\delta^{18}O$ and $-52.8 \pm 1.0\,\delta^{2}H$). $Wvmr$ in a range from 4500 to 25000 ppmv were obtained by increasing the stream of dry air diluting the sample gas. For each of the three water sources, measurements were carried out on two separate days. The CRDS analyzer showed a clear positive correlation between $wvmr$ and $\delta^{2}H$. Slopes were significantly increasing with higher

isotopic composition ($R^2 = 0.997$, p-value = 0.04). For $\delta^{18}O$ an effect of *wvmr* was observed but, taking into account *sd*, negligible in the *wvmr* range of measurements. Observed relationships and derived equations of linear regression for δ^2H are shown in figure A.2 in appendix A.3. All isotope measurements were corrected to a reference level of 15000 ppmv according to their individual isotopic composition and *wvmr* measured.

Assuming thermodynamic equilibrium, isotopic composition of liquid water was calculated from vapor composition using the nearest temperature sensor and the empirical equation proposed by Majoube (1971). As there were no sensors installed in column III, temperature measurements from the neighboring column I were used. Liquid values for standards were interpolated in time to obtain values at the time of each sample point. A linear regression was calculated herewith to account for device specific drift. Finally measurements in different soil depths were interpolated to obtain an isotope soil profile for one specific time each day (17:00).

3.6.3 Event fractions

To visualize water movement in the soil column, recovered fractions of event water f_{eve} were calculated for every investigated soil depth and both isotopes separately for section b) and c). Equation 3.7 shows the used linear two source mixing model for $\delta^{18}O$ exemplary (Piayda et al., 2017). Hereby $\delta^{18}O_{act}$ is the stable oxygen isotope ratio of soil water at a certain time after the event, $\delta^{18}O_{pre}$ represents the isotopic composition on the day before the respective event and $\delta^{18}O_{eve}$ is the event water composition. The seperate calculation with both available isotopes allows for the exclusion of uncertain data points. The remaining data was averaged to obtain one event fraction value per day. Because soil moisture content was not equally distributed across the profile prior to events and the addition of water altered the amount of water contained in different depths, calculated event fractions were translated into shares of Θ. For soil depths that had no assigned soil moisture sensor, i.e. 3, 5 and 7 cm, values were linearily interpolated.

$$f_{eve} = \frac{\delta^{18}O_{act} - \delta^{18}O_{pre}}{\delta^{18}O_{eve} - \delta^{18}O_{pre}} \tag{3.7}$$

3.6.4 Error propagation

To evaluate the error associated with the calculation of measurements in the soil column and δ_E, a conclusive standard deviation is calculated using partial derivates taking into account uncertainties of input variables in the different steps of data processing. Assuming that variables are measured independently, the standard deviation can be calculated by means of a first-order Taylor series approximation (Phillips & Gregg, 2001). For calculating plant transpiration from chamber in and outflows for instance, the squared standard devaition $\sigma^2_{\delta E}$ is calculated with equation 3.8. A list of all formulas and corresponding partial derivates used along the different steps of data processing is provided in appendix A.5.

$$\sigma^2_{\delta E} = \left(\frac{\partial \delta_E}{\partial w_{in}}\right)^2 \sigma^2_{w\,in} + \left(\frac{\partial \delta_E}{\partial w_{out}}\right)^2 \sigma^2_{w\,out} + \left(\frac{\partial \delta_E}{\partial \delta_{in}}\right)^2 \sigma^2_{\delta\,in} + \left(\frac{\partial \delta_E}{\partial \delta_{out}}\right)^2 \sigma^2_{\delta\,out} \quad (3.8)$$

3.7 Estimating root water uptake with a multi-source mixing model

Root water uptake does not occur at one unique depth but potentially takes place in all parts of the soil, where roots are present. Isotopic composition of transpiration hence shows the integrated value of all water taken up by roots. An attempt to gain insight into this complex nature of root water uptake was made by implementing a multi-source mixing model drawing upon isotopic mass balance. With the two isotope species measured, a mathematical solution can be obtained for three different water sources (Phillips & Gregg, 2003).

When more than three possible sources exist, like along a soil profile, the system is underdetermined and the mixing model cannot be solved to obtain one unique solution. To deal with this, iterative algorithms are used, producing a multitude of suitable combinations of source contributions in line with isotopic mass balance (Parnell et al., 2010). To incorporate uncertainty arising from the measurement of the isotopic composition in source waters and to obtain an assessment of the likeliness of obtained solutions, bayesian inference is incorporated into the stable isotope mixing model. Accordingto this, Parnell et al. (2010) developed a package for stable isotope analysis in R (SIAR).

In the model the inital (prior) distribution for the relative proportion to RWU of a specific source is a Dirichlet distribution, a generalization of the Beta distribution. Essentially, the Dirichlet distribution is a measure of how high the chances are that a

certain probability distribution occurs. Plausible values for source contributions are thereafter calculated by fitting the model to data using a Markov Chain Monte Carlo algorithm. The result consists of probability distributions (posterior) of the relative contribution to RWU across the eight identified water sources. Additional information on model underlying principles and on stable isotope mixing models implemented into a bayesian statistical framework can be found in Parnell et al. (2010) and Parnell et al. (2013).

In the experiment presented, the function *siarmcmcdirichletv4* was used with values of 200000, 50000 and 15 for iterations, burn-in and thinning, respectively. This resulted in a matrix containing 10000 lines of water fraction contribution of the eight given water sources, each generating the isotopic composition measured in plant transpiration. To also account for uncertainty of measuring the target value (transpiration), which is not integrated into the function, each transpiration measurement is represented by its calculated value and two additional values for which the final standard deviation is subtracted or added. A most frequent value (mfv) is calculated for each depth separately by aggregating the resulting water uptake fractions in blocks of 1 %. The mfv is the interval with the highest amount of values.

4 Results

The results of the experiment are presented, starting with a general part showing an exemplary measurement sequence and the ambient conditions as well as soil moisture measurements for the whole experiment. In the second part, the evolution of soil profiles during bare soil evaporation (section 1 of the experiment) is displayed. A third part shows results of plant transpiration measurements and soil profiles during section 2 of the experiment, including an evaluation of the distribution of water added from the bottom (b) and the top (c) as event fractions in the soil profile. Finally, the results of section 2 are used as input information for the statistical RWU model SIAR, illustrating shifts of RWU profiles in response to changes of atmospheric conditions and soil water availability as well as development of the rooting system.

4.1 General - entire measurement period

4.1.1 Measurement sequence

Figure 4.1 illustrates raw measurements of *wvmr* and isotopic compositions exemplarily for a sequence of 10 h on DoE 3 showing all the different components measured. Dashed lines display times of switching between measurements. Plateaus in *wvmr* as well as isotopic compositions usually stabilized fast after switching of the valves. Measurements that did not meet this criteria were excluded from the results, because of potential condensation distorting measured values. $Wvmr$ ranged between 10000 to 17000 ppmv for soil measurements and 9000 to 28000 ppmv for plant chamber outflow.

During section 1 all soil measurements were found in the range spanned by the two standards. In section 2 the raw δ^2H composition in 1 cm depth slightly exceeded the mean value for St_{heavy} in the vapor phase on one occasion by 5 ‰ on DoE 1. On DoE 1-7 and 36-41 the raw δ^2H composition measured in the plant chamber outflow exceeded the isotopic composition of the heavy standard. The maximum value of this extent was around 16 ‰ in the first plant chamber measurement on DoE 39. The raw values for $\delta^{18}O$ of all measurements were located in between standard measurements at all times.

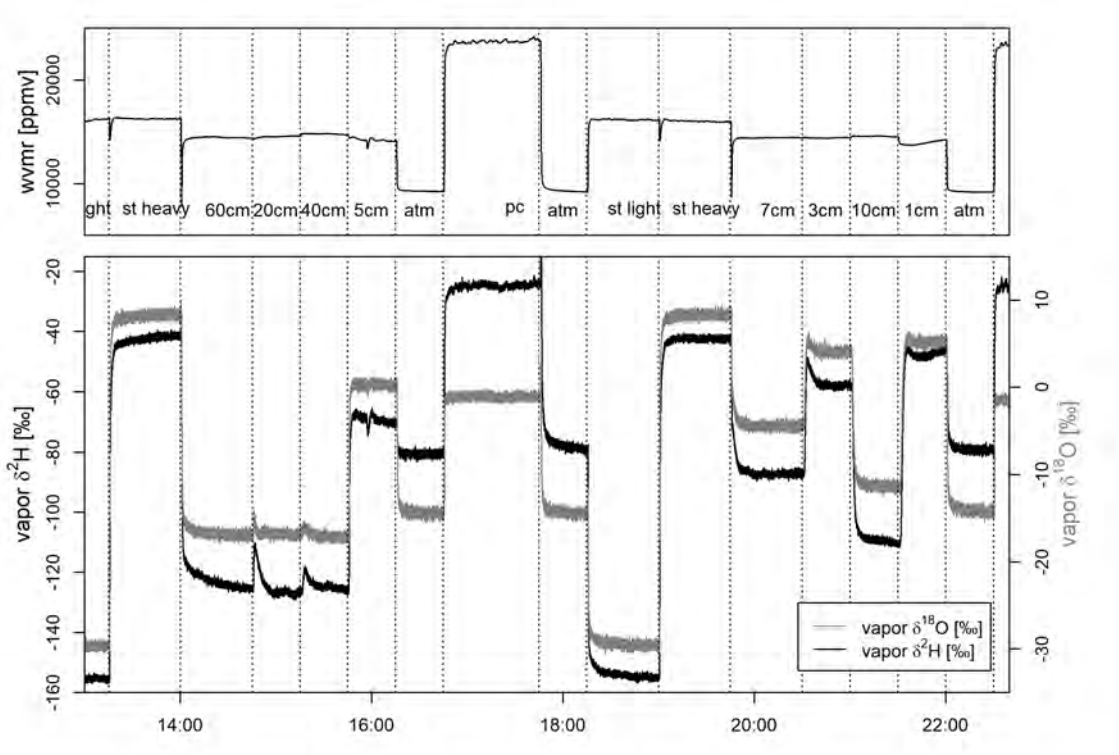

Figure 4.1: Example of the measurement sequence on DoE 3 (section 2) including measurements of standards, all available soil depths, plant chamber and ambient air. The figure shows *wvmr* and isotopic composition of the sampled water vapor. Dashed lines are the times when the opening of the magnetic valves were changed, therefore indicating switching between different measurements.

4.1.2 Ambient conditions

Over the entire experimental period air temperature and relative humidity in the laboratory ranged from 18.2 to 23.7 $°C$ and 17.7 to 51.4 %, respectively. Mean values were 20.1 $\pm$ 0.93 $°C$ and 37.4 $\pm$ 6.27 %. With the installation of the LED daylight bulbs above the setup on 26.01.2018, a more pronounced diurnal variation (in the range of around 1-2 $°C$) of the ambient air temperature is observed. Figure 4.2 shows the time series of temperature and *rh* as well as the isotopic composition of ambient air for the whole experiment.

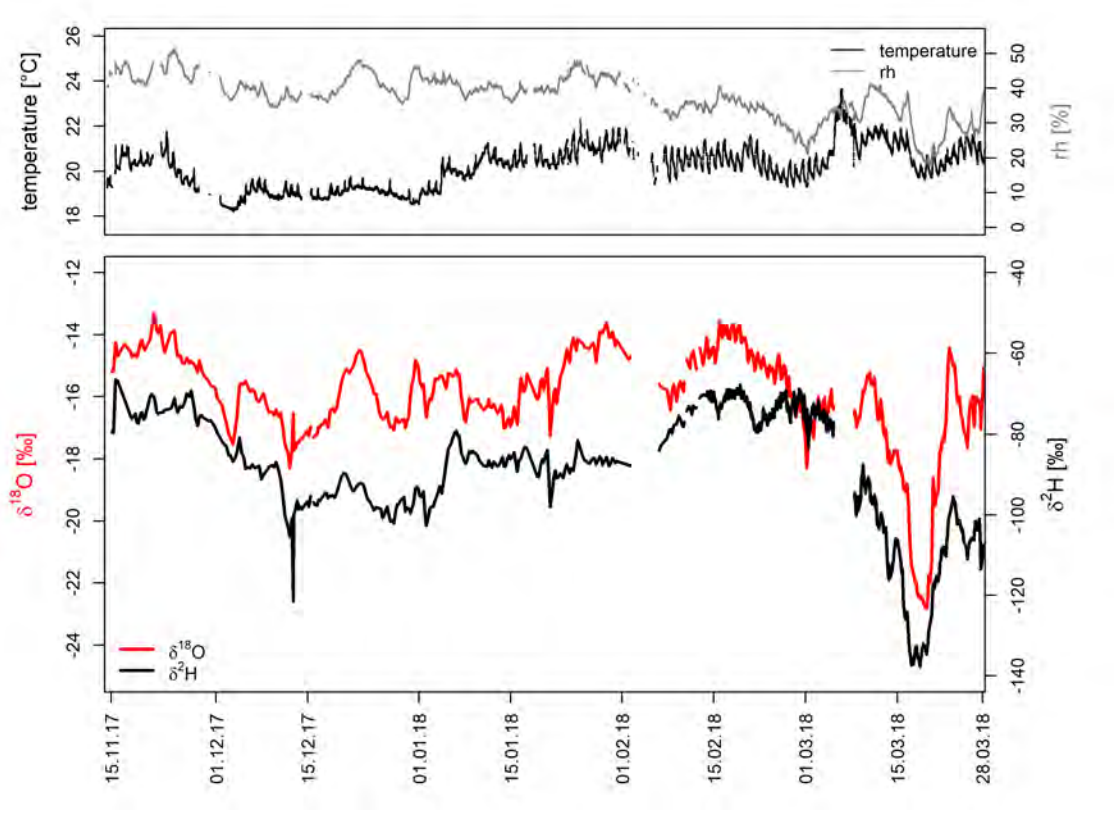

Figure 4.2: Temperature, rh and isotopic composition of ambient air over the course of the experiment. Mean values over the whole period are $20.1 \pm 0.93\,°C$ and $37.4 \pm 6.27\,\%$ for T and rh, respectively.

4.1.3 Volumetric soil moisture

Figure 4.3 shows the evolution of volumetric soil moisture content for depths equipped with sensors. For better clarity, data between section 1 and 2 appears in less saturated colors. Dashed lines indicate the start and endpoints of phases, where water was added to the column. Hereby a) marks irrigation from the top on DoE 1-3, b) is saturation of the columns bottom centimeters on DoE 7-10 and c) represents the second phase of irrigation from the top on DoE 35-38.

On the first days following the saturation of the soil column the decrease in volumetric soil moisture content was more pronounced with lower soil depths. In contrast to other depths, Θ in 60 cm depth remained constantly high during the first two weeks of bare soil evaporation. With subsequent drying afterwards the soil moisture in this depth declined faster. Around one and a half months after saturation (end of december) until the end of section 1 the decrease in soil moisture content was similar for all available depths reaching values between 29 % (depth 5 cm) and 35 % (depth 20 cm) before the transplantation of *Centaure jacea* into the column.

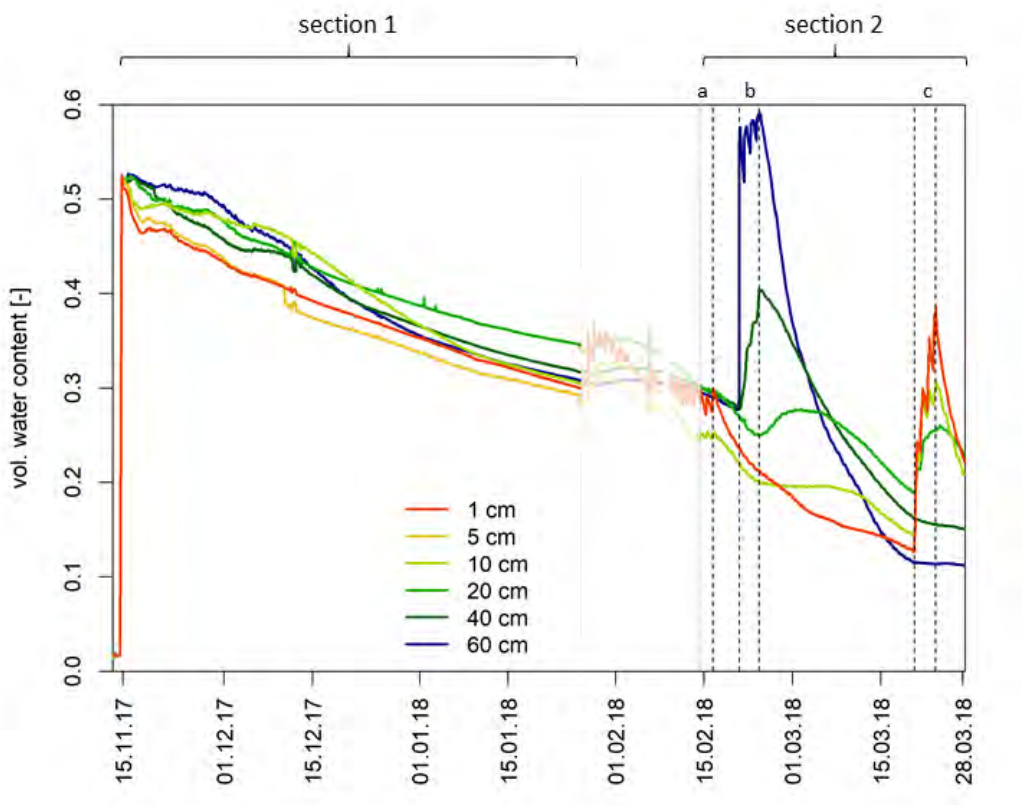

Figure 4.3: Soil moisture in different depth over the whole course of the experiment. Dashed lines indicate times when water was added to the column: a) irrigation from the top ($30\,ml\,day^{-1}$), b) saturation from the bottom ($500\,ml$ in total), c) irrigation from the top ($150\,ml\,day^{-1}$).

After the plant was inserted into the soil column, the subsequent irrigation fulfilled the purpose to compensate for a fast decline in water availability as a consequence of root water uptake. It can however still be seen that soil moisture contents in the upper few cm of the column dropped faster in comparison to bare soil evaporation in section 1. Because the sensor in 5 cm depth got damaged during the time period in between section 1 and 2 and thereafter did not give plausible measurements anymore, it was excluded for section 2.

After daily irrigation from the top was stopped, the soil moisture content decreased immediately. The sharpest decline can be seen in 1 cm depth even though the column was now covered with tin foil to minimize evaporative losses. With increasing soil depth, this initial decline was less pronounced. The saturation of the bottom centimeters immediately resulted in a reset of depth 60 cm to almost saturated conditions. At lower depths the resulting increase in soil moisture was less pronounced and associated with a higher time lag. For 1 cm soil depth this did not increase Θ, however it decelerated the decrease in soil moisture in comparison to the decline preceeding event b). Resulting from a steep decline, the soil moisture content at the column bottom was lower than in all other depths right before the repeated irrigation from

the top. Like in 40 cm depth Θ in 60 cm remained constant for the last week of the experiment.

4.2 Section 1: Bare soil evaporation

Figure 4.4 shows the soil water isotopic composition in column I for day 11 to 72 after saturation. Because standards had inexplicable jumps during this first section of the experiment that shifted soil profiles in a counterintuitive way, standardization was carried out with fixed mean values of 17.93 ‰ and 34.74 ‰ in St_{heavy} and -20.71 ‰ and -88.65 ‰ in St_{light} for $\delta^{18}O$ and $\delta^{2}H$, respectively. Days 1 to 10 after saturation had to be discarded, because the infrared light installed during that period caused condensation that led to non-reproducible isotopic compositions. Missing data points afterwards were linearly interpolated in time. Columns II and III, which were measured alternatingly, showed similar results and are therefore not displayed.

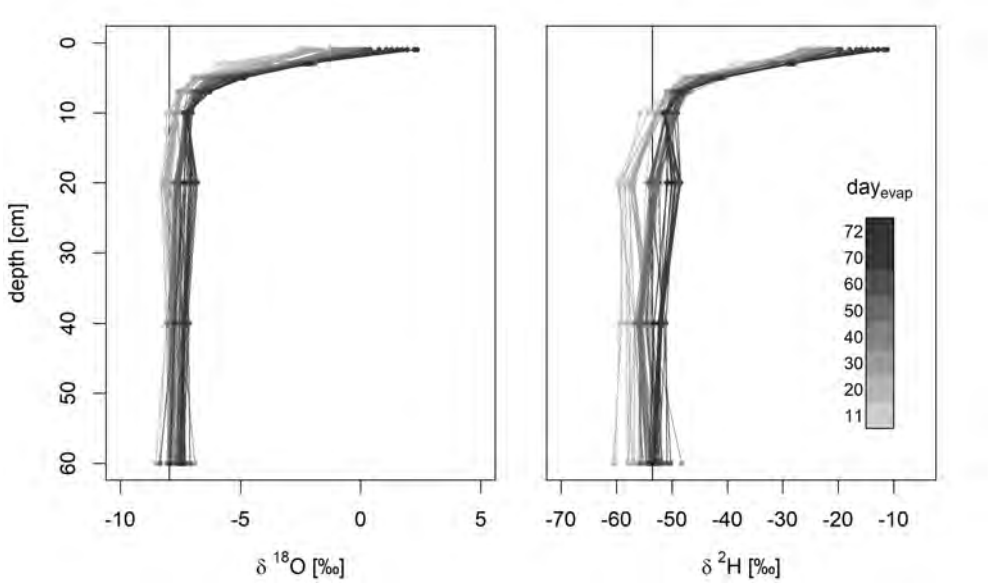

Figure 4.4: Profiles of $\delta^{18}O$ and $\delta^{2}H$ for days 11 until 72 of bare soil evaporation. Averaged standard deviations over all depth and displayed days are 0.32 and 0.75 for $\delta^{18}O$ and $\delta^{2}H$, respectively. Vertical lines indicate the isotopic composition of water used for saturation.

For depths 60, 40 and 20 cm soil isotopic compositions measured scatter on top of the composition of saturation water. With decreasing soil depth, the share of heavy isotopes in soil water increases in an exponential shape. After 72 days of bare soil evaporation (the heaviest) values of 2.35 ‰ and -11.24 ‰ were reached in 1 cm depth for $\delta^{18}O$ and $\delta^{2}H$, respectively.

During bare soil evaporation no systematic change of the isotopic composition with time could be observed for measurements in 40 cm and 60 cm. Therefore these depths can be used to estimate precision of the in-situ method over an extended time period and to also validate measured compositions with the water used for saturation of the soil column, i.e. the methods accuracy. Table 4.1 summarizes mean isotopic compositions and associated *sd* in both depth for the time period 11 to 72 days after saturation. They are compared to mean *sd* values calculated with the error propagation functions and the isotopic composition of saturation water.

Considering measurement precision, the in-situ method was able to reproduce the isotopic composition of water used for saturation. For $\delta^{18}O$ the *sd* calculated over the period of soil evaporation was lower than the mean *sd* of values calculated with the described error propagation method. $\delta^{2}H$ shows a 0.7 ‰ higher deviation from the mean.

Table 4.1: Isotopic composition in 40 cm and 60 cm depth measured in-situ in comparison to values of saturation water.

	$\delta^{18}O$ [‰]		$\delta^{2}H$ [‰]	
	40 cm	60 cm	40 cm	60 cm
$mean \pm sd$	-7.63 ± 0.25	-7.73 ± 0.30	-54.61 ± 2.08	-54.10 ± 2.07
$water_{sat}$	-7.97 ± 0.05		-53.50 ± 0.37	
sd_{ep}	0.41		1.32	

The relationship between $\delta^{18}O$ and $\delta^{2}H$ values in soil profiles during bare soil evaporation can be seen in figure 4.5. Only measured values are displayed, interpolated data was not considered for this visualization. The crosses for each data point represent their respective *sd* calculated with the error propagation approach described in chapter 3.6.4. For reference the GMWL water line ($\delta^{18}O = 8\delta^{2}H + 10$) was added. The linear regression through all plotted soil column data points has a slope and intercept of 4.62 and -17.46 respectively ($R^2 = 0.96$). Isotopic composition in higher soil depths (>10 cm) plot close to the GMWL, with decreasing soil depths points deviate from it increasingly.

Isotopic composition in ambient air fluctuated over the course of the experiment and showed no obvious trend over time (compare figure 4.2). The point cloud that scattered more randomly in the dual isotope space compared to soil measurements plots around the extension of the linear regression through soil measurements to the other side of the GMWL. The linear regression through all data points in the ambient air has a slope and intercept of 3.31 and -38.08, respectively. Its R^2 of 0.14 is lower compared to soil meausrements.

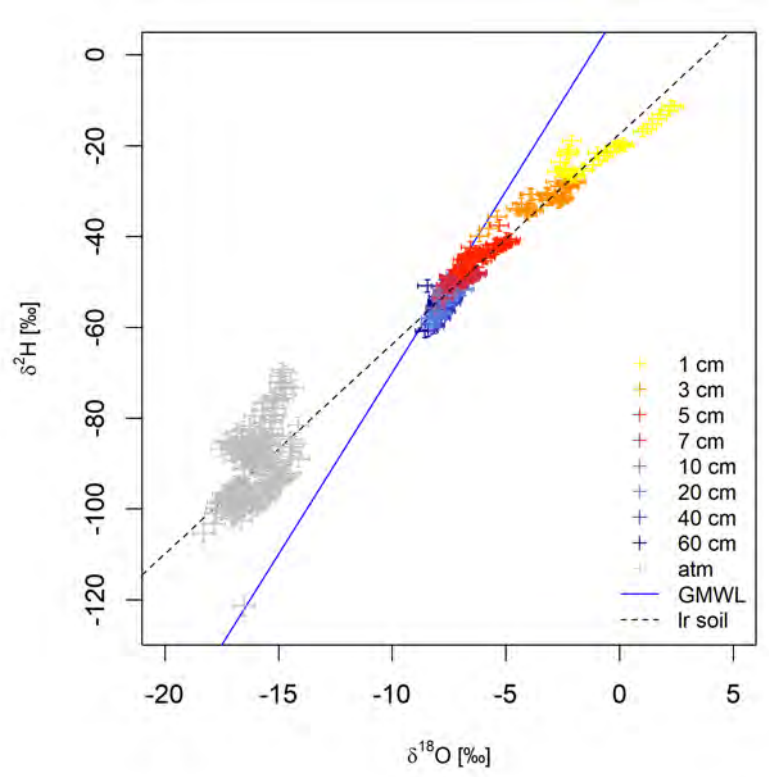

Figure 4.5: Dual isotope plot for days 11 until 72 of bare soil evaporation and ambient air (atm). The crosses mark the standard deviation of measurements calculated with the error propagation approach. Also shown is the linear regression line through all soil measurements (dashed line) and the GMWL (blue line) as reference.

Visually soil measurements were grouped according to soil depth and evolution of isotopic composition. The parameters (slope and intercept) of the resulting regressions as well as their coefficients of determination are summarized in table 4.2.

Table 4.2: Slopes, intercepts and coefficients of determination for linear regressions calculated for soil measurements divided in groups.

soil depth [cm]	slope	intercept	R^2
all depths	4.62	-17.46	0.96
60, 40, 20, 10	6.58	-3.41	0.74
7, 5	3.82	-21.46	0.76
3, 1	3.39	-19.86	0.88

The highest slope and intercept is found for the regression through soil depths from 60 cm to and including 10 cm. The observed slope is still lower compared to that of the GMWL. The deviance from the ratio in equilibrium fractionation factors calculated for the mean lab temperature (8.68 for 20.1 $°C$) is even higher. The slopes for soil depths above 10 cm are increasingly lower with decreasing soil depths. For measurements in 7 and 5 cm as well as in 3 and 1 cm the intercept is also significantly lower.

4.3 Section 2: Plant chamber and soil profiles

4.3.1 Standard measurements and soil temperature

From 14.02.2018 until 28.03.2018 isotopic composition was measured both in the soil profile and plant transpiration. During these six weeks the isotopic composition of standards was more stable and no systematic jumps, resulting in inexplicable shifts in the isotopic soil profiles, were observed. Therefore standardization in this section was carried out as planned and described in chapter 3.6.2. Figure 4.6 shows the timelines of mean and *sd* in both isotopes for all standard data points used in data processing. Temperatures measured inside the insulated standard box and used for calculation of liquid isotopic compositions with equilibrium fractionation are provided as well.

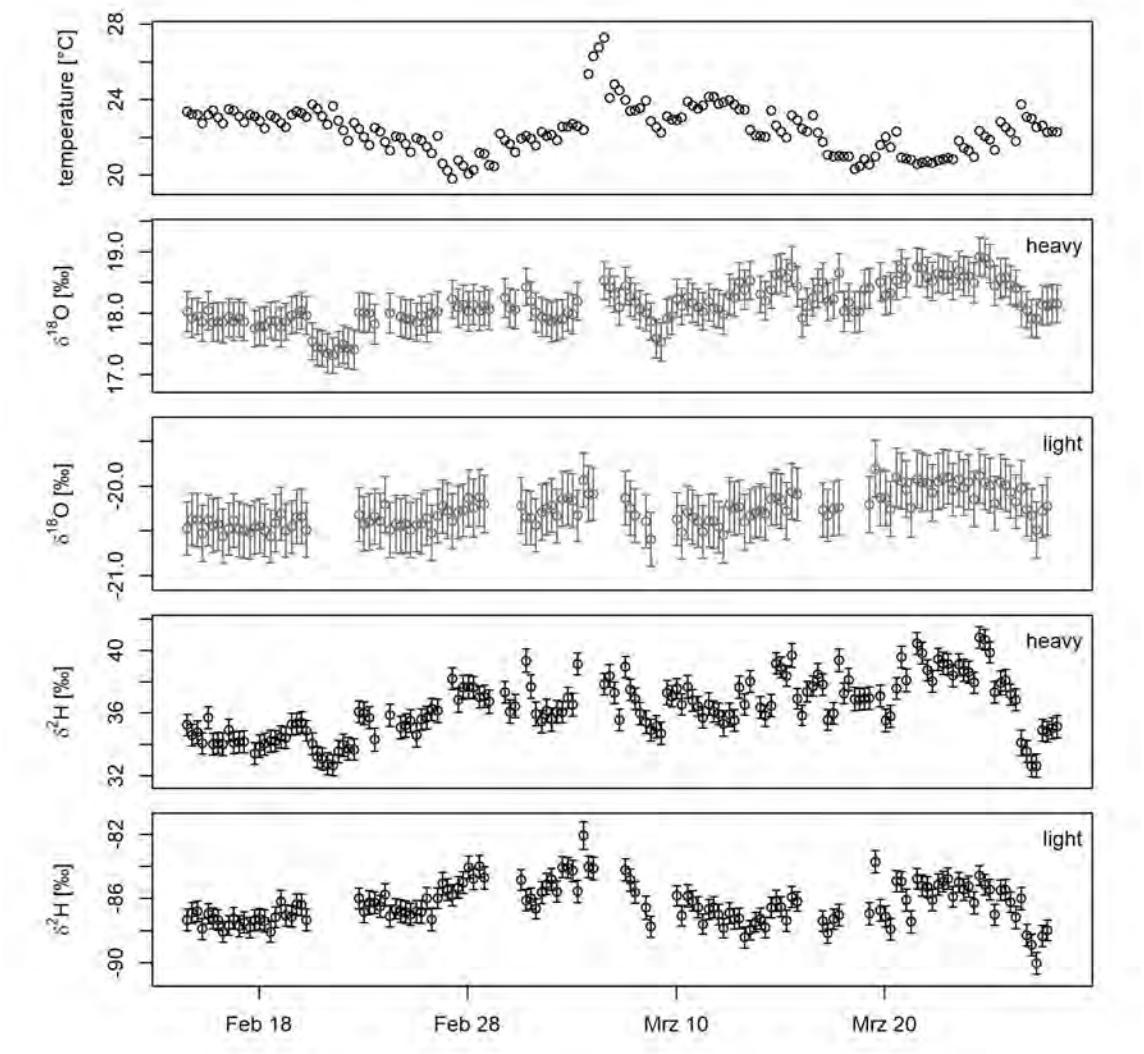

Figure 4.6: Timeline of processed and sorted measurements for St_{light} and St_{heavy} and the temperature measured in the insulated standard box. Isotopic compositions are reported as mean values with their respective standard deviations.

There is no apparent drift in standard isotopic composition. Also no relationship between any of the processed isotope ratios and the measured temperature was observed. This implies that the temperature dependency of equilibrium fractionation between liquid and vapor phase was accounted for by data processing.

Table 4.3 provides statistics for both standards over all measurements included in data processing. The mean values for section 1 were similar but slightly lighter than those calculated for section 2. However, all values except $\delta^{18}O$ for St_{Light} lie inside the range of standard values in section 2.

Table 4.3: Statistics for standard measurements used for calibration of all measurements in section 2.

		min	max	mean	sd
St_{light}	$\delta^{18}O$	-20.59	-19.81	-20.27	0.18
	$\delta^{2}H$	-90.05	-82.09	-86.34	1.26
St_{heavy}	$\delta^{18}O$	17.31	18.92	18.13	0.34
	$\delta^{2}H$	32.62	40.82	36.36	1.84

Soil temperature had a higher diurnal variation during section 2 compared to section 1 and also fluctuated more than the ambient temperature, due to the light cycle of installed LED lamps. As expected, the diurnal cycle was more pronounced in upper soil compartments, with daily differences of up to $4\,°C$ in 3 cm depth. At lower soil compartments recorded temperatures were lower overall and had a diurnal amplitude of $1-2\,°C$ in 60 cm depth. Timelines of ambient air and soil temperatures in column I are displayed in figure A.3 in appendix A.6.

4.3.2 Soil profiles

Because water either enriched or depleted in the heavier isotopes was added to the column in section 2, the soil water isotopic composition changed to a larger extent and in the entire profile. Figure 4.7 displays soil profiles of $\delta^{18}O$ and $\delta^{2}H$ next to soil moisture profiles in daily resolution. For better clarity and to avoid overlapping of profiles, data was divided into three different sub-sections, each indicating the start of additional water being added to the system.

In the first six days, soil water $\delta^{18}O$ and $\delta^{2}H$ profiles remained stable. A systematic decrease in heavy isotopes is only observed in 1 cm soil depth for $\delta^{18}O$. The profiles exhibit an exponential shape and are more enriched in the top compared to section 1, due to preceding irrigation with enriched water. The isotopic compositions for depths below and including 20 cm were not distinguishable and represent the composition of

water used for column saturation three months ago.

To make the three bottom depths distinguishable and maintain a monotonic profile over the whole column depth, the bottom of the column was saturated with depleted water on the first four days in section b). On the first day, 2 h after the start of the saturation, $\delta^{18}O$ only slightly decreased in 60 cm depth, while $\delta^{2}H$ featured no observable change, whereas soil moisture had already increased by 10 %. On the second day the bottom of the soil column was fully saturated again and isotopic composition was close to that of saturation water. A clear systematic increase in $\delta^{18}O$ and $\delta^{2}H$ at the column bottom could be observed two weeks after saturation from DoE 20 onwards. Before that, mean $\delta^{18}O$ and $\delta^{2}H$ in 60 cm depth were somewhat lighter than the water added with -18.58 ± 0.15 and -72.28 ± 1.04, respectively.

An increase in soil moisture was only observed in 60 and 40 cm depth and decreased fast during the first days after saturation, especially in 60 cm depth. Apart from the highest depth, the whole isotope profile shifted towards lighter values in reaction to saturation from the bottom in the four weeks of section b). Isotopic composition in 1 cm depth decreased faster than in 3 cm especially for $\delta^{2}H$ with decreasing soil moisture. This results in depth 3 cm featuring the highest isotopic composition in both isotopes from DoE 18 onwards.

It should be noted that the linear interpolation between depths 40 and 60 cm is presumably not representive of the shape of the isotopic course between those depths, at least at the first days after saturation as will be discussed in chapter 5.3. For better visualization of the evoluation of the isotopic composition in both depth the connecting line was plotted nevertheless.

In the first four days during section c) 150 ml of enriched water were added from the top each day. In 1 cm depth the isotopic composition only increased slightly on the first day and kept increasing systematically along with volumetric soil moisture content during the irrigation period. After irrigation was stopped, a systematic increase with lower extent could still be observed for $\delta^{18}O$ in depth 1 cm. Depth 20 cm also increased during irrigation, while it remained constant afterwards. All depths between 1 and 20 cm in contrast showed a more evenly spaced increase from the first day in section c) until the end of the experiment.

Overall, the treatments led to soil profiles that are monotonic and exhibit distinguishable isotopic compositions for every depth spanning a range from -16.32 ‰ to 13.98 ‰ for $\delta^{18}O$ and -64.53 ‰ to 31.65 ‰ for $\delta^{2}H$.

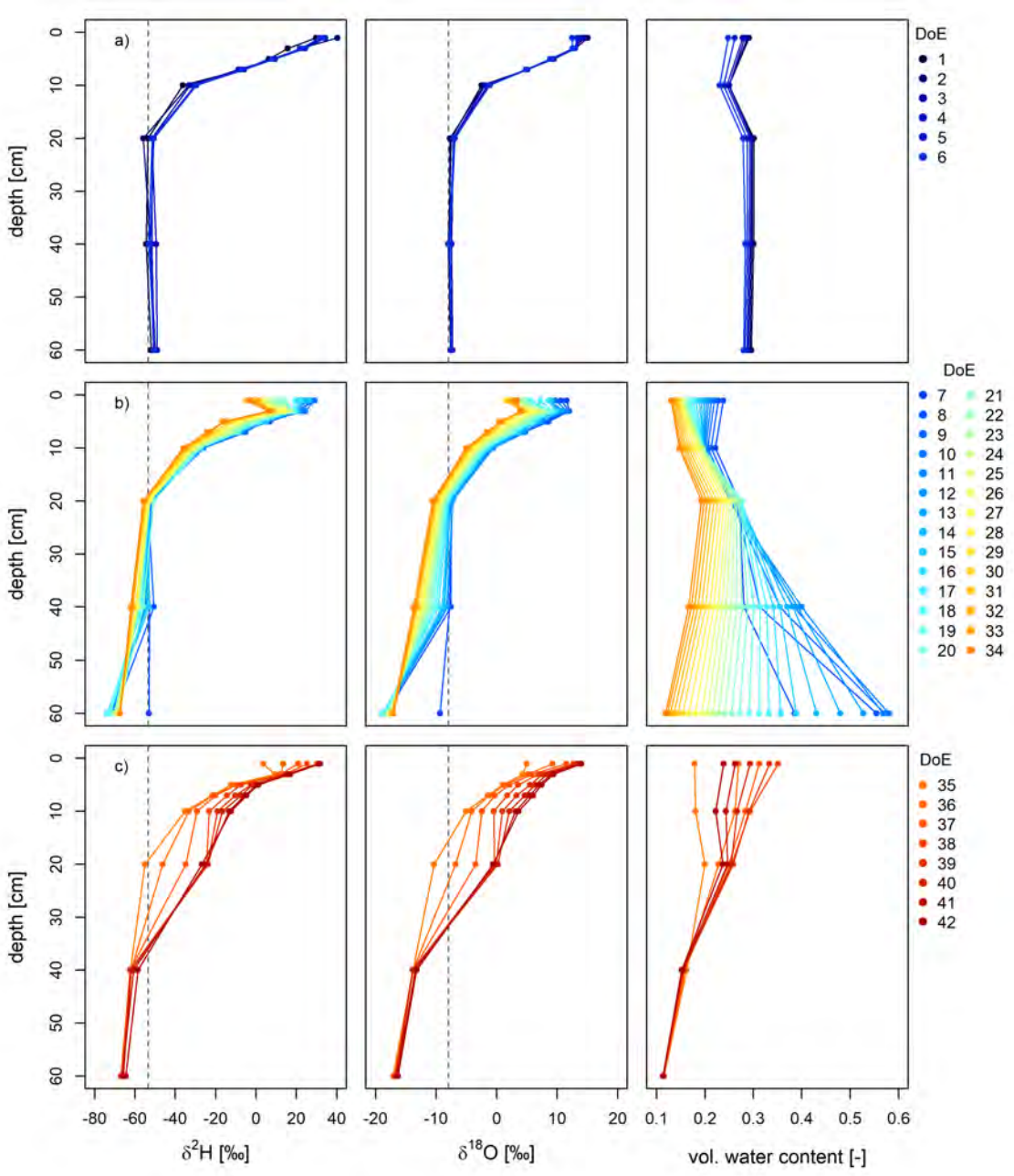

Figure 4.7: Soil isotopic composition and moisture content as profiles over depth and time. The timeseries was divided into sections a), b) and c) that each indicate addition of isotopically distinct waters.

4.3.3 Movement of event water in soil profiles

To gain a better understanding of the subsequent distribution of water added to the soil profile, fractions of the event water in seperate soil depths were calculated using the isotopic composition of irrigation water and pre-event water (see chapter 3.6.3). Because soil moisture contents change with water transport, those fractions are visualized in relation to the volumetric soil moisture content in a specific depth.

Figure 4.8 shows the event water fractions along the soil profile for the day before (DoE 6) and for selected days after saturation from the bottom. In 60 cm depth all pre-event water was replaced by event water on the second day of water addition, accompanied by a pronounced increase in Θ, while event water was not found in the soil depth above, even though Θ already increased slightly by 3.3 % vol. Soil moisture content in 40 cm depth was highest after the last day of saturation with a value of 40.0 % vol. In contrast to the increase in soil moisture by 12 % as compared to before the event, event water only accounted for 2 %vol at that time, corresponding to 5 % of water contained in that depth. The share of event water increased in all depths apart 60 cm until the end of section b) and along with soil water was distributed more evenly across the profile in the end. Fractions of soil water ranged from 90 % in 60 cm depth to 20 % in 10 cm depth.

Differences in event fractions calculated separately for δ^2H and $\delta^{18}O$ were constantly higher than 10 % in 3 cm depth from DoE 22 onwards. This suggests, that other processes than the redistribution of water from further down in the profile due to water potential gradients is causing the increase of heavy isotopes in this depth.

The calculation of event fractions was also carried out for section c), using the isotopic compositions on the day before reirrigation (DoE 34) as baseline. Due to the shorter time frame and faster change in isotope ratios all subsequent days are displayed in figure 4.9. Because the initial values in 3 cm depth were similar to irrigation water, event fractions could not be resolved in this depth and are therefore not displayed. On the first day of reirrigation soil water in 1 cm depth consisted of around 50 % event water, in 2 cm depth only 9 % were found and the share decreased further with soil depth. From DoE 36, with additional water added, soil water in 1 cm depth was fully composed of event water. While during the irrigation period the share of event water was higher in 20 cm depth compared to 5, 7 and 10 cm, this balanced out in the proceeding days, resulting again in a profile with rather equally distributed soil moisture content and share in event water. In that occasion this was only seen for the soil compartments above 40 cm, which were impacted by the irrigation event.

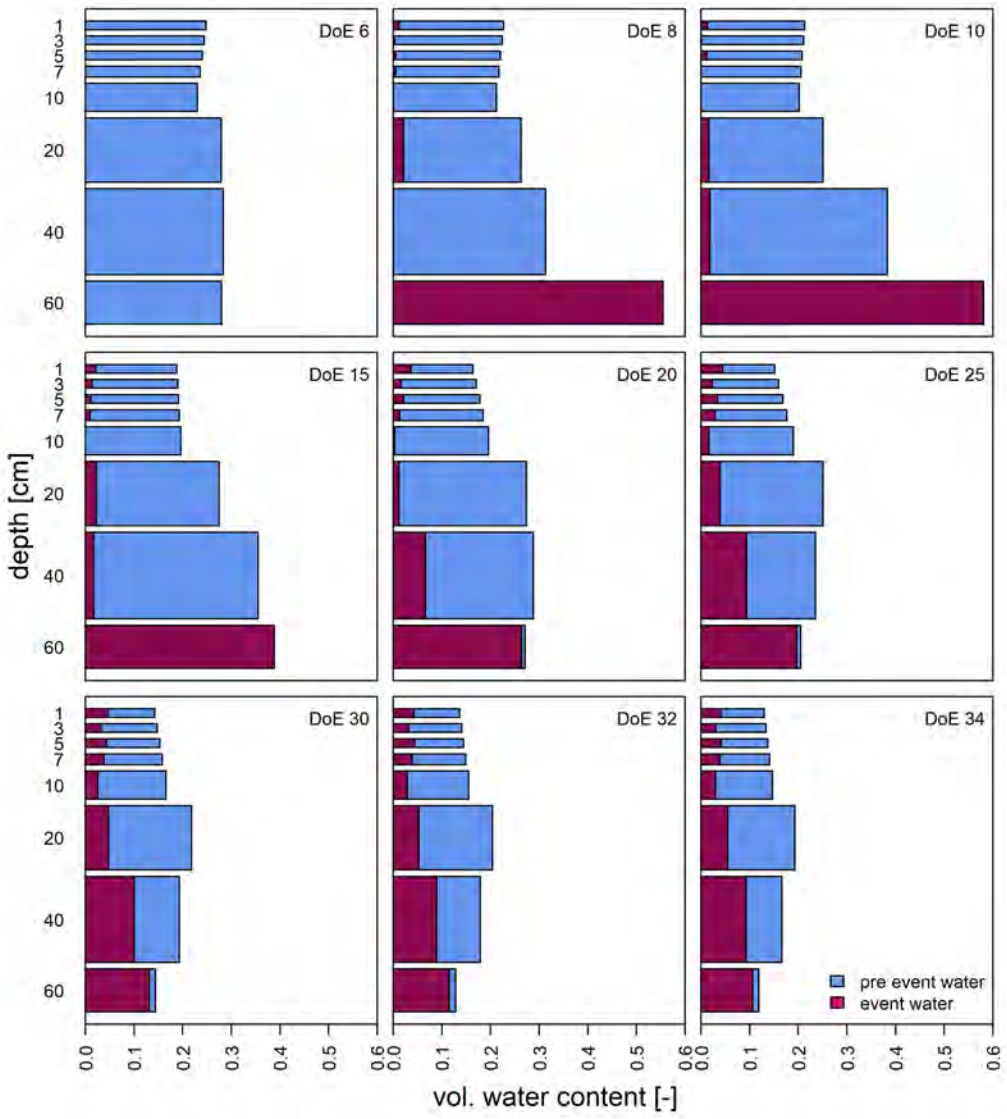

Figure 4.8: Fraction of soil water from pre-event and event water in different soil depths for event b) (saturation from bottom on DoE 7-10). For the display, eight out of the 28 days were selected.

Soil moisture in 40 and 60 cm depth decreased slightly during all days while no isotopic trace of event water was detected in these depth. Therefore infiltration of event water did not reach below 40 cm. From DoE 40 onwards the decrease in soil moisture in 40 cm depth and under was lower by one to two orders of magnitude, compared to soil layers down to 10 cm.

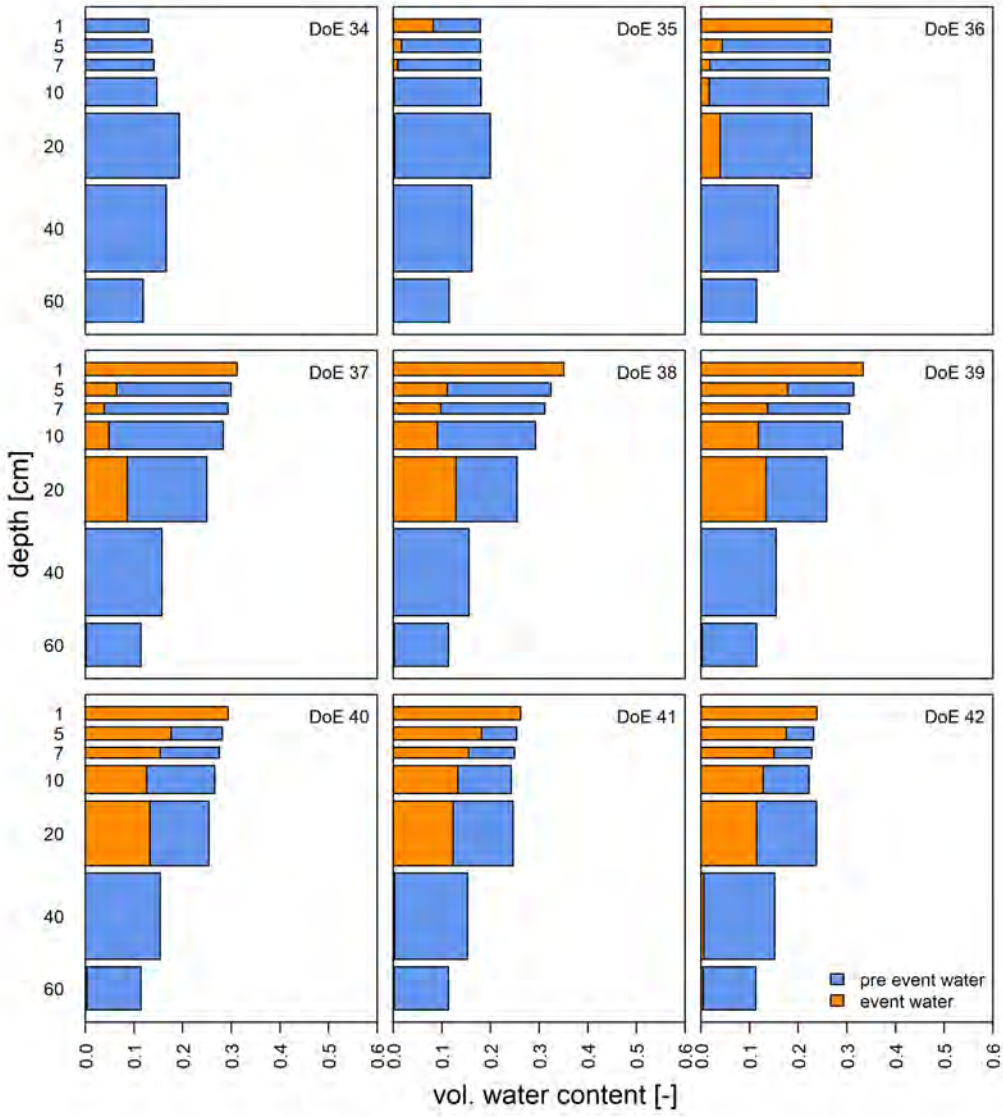

Figure 4.9: Fractions of soil water from pre-event and event water in different soil depths for event c) (irrigation from the top on DoE 35-38).

4.3.4 Plant chamber

Figure 4.10 shows *vpd*, transpiration rate normalized to the surface area of the soil column, and isotopic composition in transpiration. Also provided is the value of flow rate into the chamber, as it affects the ambient conditions inside the chamber. From DoE 18 until 22, all transpiration measurements had to be discarded due to condensation in the tubing, that connected the plant chamber with the measuring device. As a result, plateaus were not stable and data points did not plot on top of soil measurements in the dual isotope space.

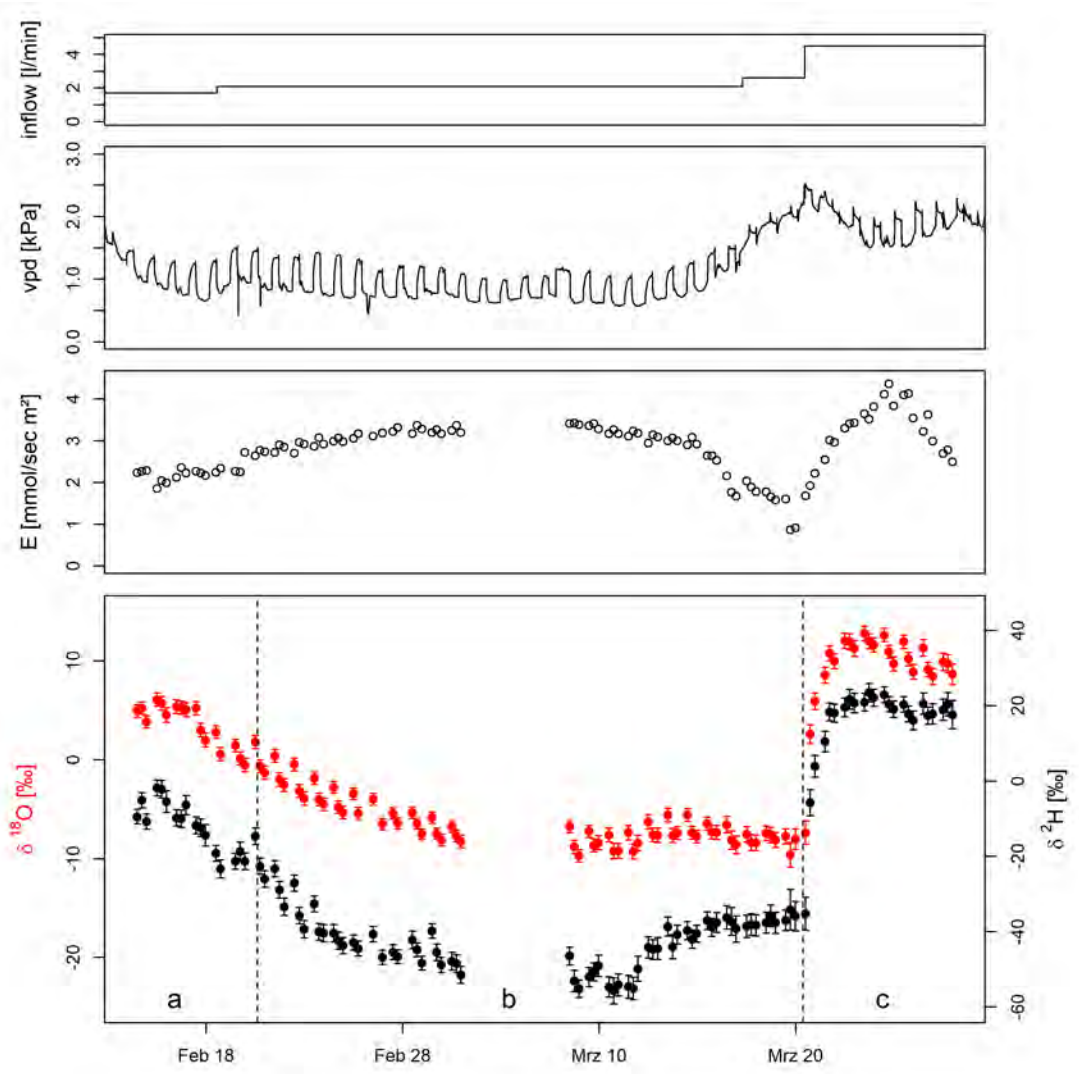

Figure 4.10: Timeline of the isotopic composition in transpiration as mean values with standard deviations. Also provided is a timeline of the transpiration rate, the air flux into and the *vpd* inside the chamber, calculated from the sensor measuring rh and T. Dashed lines indicate times when new water was added.

The *vpd* followed a clear diurnal pattern while on average it remained constant until DoE 30. Each day, when lights were switched on, it increased fast despite the increase in temperature of up to 4 °C, which is associated with a sharp increase in rh from 50 to 60 % to values of 75 to 80 %. Daily maximum values of rh measured in the plant chamber already slightly decreased on DoE 27 but experienced a sharp decline after DoE 29 resulting in an increasingly higher *vpd*. The lowest daily maximum of 32 % was measured on the first day of irrigation from the top (DoE 35), one day after the inflow into the chamber was almost doubled. This was followed by an increase of rh to values around 55 % on DoE 37-39 with a repeated decline afterwards.

Until DoE 17 the transpiration rate increased consistently and decreased from DoE 23 up to the last day before reirrigation from the top, when it showed the lowest value of 0.87 $mmol\,sec^{-1}\,m^{-2}$ in the afternoon. From DoE 35 onwards a faster increase than before is observed with the overall highest value of 4.36 $mmol\,sec^{-1}\,m^{-2}$ measured on DoE 39 one day after the last water input.

To validate the calculated transpiration rate, it was integrated for each day and compared to daily water loss from the column calculated by means of a water balance using the change in volumetric soil moisture content. Results for all days during section 2 that were not influenced by water addition to the column is shown in figure A.5 in appendix A.8.

Similar to the course of E, isotopic composition in plant transpiration changed gradually towards heavier compositions after the first irrigation from the top and stayed more or less stable in $\delta^{18}O$ and increased slightly in $\delta^{2}H$ after DoE 23 until the beginning of section c). The extent of calculated standard deviations is linked to the differences in the *wvmr* between inflow and outflow. Values were highest with 1.23 for $\delta^{18}O$ and 5.35 for $\delta^{2}H$ in the afternoon on DoE 34, when the difference in *wvmr* was only 4300 ppmv. Like the transpiration rate the isotopic composition of plant transpiration showed a fast reaction to the irrigation. The first significantly higher value was registered in the afternoon on DoE 35, but the most enriched values in isotopic composition are reached faster, as compared to the transpiration rates. At the time when the transpiration rate reached its maximum isotopic composition already started to decrease again. Overall, transpiration measurements are found in a range from -9.73 to 12.77 and -55.75 to 23.42 in $\delta^{18}O$ and $\delta^{2}H$, respectively.

For most days during the experiment the first transpiration measurement, 2.5 h after lights were switched on, showed systematically and significantly higher values compared to measurements later in the day, which were mostly not statistically distinct. On DoE 9 the range of diurnal differences was highest with 3.43 ‰ and 12.20 ‰ in

$\delta^{18}O$ and $\delta^{2}H$, respectively. On average transpiration isotopic composition during one day varied by 1.97 ‰ and 4.39 ‰. Figure A.6 in appendix A.9 provides exemplary plots of the diurnal variation in *rh* and *vpd*, also showing the time points of plant chamber measurements, to investigate potential connections of ambient conditions with transpiration measurements. Selected was Doe 9 with the highest diurnal variation in transpiration isotopic composition and DoE 33 with a comparably small deviance over the day. Diurnal variations are discussed in chapter 5.4

4.3.5 Comparison of soil and transpiration data in the dual isotope space

Visualizing both isotopic composition in the soil profile and plant transpiration allows for an investigation of the water pools sampled in both systems. It was also used to reveal possible problems, like for instance condensation or incomplete mixing of plant chamber air. Figure 4.11 shows both data sets in the dual isotope space divided in the sections a), b) and c) that are defined by new water input into the system. In contrast to the display of soil profiles, section b) was further split into data before and after the data gap due to the large number of points in this section. Section b1 therefore represents data points during a period when isotopic composition in transpiration showed a steady decrease, b2 includes measurements for which transpiration ratios remained stable and increased again. Each data point is displayed as the associated *sd* calculated by means of error propagation. Mean values for *sd* in transpiration and soil measurements for the different steps of data processing are displayed in table 4.4. Every plot provides the GMWL for comparison as well as linear regressions through all soil data points and transpiration measurements. Table 4.5 summarizes the parameters and coefficients of variation for the linear regression through soil and transpiration data.

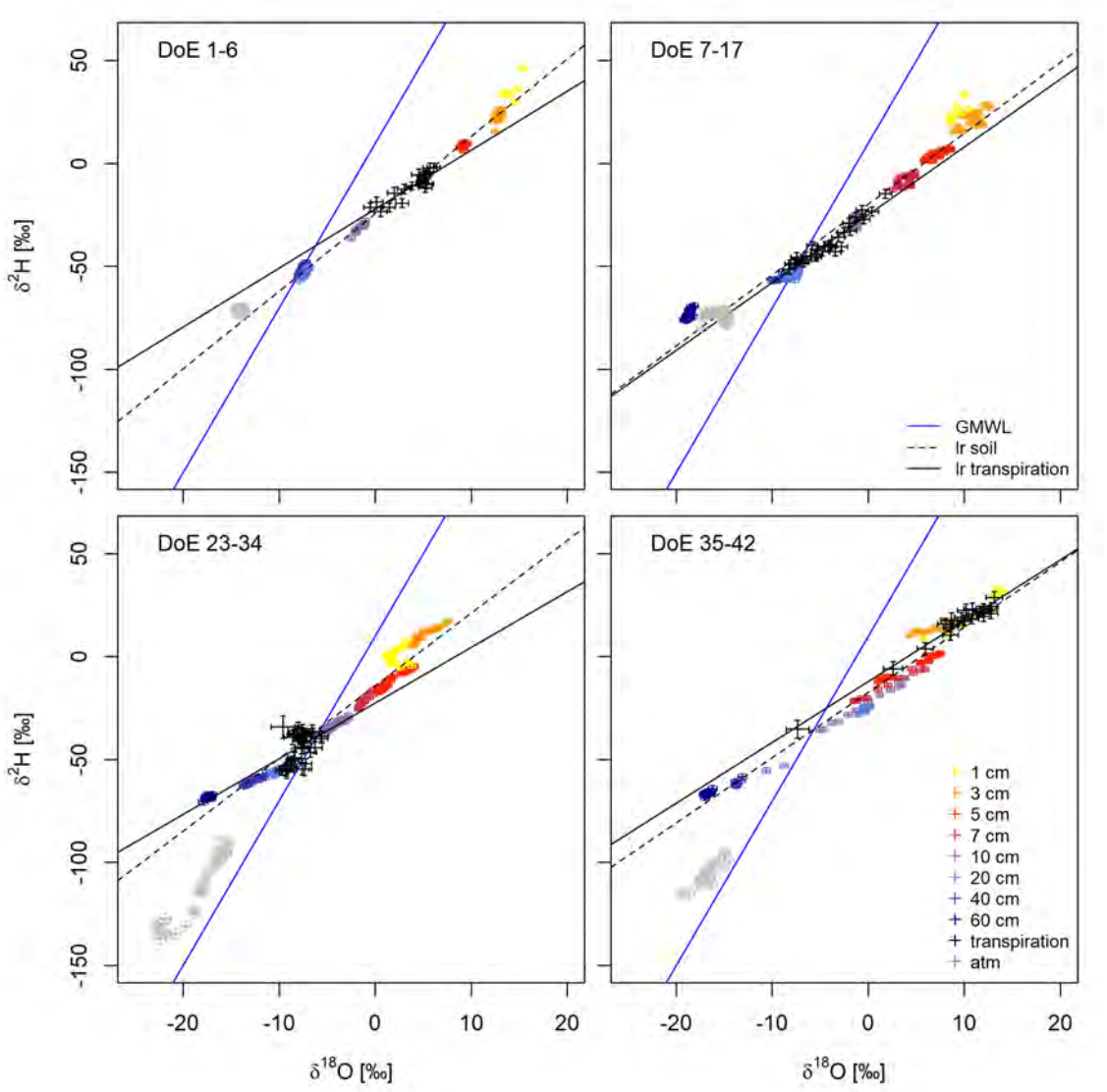

Figure 4.11: Isotopic composition of soil profiles and transpiration in the dual isotope space. For better clarity, the data set of section 2 is divided into the different stages, when water was added to the column. Because section b) is rather long, it was further divided into two parts. Crosses show the respective *sd* for data points. Dashed lines show the linear regression through all soil depths, solid lines show linear regressions through transpiration data. The GMWL is also displayed as blue solid line.

Table 4.4: Averaged standard deviations for $\delta^{18}O$ and $\delta^{2}H$ in transpiration and soil measurements for the different steps of data processing, calculated by means of error propagation.

measurement	WS-CRDS	*wvmr* correction	vapor to liquid	standardization	transpiration
$\delta^{18}O$ soil	0.316		0.320	0.405	
$\delta^{2}H$ soil	0.652	0.653	0.738	1.227	
$\delta^{18}O$ transpiration	0.299			0.407	0.712
$\delta^{2}H$ transpiration	0.764	0.769		1.406	2.533

Despite the preceding irrigation with enriched water from the top, soil measurements of all depth still plot on one line. Compared to bare soil evaporation, values are spread across a wider range in both isotopes and the slope of the resulting linear regression is lower. During section 2 slopes of the linear regressions through soil measurements stayed similar with a consistently high R^2. However soil measurements are slightly less linearily correlated with water from other sources added to the bottom and the top of the column, as well as ambient air intrusion. This leads to the expansion of the one dimensional evaporation line into a narrow, two dimensional polygon.

Table 4.5: Slopes, intercepts and coefficient of determination for linear regressions calculated for soil and transpiration measurements in the dual isotope space. The time series was divided according to figure 4.11. Because transpiration plotted close to values in 1 and 3 cm depth during the last seven days of section 2, regressions were calculated separately.

DoE	data	slope	intercept	R^2
1 - 6	all soil depths	3.76	-24.42	0.99
1 - 6	transpiration	2.86	-22.20	0.79
7 - 17	all soil depths	3.44	-19.66	0.96
7 - 17	transpiration	3.30	-24.90	0.91
23 - 34	all soil depths	3.53	-14.13	0.96
23 - 34	transpiration	2.70	-22.52	0.12
35 - 42	all soil depths	3.17	-17.36	0.97
35 - 42	transpiration	2.96	-12.04	0.96
36 - 42	1 and 3 cm	2.25	-2.12	0.85
36 - 42	transpiration	2.07	-2.37	0.67

Transpiration isotopic composition of valid data points generally plots inside the area enclosed by soil measurements over the whole experiment. Like in soil measurements, the regression slopes for transpiration measurements are much lower than that of the GMWL. All calculated slopes are also lower than those for soil data. In the time frames of DoE 7-17 and 35-42 transpiration isotopic composition transitioned more compared to the other sections. The respective linear regressions in the dual isotope space are better determined ($R^2 > 90\,\%$). For those periods, slopes calculated for transpiration and soil measurements are very similar, only deviating from each other by about 0.2.

In the bottom right plot showing DoE 35-42, the three lighter measurements that are isolated from the point cloud, represent the first day of event c), highlighting the fast transition in the combination of water sources transpired by the plant. Because from DoE 36 onwards transpiration values plot close to those in 3 to 1 cm soil depth, linear regressions were calculated separately for this time period, for soil measurements only including the two uppermost depths (compare table 4.5). Even though R^2 was below 90 % for the two measurements, the resulting regression lines show both a similar slope and intercept.

Until DoE 17, data points of ambient air, like in section 1, are located close to the extension of the linear regression through all soil measurements. From DoE 23 onwards they show a lower composition in both isotoplogues and plot closer to the GMWL. This change in the isotopic composition of background air provided to the plant chamber in turn had no apparent effect on transpiration measurements.

4.4 Modeling root water uptake

Having shown that transpiration vapor can be led back to soil water, a statistical computation of RWU fractions from both data sets is possible. Due to uncertainty in the course of the diurnal variation in the isotopic composition of transpiration, a daily value for transpiration was calculated as mean between measurement two and three for each day. Because it was systematically heavier on most days, the first measurement was generally excluded from averaging. Plausible methodological and physiological reasons for the observed diurnal devaitions will be discussed in chapter 5.4.

For reasons of completeness, figure 4.12 displays computed diurnal variations in RWU profiles exemplary for DoE 9 and 33 that showed pronounced and small diurnal deviations, respectively. Because for those days, isotopic composition along the soil profile was stable, all three transpiration measurements were related to the same isotopic soil profile of the respective day. Additionally, ambient conditions in the plant chamber for these days are provided in figure A.6 in the appendix, as mentioned before. The differences in calculated transpiration values resulted in differing RWU profile on DoE 9, while profiles on DoE 33 are similar.

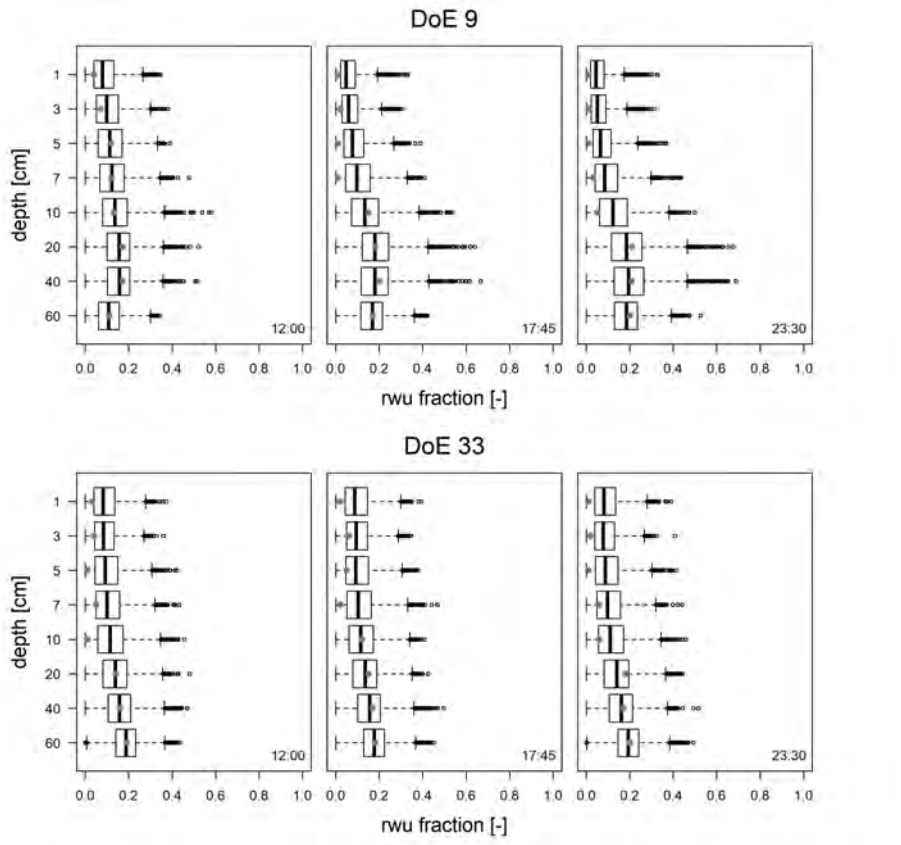

Figure 4.12: Exemplary display of diurnal variations of RWU profiles, separately calculated for all three transpiration measurements with the statistical mixing model SIAR on DoE 9 and 33. These days were selected, because they exhibited the highest and lowest deviation in isotopic composition of transpiration. The box and the line inside represent the interquartile range and the median of the data set, respectively. Whiskers extend to one and a half times of the box width. RWU fractions outside the whiskers range are displayed as separate points. Grey points indicate the mfv for each depth.

The results of statistical modeling are summarized in figure 4.13 as boxplots for selected days in section 2, showing an overview of differences in daily uptake profiles. Boxplots of RWU fractions for all days can be found in figure A.7 in appendix A.10. In general, mfv calculated on the basis of 1 % increments often plot close to the median of the respective depth and also show a similar depth profile.

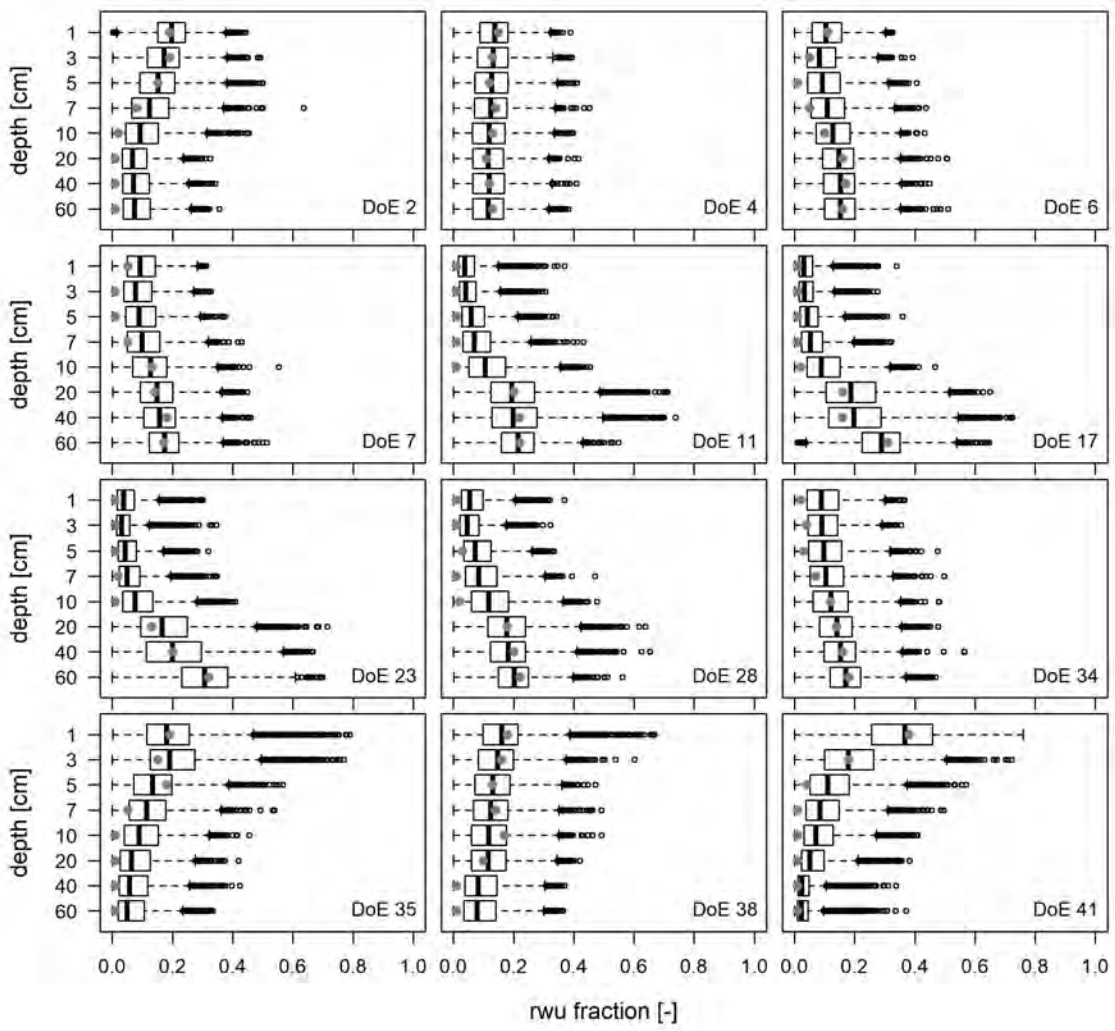

Figure 4.13: Boxplots of 10000 RWU fractions in the measured soil depths on selected days of section 2 calculated with the statistical mixing model SIAR. The box and the line inside represent the interquartile range and the median of the data set, respectively. Whiskers extend to one and a half times of the box width. RWU fractions outside the whiskers range are displayed as separate points. Grey points indicate the mfv for each depth.

Despite the wide range of possible contributing fractions in every depth, a clear pattern in the change of RWU along the soil profile can be observed. While from DoE 1 to 3 RWU profiles were similar, exhibiting higher uptake fractions with decreasing soil depths and mfv were close to 0 for 20 cm depth and below, it shifted towards a more equal contribution of all soil depths on the first day without irrigation. The share of deeper soil compartments (20 cm and below) increased the following days, especially during saturation of the column bottom from DoE 8 to 10. The pattern of augmented uptake from even higher depths first increased and then stabilized until DoE 26. From DoE 27 until 34 uptake fractions converged again, while higher uptake fractions still occured in lower depths.

Reirrigation from the top on DoE 35 immediately reversed the profile. From that day on mfv in 40 and 60 cm depth approximated 0 again. Uptake from 1 cm soil depth was especially high during the last three days, even though the soil moisture content was not considerably higher than in 3 to 20 cm depth.

To provide a better overview of the changes in the RWU profile over the course of the experiment, figure 4.14 (bottom) shows most frequent values over the soil profile in time. Therefore daily RWU profiles were interpolated in hourly time steps. For the depth profile, values were normalized to RWU fraction per cm, to account for differing volumes that the respective soil depth refers to, and thereafter linearly interpolated in a resolution of 1 cm. RWU is driven by the water potential gradient along the soil-atmosphere-continuum and a reaction in the isotopic composition of transpiration to changes in water availability in the profile were observed. Therefore figure 4.14 also shows volumetric soil moisture content and water potential, combining matric and gravitation potential. The data basis for this visualization are mean hourly values of Θ in depths 1, 10, 20, 40 and 60 cm also interpolated in 1 cm depth resolution. Matric potential was derived from the water retention curve (see figure 3.2) for every soil moisture value separately. The baseline for gravitation potential was defined as the column bottom, where it represents a value of 0 and becomes more positive with increasing column height, therefore resulting in less negative values of water potential.

The two color ramps divide water potential data into values below and above the peramenent wilting point (pwp) at a value of -15000 hPa (-1.5 MPa) translating into pF 4.2. Naturally volumetric soil moisture content and water potential follow the same pattern, because matric potential is derived from Θ and, compared to this component, gravitation potential is negligibly small. Nevertheless, the calculation of water potential and the visualization in water resources that are accessible or not accessible to plants should help to improve the interpretation of RWU patterns.

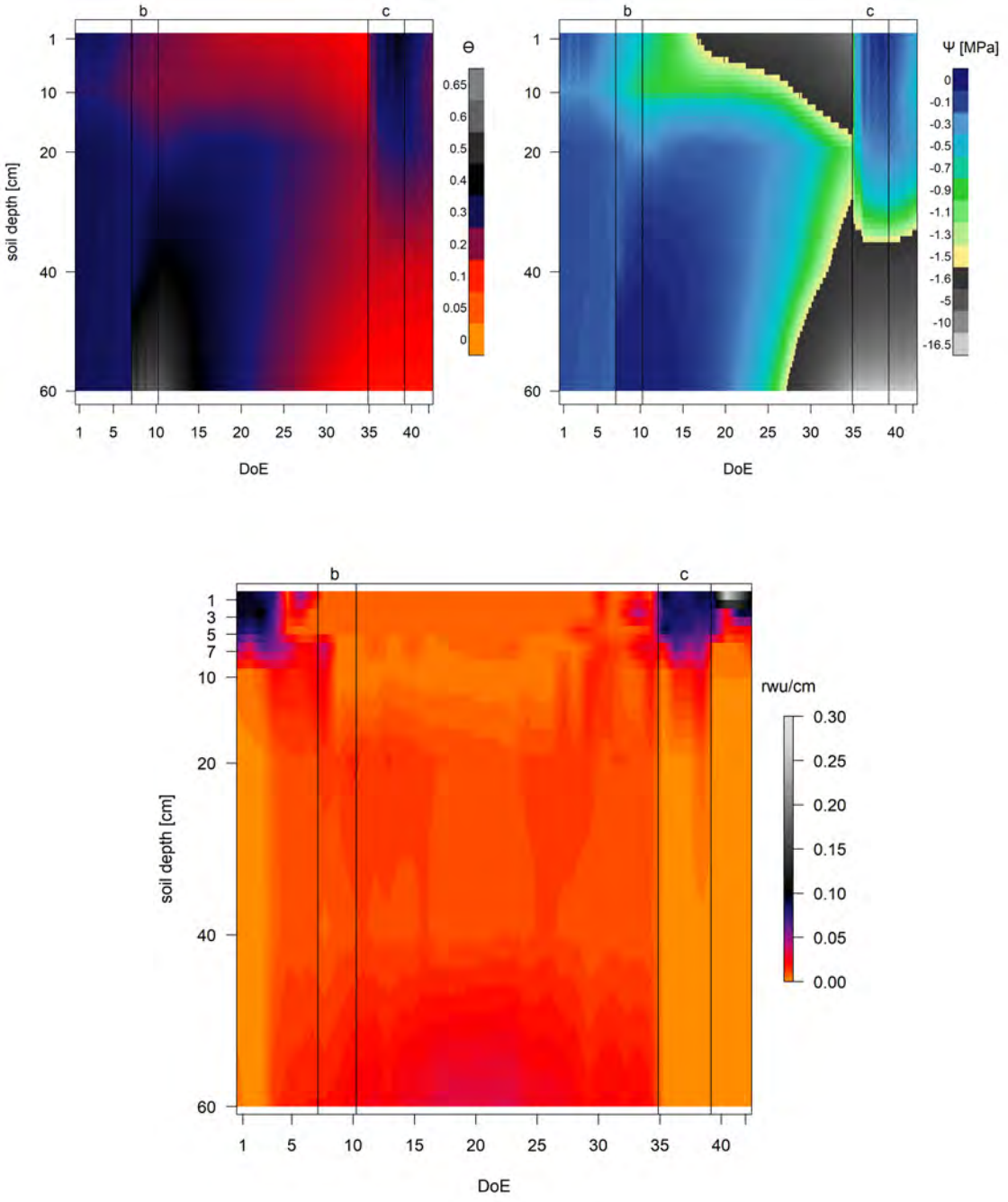

Figure 4.14: Evolution of volumetric soil moisture content (top left), water potential (top right) and most frequent RWU fractions (bottom) along the soil profile in hourly time resolution. $Mfvs$ were normalized to water uptake fraction per cm. The two color ramps in the water potential plot divide data into values below (grey) and above (colored) the pwp. Start- and endpoints of times when water was actively added from the bottom (b) and the top (c) are indicated by vertical lines.

It has to be noted that derived RWU fractions, i.e. the mfv, on particular days do not sum up to 1, i.e. 100 % over all depths. On average, most frequent values add up to 0.71 $\pm$ 0.09 and lie in the range of 0.48 to 1.03. From DoE 35 until the end of

the experiment sums varied more between days and also showed a decreasing trend. Mean values for days before and from DoE 35 are 0.72 ± 0.014 and 0.66 ± 0.049, respectively. As an exception, here the standard error is provided as a measure of variance due to varying sample sizes.

During the first days, with irrigation from the top, water potential was constantly high and evenly distributed across the profile, whereas RWU was concentrated in the top 7 cm. With saturation from the bottom and consequently higher water potentials with soil depth, RWU gradually shifted towards deeper compartments. From Doe 9 to 28 RWU from all depth in the top 10 cm never exceeded a value of 0.03 (value not normalized to 1 cm). Afterwards, RWU from those depths increaseed slightly especially in 10 cm depth until the beginning of event c), even though the water potential already dropped below -1.5 MPa. For 3 cm depth, for instance, a fraction of 0.09 was calculated with the statistical model on DoE 33. Water potential in the top soil was at its minimum of -8.7 MPa in 1 cm depth right before reirrigation.

In 60 cm depth values below -1.5 MPa were observed from DoE 28. The lowest overall value in water potential of -16.5 MPa was found on DoE 42 at the column bottom. Like in the upper soil, RWU was still calculated for higher depths until reirrigation from the top, when the fractions in 40 and 60 cm dropped to a constant value of 0.01. During the four days of reirrigation an initial fast change could be observed, shifting all modeled RWU to the top 7 cm. With further infiltration of water and a pronounced increase in soil moisture content up to 20 cm, also derived RWU expanded towards higher depths. On DoE 38 values of 0.10 and 0.17 were calculated for 20 and 10 cm, like depths below dropping to 0.01 again the day after and staying there until the end of the experiment.

5 Discussion

5.1 Evaluation of the in-situ measurement system

The goal of this study was to modify an existing setup for monitoring water stable isotope ratios in a soil profile (Rothfuss et al., 2015), in order to assess its suitability for RWU estimation in high time resolution. Therefore, the setup was tested with a natural soil, which had a high silt content. A plant was inserted into the column and a plant chamber and daylight bulbs were added to the setup. Potential effects of setup changes on measurements of the soil isotopic composition will be discussed in detail in the next chapter, followed by a critical investigation of transpiration measurements (see chapter 5.1.2) and a comparison of calculated measurement precision to other studies using direct equilibration methods as well as established water extraction techniques (see chapter 5.1.3). Finally, the tested method is evaluated with respect to advantages and limitations and in comparison to established water extraction methods using destructive sampling.

5.1.1 Soil measurements

During the entire experiment the polypropylene tubing remained water-proof and no traces for the influence of the natural soil, i.e. silting of tube micropores or isotopic fractionation by soil properties were observed. A thorough discussion of potential differences in sampled water pools follows in chapter 5.2.

Because the method samples isotopically depleted vapor, the question arises, whether the sampling technique systematically increases the isotopic composition of remaining soil water during a long-term experiment. Both standards that, compared to soil measurements, were exposed to a longer daily sampling time of 3 h, did not show an unidirectional increase in their isotopic composition. If water vapor extraction affected the remaining water pool, influences were extraneous compared to the fluctuation of measured vapor values, impacted by the lasers drift and also potential condensation problems. This is not surprising, as for standards the amount of liquid water extracted with the method is about $0.11\,ml\,day^{-1}$ and accumulates to as little as $14.5\,ml$ over the whole 19 weeks of the experiment.

Rothfuss et al. (2013) examined the time needed until the polypropylen material fully adjusted to an induced change in isotopic composition of pure liquid water. The authors showed that it took up to a few hours before stable values were reached again. This time lag was explained with old water contained in the micropores of

the polypropylene tubing that first had to be replaced by the isotopically new water mixture. Because the soil isotopic composition was only recorded in daily temporal resolution and the soil was also not saturated for most parts of the experiment, this reaction time was sufficient in the presented study. Only the missing instantaneous reaction in 60 cm depth on DoE 7, 2 h after saturation from the bottom, points towards the time lag issue.

Minor condensation that was observed during section 1 in the tubing right at the exit from the soil column should not have impacted the isotopic composition of measured soil depths, as long as temperatures in the column and at the condensation site are similar (equilibrium fractionation) and sample air equilibrates with condensation water. Because soil measurements seemed more reproducible with regular daily flushing of the outlet tubings in section 2, this assumption is only partially supported. Flushing in the applied manner did not have an obvious impact on the isotopic equilibrium between liquid and vapor phase. Therefore, it is concluded that the time difference of 4 h between flushing and the first soil measurement was sufficient in respect thereof. The presented experiment shows that condensation of sampled vapor potentially affects the precision and reliability of soil measurements and should hence be considered in future applications of the method. This is especially true for experiments with pronounced diurnal variations in temperatures, e.g. in the field, as problems with determining isotopic compositions increased when daylight bulbs were installed and daily flushing was not exerted yet (data not shown). An alternative solution could come from heating all sample lines, beginning at the outflow of each soil depth until the sample air inflow into the measurement device, or from including the possibility for purging with dry air in between measurements right after the column outlet.

5.1.2 Transpiration measurements

Due to air leakage from the plant chamber, there was a large difference in the air flux flowing into and out of the chamber. In combination with supposed gradients, e.g. of rh inside the chamber, thorough and instantaneous mixing is essential to obtain reliable transpiration measurements. Hereby the fans were indispensable, as a quick decline in $wvmr$ and measured isotopic ratios was observed immediately, when the fans were turned off.

A systematic offset of measured $wvmr$ from water vapor content calculated with rh and T measured inside the plant chamber could have arose from condensation due to the temperature drop between the plant chamber and the subsequent tubing. As

heating of the tubing from DoE 21 on did not solve this discrepancy, this does not provide a sole explanation. With lower transpiration rates, an increase in inflow and therefore overall lower values of rh inside the plant chamber, measured $wvmr$ matched calculated ones. Consequently, a possible explanation could also be a less pronounced chamber gradient due to a faster exchange of the chamber air and a more turbulent mixing in response to increased inflow. However, the resulting decrease in the difference between chamber air in- and outflow $wvmr$ values deteriorated the precision of measured isotopic compositions, especially when transpiration rates became limited by water supply. This illustrates that boundary conditions, in particular the amount of air flux, should be carefully chosen as a compromise between preventing condensation during the whole diurnal cycle, avoiding ambient air intrusion due to air leakage, resulting chamber conditions (especially rh and vpd), while also aspiring to maximize measurement precision. The utilization of calculated instead of directly measured $wvmr$ in computing transpiration isotopic composition resulted in a higher fraction of transpiration of the chamber outflow. It consequently shifted derived transpiration values towards more depleted compositions but only in the range of their standard deviation.

Uncertainties and systematic errors in the calculation of plant gas exchange fluxes with whole-plant chambers were investigated by Pérez-Priego et al. (2015). In contrast to chamber systems that only enclose plants during measurements, disturbance of ambient conditions and a following stabilization period must not be taken into account for the permanent installation, realized in the presented experiment. On the other hand, this entails the disadvantage that the chamber continuously alters boundary conditions driving plant transpiration, like stomatal conductance (Pérez-Priego et al., 2015) and therefore does not necessarily simulate natural conditions. In comparison to other plant individuals growing in the laboratory, for instance, the individual inside the chamber showed stronger branching, which might have been induced by the constant air movement it was exposed to.

5.1.3 Measurement precision

The error propagation approach allowed for the estimation of uncertainties along the steps of data processing. On average, final calculated values for transpiration measurements were 0.71 ‰ and 2.53 ‰ for $\delta^{18}O$ and $\delta^{2}H$, respectively. Values for soil measurements (0.40 ‰ and 1.23 ‰) were noticeably lower. This mostly emerged from the data processing step of calculating transpiration isotopic composition from chamber in- and outflows that almost doubled the sd for both isotopologues.

Certainly, it should be evaluated in the future, if the applied error propagation approach yields a realistic approximation of the measurement precision. Irrespective of this fact, calculated standard deviations are comparable with measurement precisions of other methods determining water stable isotopes in soil and plant material. For water contained in silty and clayey soils, extracted by means of cryogenic vacuum extraction, Koeniger et al. (2011) found standard deviations of up to 0.21 ‰ and 1.1 ‰ for $\delta^{18}O$ and $\delta^{2}H$, respectively. For plant samples they report deviations in the range of 0.45 - 0.63 ‰ in $\delta^{18}O$ and 1.5 - 4.7 ‰ in $\delta^{2}H$. Averaged over the two soil types and variable water contents tested, Orlowski et al. (2016a) reported values of 0.77 ‰ and 3.19 ‰ for the direct vapor equilibraion method in $\delta^{18}O$ and $\delta^{2}H$, respectively. For their in-situ method in soil profiles, Volkmann and Weiler (2014) report slightly higher *sds* of 0.22 ‰ and 1.6 ‰ for repeated in-soil measurements. For their in-situ measurement of transpiration in a chamber system, Volkmann et al. (2016a) state a general measurement precision of 2.5 ‰ for $\delta^{2}H$. In their experiment measuring isotopic composition in tree xylem in-situ, Volkmann et al. (2016b) calculated mean precisions of 0.33 ‰ and 2.8 ‰ for $\delta^{18}O$ and $\delta^{2}H$ respectively over the daily experimental periods of seven hours.

5.1.4 Methodological advantages and limitations

In contrast to traditional techniques that require water extraction prior to analysis, the tested method enables non-destructive in-situ measurements in both soil and transpiration. However, an investigation is only possible on the single-plant scale with the laboratory setup. The work input necessary for the initial installation is considerable and even though measurements are automated, continuous supervision and maintenance was necessary, in order to obtain reliable results. In comparison to cryogenic vacuum extraction that is accompanied by high capital and running costs (Orlowski et al., 2018), running expenses are manageable once the system is installed.

The high temporal resolution of processed data, together with the additional recorded parameters, facilitated the screening for invalid measurements and therefore increased confidence in the results. The combined assessment of variability in measurements between days and the course of measured raw values, i.e. stability of plateaus in *wvmr* and isotopic compositions, also proved to be helpful in this respect.

While the extent of the soil column constrains water movement in the soil column, which potentially hampers the transferability of obtained results to RWU under natural conditions, it also offers a unique possibility for testing RWU models under restricted and well-known boundary conditions. Additionally, horizontal heterogen-

ities are less pronounced than in natural systems and are accounted for, due to the length of the tubing across which sampling takes place. The method proved to yield plausible results even in natural soils with very low moisture contents, which can be a limiting factor in some methods using water extraction (see e.g. Orlowski et al. (2018, 2016a)). This was also concluded by Rothfuss et al. (2015) for standardized sand.

Laser-absorption instruments were shown to be sensitive towards organic contaminations of sampled water (West et al., 2010). Most likely, organic contaminations did not impact measurements in the presented experiment due to the sampling of transpired water as vapor and the soil material used. However, this potential error source has to be considered and, where necessary, be corrected in future applications. Post-processing software to correct for the impact of known concentrations in various organic compounds are already available (Schmidt et al., 2012). It should be further investigated, whether obtained correction functions are equally applicable to direct vapor sampling.

5.2 Water pools sampled

Together with the recovery of event water in the lowest and uppermost soil depth after event b) and c), the agreement between values of saturation water and measured in-situ, increases confidence in the method and also indicates that within measurement precision water pools in the soil column are well mixed. In contrast to Gaj et al. (2017); Orlowski et al. (2016a, 2016b) and Orlowski et al. (2013), who observed isotopic differences from spike water in samples with high clay and silt content, when using cryogenic vacuum extraction, a fractionation effect arising from soil texture was not observed in the presented experiment.

Partly for soil measurements the problem of isotopically different water pools due to soil properties and its effect on the sampled isotopic composition was circumvented by using a standard, which contained the same soil type at a similar bulk density. As for silty and clayey soils the fractionation in vapor equilibration techniques was shown to also depend on water content (Orlowski et al., 2018, 2016a; Meißner et al., 2014) and standards stayed close to saturation the whole time, a fractionation effect in processed data could still have been observable. This would support the proposed hypothesis that two distinct water pools supplying plant transpiration on one hand and stream and groundwater recharge on the other hand arise from istopically distinct soil water pools with different mobilities (McDonnell, 2014). At least for soil moisture contents between saturation and 28 % a fractionation effect was not observed and

initial saturation water was recovered in the bottom 40 cm until saturation with isotopically distinct water on DoE 7. Comparably, no isotopic difference in soil water due to a separation in mobile and immobile water was found by Sprenger et al. (2016) and McCutcheon et al. (2017). Sprenger et al. (2016) argue that a different isotopic signal in recharge arises from subsequent mixing of waters with soil depth. Therefore, the effect of evaporatively enriched water in the top soil diminishes with soil depth and isotopic differences do not originate from the fact that plants use an isotopically different, more tightly bound soil water source. A subsequent mixing of the isotopic signal of event water with longer travelling distance along the soil column was also observed in the presented experiment, supporting this theory.

Regardless of the uncertainty in the water pools investigated by the method and fractionation effects between these pools, the accordance between soil and transpiration isotopic compositions suggests that the applied soil method integrated water pools also available for root water uptake. This accordance was not only met in a well watered soil but also for low soil moisture contents, when most of the remaining water was presumably not available to the plant anymore, due to very negative matric potentials.

5.3 Isotopic evolution of soil profiles and water movement inside the column

Bare soil evaporation over 2.5 months continuously increased the magnitude of the exponentially shaped isotopic soil profile. The observed shape is typical and well-documented in the literature (see e.g. Barnes and Allison (1988); Rothfuss et al. (2015); Gangi et al. (2015)). In contrast to those studies, that found depleted compositions in the topsoil, most enriched water was found in the uppermost soil depth during the entire section 1. This can be attributed to the soil texture that was only partly composed of sand but dominated by the particle size silt. For a groundwater depth of 1 m below the soil surface Raes and Deproost (2003) report a capillary rise of 3 and 3.6 $mm\,day^{-1}$ for the soil type loam compared to 0.8 and 1.8 $mm\,day^{-1}$ for sand for bare soil and cropped soil, respectively. Therefore, compared to Rothfuss et al. (2015), the soil had a stronger ability for capillary rise and higher soil moisture contents were maintained until the end of section 1 (30 % in 1 cm depth). The subsequent delivery of water from lower soil compartments is also illustrated by the similar decline of soil moisture in all depths 11.5 months after complete saturation of the column. This is additionally supported by the fact that after 72 days, compared to Rothfuss et al. (2015) in the same time step, the heaviest isotopic compositions

measured were lower by approximately 12 ‰ and 23 ‰ for $\delta^{18}O$ and $\delta^{2}H$, respectively. Also evaporative enrichment at that point mostly affected the top 7 cm, while Rothfuss et al. (2015) observed a clear enrichment in 10 cm depth.

The before-mentioned decrease of $\delta^{18}O$ and $\delta^{2}H$ at the column top was however observed with lower Θ in section 2. It is the result of the movement of the evaporation front further into the soil and a following diffusion of depleted water vapor towards the surface (Barnes & Allison, 1988) and the simultaneous invasion of ambient water vapor (Rothfuss et al., 2015). Similar to Rothfuss et al. (2015), but in opposite order of investigated isotopes, water was not any more most enriched in 1 cm depth for $\delta^{18}O$ on DoE 6 ($\Theta_{1\,cm} = 24.8\,\%$) and with a time lag of 12 days on DoE 18 for $\delta^{2}H$ ($\Theta_{1\,cm} = 17.0\,\%$). In comparison to the above-mentioned experiment with sand, where this happened at $\Theta = 0.09$, the soil moisture content was still substantially higher.

Reported slopes for soil water were continuously lower than the slope of the GMWL both for all soil depths but also for regression lines calculated for grouped soil depths, indicating that evaporative enrichment had an impact on all of them. The slope for the bottom 50 cm, below the evaporation front, was also lower than 8 during section 1, even though no systematic increase in heavy isotopes was observed. This suggests an influence of the enrichment in the top centimeters by means of (back)diffusion. As expected, the slope is higher than for soil compartments above and due to a less pronounced movement along the evaporation line also not satisfactorily described by the linear regression. The value of 4.62 calculated for bare soil evaporation over all depths is well in the range reported in the literature (Gibson et al., 2008; Braud et al., 2005) and somewhat higher than the slope of 3.1 determined by Rothfuss et al. (2015) for the first 100 days of their experiment.

Irrigation with enriched water from the top further decreased the evaporation line slope that remained rather constant during section 2, despite the addition of other water sources in section b) and c). Regardless, event water had a pronounced isotopic influence on the soil profile. Especially the addition of depleted water from the bottom resulted in a clear shift towards lighter isotopic compositions in all soil depths. Backdiffusion and a consequential isotopic convergence was hereby clearly observed for 60 cm depth. In contrast reirrigation from the top only influenced the top 20 cm, even though induced water potential differences along the soil profile had a similar range for both events. One explanation comes from the overall higher water content and therefore larger share of less tightly bound water in section b). The only depth and time during section 2 when matric potential is above field capacity (-60 hPa) is found in 60 cm depth from the start (20.02.2018 15:00) until two days after saturation

from the bottom (25.02.2018 22:00).

There are two basic processes to explain water movement in soils in immediate reaction to event water that lead to different isotopic profiles: Either new water replaces existing soil water pushing it downwards or upwards (translatory flow) or event water movement happens preferentially along macropores, e.g. formed by decayed plant roots, therefore bypassing old soil water (Gazis & Feng, 2004). Partitioning soil water into pre-event and event water revealed that saturation from the bottom replaced all existing water in 60 cm depth by the second day of event b). Meanwhile Θ in 40 cm depth and to a smaller extent in 20 cm depth increased, while no isotopic trace of event water was found. This indicates that preexisting water is displaced by added water without considerable mixing. The sharp isotopic front that is associated with this process (Gazis & Feng, 2004) could not be observed due to the limited spatial resolution of isotopic measurements at the column bottom. This reinforces the before-mentioned uncertainty in the shape of the isotopic profile after event b) with a more or less pronounced step change being likely, at least for the days during and right after saturation from the bottom. However, capillary rise as a result of water potential differences and diffusion in consequence of concentration gradients smoothens the profile progressively afterwards.

Event c) partly refilled soil water resulting in a mixture of event and pre-event water on the first day of irrigation. In the same time, the increase in Θ in 5 cm depth is only partly explained by event water influence, indicating that also in this event old water is pushed down the soil profile. On DoE 36 the importance of this process becomes even more clear, with soil water at the column top being completely comprised of event water and a further increase in Θ in soil depths below, without an equivalent simultaneous increase in the event fraction shares. In contrast to event b), the greater increase in event fraction share in 20 cm soil depth on the second to fourth day of irrigation (DoE 36 - 38), as compared to 5, 7 and 10 cm depth, points towards a preferential flow component during water infiltration. This seems plausible with the planting of *Centaurea jacea* about 2 months before in mind, because the predrilled hole of 17 cm depth likely resulted in a more permeable soil volume that in addition featured soil compaction along its walls and especially at its bottom. Certainly following root growth weakened these differences in soil densities but still explains the infiltration pattern of event c).

Overall, the addition of depleted water in event b) fulfilled the initial goal of isotopically distinguishable soil depths, providing an important prerequisite for a more accurate and better resolved RWU modeling. Due to the isotopic depletion of soil water in 1 cm depth, as a result of interference with ambient air at low soil moisture

contents, the profile was not completely monotonic for a substantial period during section 2. Because of the high spatial resolution in the uppermost column centimeters this should have a rather small effect on the RWU estimation though. On the contrary, this process moved isotopic compositions in 1 and 3 cm away from the linear soil evaporation line, which is favorable for the modeling approach because information for both invested isotopologues is less redundant.

5.4 Transpiration

The setup allowed for observing significant changes in transpiration isotopic composition over a period of six weeks. Previous studies, which draw upon laser spectroscopy for combined measurements in transpiration and soil isotopic composition and derived at least transpiration composition in-situ (Piayda et al., 2017; Volkmann et al., 2016a), followed plant water uptake in response to heavily labelled irrigation pulses. In contrast, the presented experiment was conducted in a range that is close to plausible natural isotopic abundances. Therefore the method could potentially also be applied in laboratory and field experiments that aim at investigating natural conditions without the addition of labelled event water.

The change in transpiration isotopic composition arises from different simultaneous processes: A change of the composite isotopic signature of the complete soil water pool, growth and development of the plant root system (slow process) and variations in the root components that actively take part in momentary water uptake. The latter is influenced by both water potential differences between plant roots and their surrounding soil areas and (active) alterations in root hydraulic conductivity, e.g. by means of aquaporin activity.

For the gradual decrease in the share of heavy isotopes in transpiration from DoE 4 to DoE 23, the predominance of underlying causes is not resolvable. In this time period the isotopic composition in the soil column water pool decreased due to the event in section b), likely also depleting the water pool accessible to the plant. Because transpiration isotopic values started to decline immediately after irrigation was discontinued, while soil profiles did not undergo pronounced shifts, this does not serve as the only explanatory reason though. With reirrigation from the top, isotopically different water was added to the soil water pool another time, again altering transpiration in the same direction. Because of the magnitude and short time frame of the step change, in comparison to a steady increase in soil isotopic composition over the following days with irrigation, also with this event an exclusive change in source water can not explain the isotopic time course in transpiration. Because of the

short time frame, adjusted root system growth also plays a subordinate part. Implications from the change in transpiration isotopic composition and as just described also RWU depth on root development, root activity and water potential differences will be discussed in detail in chapter 5.5.

A closer look at the time course of the transpiration rate provides insight into ambient conditions limiting daytime RWU. Plant aboveground biomass still increased noticeably especially in the beginning of section 2, which typically also results in higher belowground biomass (Niklas, 2004) and therefore better access to soil water resources. However the transpiration rate only slightly increased in the time frame from DoE 1 to DoE 17. Together with the daily step increase in rh, which stayed on a constant level until lights were switched off, this indicates that transpiration is limited by the high rh and accordingly low vpd as a result of plant transpiration and the amount of inflow, which affected the time needed to exchange the complete chamber air volume.

The gradual decrease in transpiration rate with an increase in vpd from DoE 23, until water is added in event c), points towards water availability as the limiting factor for plant transpiration. This is supported by the fact that the transpiration rate further decreased, despite the second increase of the amount of chamber air inflow. The last and most pronounced increase in air influx clearly lowered maximum daily rh and consequently increased vpd. Subsequently, the transpiration rate was more impacted by available soil water and root water uptake rates, than vpd in the plant chamber.

The systematic enrichment of the first measurement each day, compared to the second and third measurement, could not explicitely be related to a diurnal variation in RWU, as observed for instance by Doussan et al. (2006). By means of light transmission imaging, the authors followed changes in soil moisture content in a rhizotron planted with *Lupinus angustifolius* and compared it to modeled values. Figure 5.1 shows their observed (top) and modeled values (bottom) for a tap-root system during the first hours of the experiment. Even though the images do not show root activity directly, they illustrate with the depletion in soil moisture content that water uptake was first concentrated near the plant base and within hours spread to more distant parts of the root system.

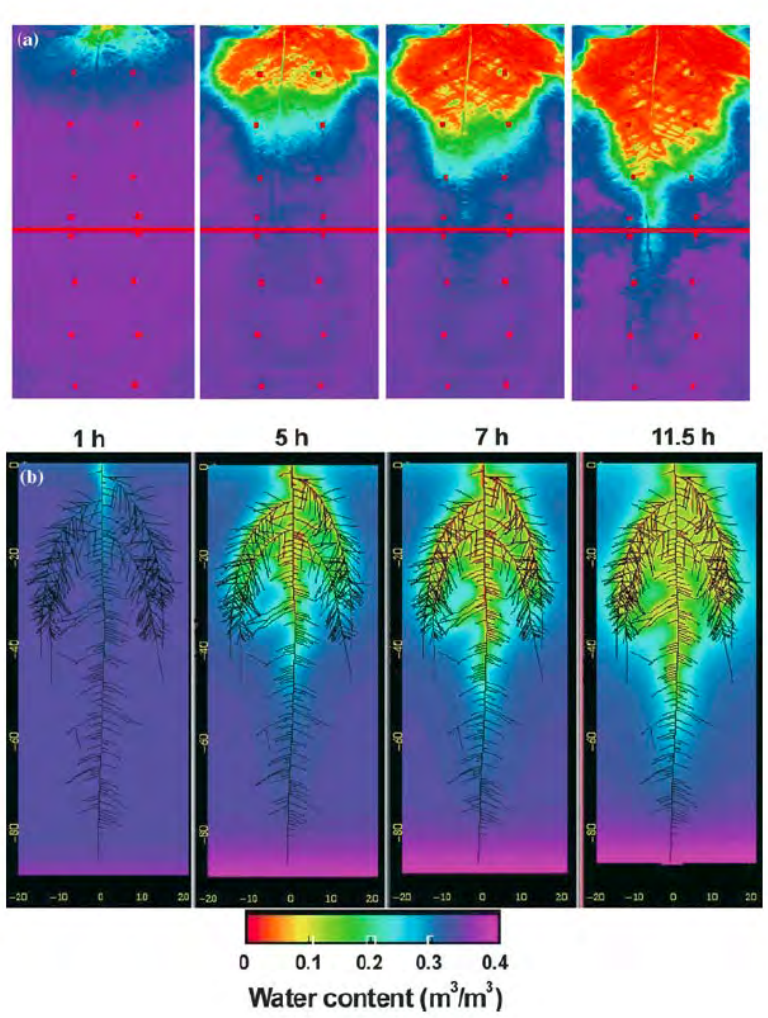

Figure 5.1: Images of short-term changes in observed and modelled soil moisture contents in a rhizotron containing *Lupinus angustifolius* with a taproot system (figure adopted from Doussan et al. (2006)).

Even though increased uptake from upper soil compartments due to higher soil moisture content and/or lower transpiration rates would also be a possible explanation in the presented experiment, enriched values can also be explained by a violation of the steady-state assumption. At first this seems contradictory to recent studies, which observed a depletion of transpiration isotopic composition as compared to steady-state values during the day (Dubbert et al., 2014, 2013; Lai et al., 2006). In these studies the underlying cause for the depletion was a decrease in rh during the day. In contrast to a typical diurnal cycle under field conditions, in the presented experiment, as a result of increased transpiration, rh was higher during the light period. However, 2.5 h after lights are switched on, ambient conditions in the plant chamber had usually reached a stable level.

Dubbert et al. (2017) investigated transpiration isotopic adjustment in reaction to a

decrease in rh from 60 % to 30 %, followed by an increase back to the initial value. While the decrease in rh resulted in a depletion of transpiration isotopic composition compared to source water, an increase in rh led to an immediate increase in the ratio of heavy oxygen isotopes and a subsequent return to source water isotopic compositions afterwards. Additionally, they observed pronounced differences between species. This observation is supported by the comparison of the diurnal course of rh and vpd in the plant chamber (compare figure A.4 in the appendix). For DoE 33 that featured a less pronounced and more gradual step change, compared to DoE 9, transpiration isotopic composition was rather stable. This also suggests that transpiration isotopic composition takes longer to return to steady-state values with a more pronounced change in ambient conditions. Nevertheless, the highest deviation in $\delta^{18}O$ was less than half compared to the increase observed by Dubbert et al. (2017) immediately after the rh step change. This can be explained with the less abrupt change in ambient conditions and the incorporated waiting time for plant adjustment. Additionally, in the dual isotope plot all valid transpiration measurements plot on the space enclosed by soil measurements, suggesting that transpiration was close to steady-state considering measurement precision.

5.5 Ecohydrological interpretation of observed differences in root water uptake

The observed daily shifts in soil isotope profiles demonstrated the importance of simultaneous high time resolution measurements in both soil profiles and transpiration for a reliable estimation of RWU within natural abundance levels. The ability to trace changes of both setup compartments offers an opportunity for a better separation of the potential influences on the time series of isotope ratios in transpiration. Both gradual and sudden changes in RWU could be observed with the new method. Ecohydrological explanations for and conclusions derived from observed changes of RWU profiles will be discussed hereafter.

With a consistently well-watered soil profile in the beginning of the experiment, the RWU profile showed an exponential shape. As water availability was not limiting, RWU likely reflected the root density profile (Draye et al., 2010). The uptake profile was therefore in line with the common perception of an exponential profile of root length densities in vertically homogeneous soils (Gregory, 2006).

It has been shown that plants often optimize their root growth to prevailing environmental conditions in order to maximize the utilization of available resources in space and time (Rothfuss & Javaux, 2017; Topp, 2016). This directional growth of the

root system, also known as root plasticity, could have been induced by the increasing difference of water availability along the soil column during section b) and provides a plausible explanation for the RWU profile gradually moving towards uptake from deeper soil compartments. It is also possible that root development had not reached a steady-state yet, when measurements were conducted and that a deeper penetration of the root system is not triggered by heterogeneously distributed water resources.

The shift in transpiration isotopic composition and the resulting predicted RWU from deeper soil compartments, where less tightly bound water was available, while a constant transpiration rate was maintained, strongly suggests the concept of compensated RWU. Šimůnek and Hopmans (2009) refer to multiple studies in the last 40 years that observed compensation of water stress in one part of the root zone by relocating the root water uptake to regions where water is less tightly bound. Therefore, the authors incorporated this compensation mechanism into their modeling approach by including a root-adaptability factor. In the presented experiment the transpiration demand could no longer be preserved by compensation, only when plant available water became scarce in larger soil compartments.

The simulated contribution of the column bottom to water uptake diminished again with a decrease in the transpiration rate. With regards to the very low water potentials both at the column top and bottom, this observation can be explained with the prevailing water potential profile. A pronounced decrease in the transpiration rate was only observed one day after water potential at the column bottom also fell below -1.5 MPa. In 1 cm depth the pwp had already been exceeded for 11 days. Before, given the prevailing ambient conditions, the plants water demand could still be met.

It has been shown that the pwp is a dynamic value, depending on soil properties and plant species. Especially drought adapted species are able to also withdraw water from soil compartments with water potentials lower than -1.5 MPa. The highly drought tolerant desert species *Larrea divaricata* for instance can absorb water at soil water potentials up to -6.0 MPa (Kirkham, 2014). Werner et al. (2002) measured seasonal variations of plant water potentials in ten dominant species in a mediterranean macchia ecosystem. For eight of those species, the most negative monthly means observed were around -7 to -8 MPa in September 1997. Minimal values of single measurements in this study were even as low as -12 MPa (M. Dubbert, personal communication, Mai 8, 2018). In a field study, conducted in Freiburg in 2017, a minimum plant water potential of -3.5 MPa was measured in July for the investigated plant species (M. Dubbert, personal communication, March 19, 2018). While it is obvious that the subsequent drying of soil reduced the transpiration rate, the plants minimum water requirements could thus be maintained to bridge dry periods.

The induced water stress, in addition, did not permanently damage the plant, e.g. through marked embolism of xylem vessels, as reirrigation immediately restored high transpiration rates.

Further uncertainty in determining the threshold value in matric potential for water, that is still available to the plant, arises from soil heterogenity especially due to different water storage properties of the rhizosphere as compared to the bulk soil. The mucilage exuded by root caps as well as air-filled gaps between roots and the soil are often used to explain observed heterogenities (Carminati & Vetterlein, 2012). Using neutron radiography, Carminati et al. (2010) observed water content heterogenities between bulk soil and the rhizosphere of a lupine. With subsequent drying, the rhizosphere stayed wetter compared to the bulk soil. After rewetting however, the rhizosphere showed signs of hydrophobicity. A time lag of 1 to 2 days was reported until the rhizosphere became wet again. Depending on the drying/wetting history of the soil, the rhizosphere can therefore either promote or constrict RWU. Carminati and Vetterlein (2012) termed this effect rhizosphere plasticity and argued to see it as a plant trait, to extenuate steep gradients in matric potentials. The authors suppose that this could be a plant strategy to facilitate RWU in parts of the root system and on the other hand disconnect roots from the soil, for example to avoid water flow from roots back to the dry soil. Additionally, the degree of rhizosphere variability was shown to be associated with root age and tends to facilitate water uptake in young root segments (Carminati, 2013).

In the presented experiment rhizosphere plasticity could provide an explanation for prolonged uptake in water limited soil compartments and also for the time lag in reaching the maximum transpiration rate. It could also have allowed for the relatively high RWU contribution predicted for the column bottom right before reirrigation, even though matric potential was as low as -12.6 MPa in 60 cm depth and also below the pwp at a value of -2.1 MPa in 40 cm depth.

Reirrigation from the top caused a fast increase in the share of heavy isotopes in transpiration compared to the rather slow shift before, which can not be associated with root system development. From the four days, when water was added in event c), the most pronounced shift, with almost all water uptake being predicted for the top 5 cm, took place on the first day, when irrigation water did not yet reach its maximum infiltration into the soil. After the irrigation event, modeled RWU from 1 and 3 cm depth was exceptionally high, even though soil water was plant available at least in the top 20 cm. Together with the fast change in transpiration rate and RWU, this could potentially illustrate a plant strategy to efficiently use as much of, for example short and intense summer rains, as possible, before it infiltrates below

the rooting depth and also generate a competitive advantage towards other species. The calculated negligible contribution of the bottom soil compartments after event c) is in line with the low decrease of Θ in these soil depths.

The statistical model proved to be a valuable tool to account for changes of the isotopic composition in both soil and transpiration data and visualize trends in RWU profiles that allowed for an ecohydrological explanation. However, it should be noted once more that the applied RWU model calculated uptake fractions for distinct depths in a wide range of possible combinations and without incorporating any ecohydrological knowledge. Even though the lineary δ^2H - $\delta^{18}O$ - bond was somewhat broken during the experiment, the change in isotopic composition with soil depth is still predominantely linear and well described by the fitted linear regression. For the statistical modeling approach this is suboptimal, in particular, when transpiration isotopic composition is located in the middle of all soil measurements. In this case multiple combinations of water taken up from different depths result in the observed transpiration composition. Because of the models pure statistic nature, counterintuitive combinations, i.e. where transpiration is a mixture of the uppermost and the lowest soil compartment, are treated as equally valid solutions for the mixing equation, marking some limits of this modeling approach.

6 Outlook

The data set collected during this experiment is unique in its duration and temporal resolution in both soil and transpiration isotopic composition, as well as in the available information on ambient conditions, like soil moisture content, soil and ambient temperature. A destructive sampling of the root length density in the depth of isotopic measurements will be carried out shortly. This provides missing information for a usage of the data set in complex, mechanistic RWU models that now more commonly also implement the modeling of isotopes. Multiple state-of-the-art models could on the one hand help with the interpretation of observed dynamics and on the other hand also benefit from the recorded data set. Models range from rather simple structures to modeling approaches incorporating 3D root systems, root development and the influence of highly resolved soil properties in space and time.

A minimalistic, implicit model that still implements information on root hydraulic architecture and heterogenities in soil water status, while featuring high computing speed, was developed by Couvreur et al. (2012). Especially, because the modeling approach allows for the decoupling of water stress and compensatory RWU, it could add valuable information on ecohydrological functioning and validate assumptions already proposed in the presented study. Additionally, the model incorporates soil water potential as sensed by the plant in soils with heterogeneous water availability.

R-SWMS (Root-Soil Water Movement and Solute Transport) was developed by Javaux et al. (2008) and is a detailed three-dimensionel model on the single-plant scale, based on water potential differences at the soil-root interface. Heterogenity in vertical and horizontal soil moisture content can be accounted for in the model as well as differing root hydraulic characteristics. Therefore, an explicit discrimination between distinct root types would be possible. The usage of the presented data set in the model could hence provide information on the development of the root system architecture, e.g. root type and age. In addition, results from modeling and MRI measurements, which are also possible with the setup, can be compared to evaluate different methodological approaches.

Other feasible approaches come from soil-vegetation-atmosphere transfer (SVAT) models. Sutanto et al. (2012) for instance used water stable isotopes and hydrometric measurements to partition evapotranspiration with a mass-balance approach and HYDRUS-1D, respectively. SiSPAT-Isotope (Simple Soil Plant Atmosphere Transfer) couples the transfer of heat, water and stable isotopes within soils in a physical 1D model (Braud et al., 2005). In combination with information derived from other models on e.g. root hydraulic properties, simulations from SVAT can be utilized to

confront data on isotopic composition in soil profiles and transpiration acquired in the parallel field experiment.

To gain a better understanding of fractionation processes in soil water, the experiment should be conducted with various soil textures. An investigation of RWU with different herbaceous species and grasses could furthermore provide information on water uptake dynamics in contrasting ecosystems. This information is much needed for a more reliable estimation of transpiration fluxes on a local and global scale. Within the context of a more variable climate and an increase in extreme events in the future, it would be particularly interesting to examine different adaptions and plant physiological traits herein with a special focus on plant strategies and their ability to cope with e.g. water shortage.

The dimension of the soil columns was chosen in a manner that allows for MRI measurements, which would provide a momentary 3D image of the plants root system. This additional information should further facilitate an evaluation of the complex mechanisms driving RWU in space and time and enhance our understanding of ecohydrological processes on the single-plant scale.

With the setup it is also conceivable to observe water uptake dynamics in reaction to other resources, e.g. nutrients, and inhibitors that are often distributed heterogeneously across soil profiles. This could be especially interesting for nutrients whose availability is linked to water, like nitrate, that is taken up with liquid soil water.

A parallel field study at the University of Freiburg currently conducts experiments applying the same method in a grassland ecosystem, also monitoring the plant species *Centaurea jacea*. It will be interesting to compare observed processes to plant behaviour under natural conditions and also in competition with other species. An evaluation of the transferability of obtained results to field conditions should provide additional information on limitations and opportunities that are associated with the new in-situ methods.

7 Conclusion

Root water uptake is a complex process and its mechanistic functioning is currently not thoroughly understood. Especially with likely changes in water availability due to climate change and the importance of the transpiration flux in the water cycle in mind, a more realistic and mechanistic representation of RWU dynamics is urgently needed to increase the predictive power of SVAT models.

The presented study successfully tested a new method, which enables the simultaneous determination of transpiration and soil water isotopic composition, to enhance the possibilities of monitoring RWU under controlled conditions in the laboratory. The tested method allows for an on-line measurement of isotopic composition in plant transpiration and soil water, omitting the laborious and destructive sampling of water that established methods are accompanied with. The direct measurements can be conducted fast, on living plant material and result in time series with a high temporal resolution. On the single-plant scale in particular this would not be possible with destructive methods.

Measured soil water isotopic profiles were reproducible and in line with previous research. Observed shifts were plausible and could be explained by existing knowledge on soil water and isotope movement. Even though isotopic separation due to soil properties was not observed in this study, it should be kept in mind for future applications, when using different soil textures. When exposed to pronounced diurnal changes in temperature, condensation inside the setups tubing was identified as a relevant methodological difficulty. To reduce the time needed for setup maintenance, this issue should be explicitely addressed in the further development of the method, in particular when applying it in field experiments.

It was demonstrated that the determined transpiration isotopic composition originated from measured soil water values, even though the calculation of isotopic compositions in both systems involved multiple data processing steps, assumptions and uncertainties. This set the pivotal prerequisite for a subsequent usage in the applied statistical mixing model and also for the application in other RWU models in future research. To increase the explanatory power of statistical multi-source mixing models and to reduce the large range of feasible water uptake fractions in individual soil depths, efforts should be directed at further deranging the linear $\delta^2H - \delta^{18}O$ bond, thus diversifying information of separate isotopologues for the model input.

Despite the high uncertainties in calculated RWU fractions, trends in uptake profiles could logically be interpreted with existing knowledge on RWU dynamics and plasticity. From the presented ecohydrological concepts however only compensated RWU could be identified anambiguously as an occuring process. In order to separate and evaluate the importance of other contributing factors, further information, i.e. on root distribution across the soil profile, should be collected. In this respect, efforts should additionally be directed towards a mechanistic modeling of observed timeseries.

References

Barnes, C., & Allison, G. (1988). Tracing of water movement in the unsaturated zone using stable isotopes of hydrogen and oxygen. *Journal of Hydrology*, *100*(1-3), 143–176.

Berry, Z. C., Evaristo, J., Moore, G., Poca, M., Steppe, K., Verrot, L., ... McDonnell, J. (2018). The two water worlds hypothesis: Addressing multiple working hypotheses and proposing a way forward. *Ecohydrology*, *11*(3), e1843.

Beyer, M., Koeniger, P., Gaj, M., Hamutoko, J., Wanke, H., & Himmelsbach, T. (2016). A deuterium-based labeling technique for the investigation of rooting depths, water uptake dynamics and unsaturated zone water transport in semi-arid environments. *Journal of Hydrology*, *533*, 627–643.

Blum, A. (2011). Plant water relations, plant stress and plant production. In *Plant breeding for water-limited environments* (pp. 11–52). Springer.

Braud, I., Bariac, T., Vauclin, M., Boujamlaoui, Z., Gaudet, J. P., Biron, P., & Richard, P. (2005). Sispat-isotope, a coupled heat, water and stable isotope (hdo and h218o) transport model for bare soil. part ii. evaluation and sensitivity tests using two laboratory data sets. *Journal of Hydrology*, *309*(1-4), 301–320.

Carminati, A. (2013). Rhizosphere wettability decreases with root age: a problem or a strategy to increase water uptake of young roots? *Frontiers in Plant Science*, *4*, 298.

Carminati, A., Moradi, A. B., Vetterlein, D., Vontobel, P., Lehmann, E., Weller, U., ... Oswald, S. E. (2010). Dynamics of soil water content in the rhizosphere. *Plant and Soil*, *332*(1-2), 163–176.

Carminati, A., & Vetterlein, D. (2012). Plasticity of rhizosphere hydraulic properties as a key for efficient utilization of scarce resources. *Annals of Botany*, *112*(2), 277–290.

Cernusak, L. A., Barbour, M. M., Arndt, S. K., Cheesman, A. W., English, N. B., Feild, T. S., ... Farquhar, G. D. (2016). Stable isotopes in leaf water of terrestrial plants. *Plant, Cell & Environment*, *39*(5), 1087–1102.

Clark, I. D., & Fritz, P. (1997). *Environmental isotopes in hydrogeology*. CRC press.

Coenders-Gerrits, A., Van der Ent, R., Bogaard, T., Wang-Erlandsson, L., Hrachowitz, M., & Savenije, H. (2014). Uncertainties in transpiration estimates. *Nature*, *506*(7487), E1.

Couvreur, V., Vanderborght, J., & Javaux, M. (2012). A simple three-dimensional macroscopic root water uptake model based on the hydraulic architecture approach. *Hydrology and Earth System Sciences*, *16*(8), 2957–2971.

Craig, H. (1961). Isotopic variations in meteoric waters. *Science*, *133*(3465), 1702–1703.

Crosson, E. (2008). A cavity ring-down analyzer for measuring atmospheric levels of methane, carbon dioxide, and water vapor. *Applied Physics B*, *92*(3), 403–408.

Cuntz, M., Ogee, J., Farquhar, G. D., Peylin, P., & Cernusak, L. A. (2007). Modelling advection and diffusion of water isotopologues in leaves. *Plant, Cell & Environment*, *30*(8), 892–909.

Dawson, T. E., Mambelli, S., Plamboeck, A. H., Templer, P. H., & Tu, K. P. (2002). Stable isotopes in plant ecology. *Annual Review of Ecology and Systematics*, *33*(1), 507–559.

D'Odorico, P., Laio, F., Porporato, A., Ridolfi, L., Rinaldo, A., & Rodriguez-Iturbe, I. (2010). Ecohydrology of terrestrial ecosystems. *BioScience*, *60*(11), 898–907.

Doussan, C., Pierret, A., Garrigues, E., & Pagès, L. (2006). Water uptake by plant roots: Ii modelling of water transfer in the soil root-system with explicit account of flow within the root system–comparison with experiments. *Plant and Soil*, *283*(1-2), 99–117.

Draye, X., Kim, Y., Lobet, G., & Javaux, M. (2010). Model-assisted integration of physiological and environmental constraints affecting the dynamic and spatial patterns of root water uptake from soils. *Journal of Experimental Botany*, *61*(8), 2145–2155.

Dubbert, M., Cuntz, M., Piayda, A., Maguás, C., & Werner, C. (2013). Partitioning evapotranspiration–testing the craig and gordon model with field measurements of oxygen isotope ratios of evaporative fluxes. *Journal of Hydrology*, *496*, 142–153.

Dubbert, M., Cuntz, M., Piayda, A., & Werner, C. (2014). Oxygen isotope signatures of transpired water vapor: the role of isotopic non-steady-state transpiration under natural conditions. *New Phytologist*, *203*(4), 1242–1252.

Dubbert, M., Kübert, A., & Werner, C. (2017). Impact of leaf traits on temporal dynamics of transpired oxygen isotope signatures and its impact on atmospheric vapor. *Frontiers in Plant Science*, *8*.

Ehleringer, J. R., & Dawson, T. E. (1992). Water uptake by plants: perspectives from stable isotope composition. *Plant, Cell & Environment*, *15*(9), 1073–1082.

Ehleringer, J. R., Phillips, S. L., Schuster, W. S., & Sandquist, D. R. (1991). Differential utilization of summer rains by desert plants. *Oecologia*, *88*(3), 430–434.

Ellsworth, P. Z., & Williams, D. G. (2007). Hydrogen isotope fractionation during water uptake by woody xerophytes. *Plant and Soil*, *291*(1-2), 93–107.

Evaristo, J., Jasechko, S., & McDonnell, J. J. (2015). Global separation of plant transpiration from groundwater and streamflow. *Nature*, *525*(7567), 91–94.

Gaj, M., Kaufhold, S., Koeniger, P., Beyer, M., Weiler, M., & Himmelsbach, T. (2017). Mineral mediated isotope fractionation of soil water. *Rapid Communications in Mass Spectrometry*, *31*(3), 269–280.

Gangi, L., Rothfuss, Y., Ogée, J., Wingate, L., Vereecken, H., & Brüggemann, N. (2015). A new method for in situ measurements of oxygen isotopologues of soil water and carbon dioxide with high time resolution. *Vadose Zone Journal*, *14*(8).

Gazis, C., & Feng, X. (2004). A stable isotope study of soil water: evidence for mixing and preferential flow paths. *Geoderma*, *119*(1-2), 97–111.

Gibson, J., Birks, S., & Edwards, T. (2008). Global prediction of δa and δ2h-δ18o evaporation slopes for lakes and soil water accounting for seasonality. *Global Biogeochemical Cycles*, *22*(2).

Gregory, P. (2006). Roots, rhizosphere and soil: the route to a better understanding of soil science? *European Journal of Soil Science*, *57*(1), 2–12.

Gupta, P., Noone, D., Galewsky, J., Sweeney, C., & Vaughn, B. H. (2009). Demonstration of high-precision continuous measurements of water vapor isotopologues in laboratory and remote field deployments using wavelength-scanned cavity ring-down spectroscopy (ws-crds) technology. *Rapid Communications in Mass Spectrometry*, *23*(16), 2534–2542.

Huntington, T. G. (2006). Evidence for intensification of the global water cycle: review and synthesis. *Journal of Hydrology*, *319*(1), 83–95.

Šimůnek, J., & Hopmans, J. W. (2009). Modeling compensated root water and nutrient uptake. *Ecological Modelling*, *220*(4), 505–521.

IPCC. (2013). Summary for policymakers. In T. Stocker et al. (Eds.), *Climate*

change 2013: The physical science basis. contribution of working group i to the fifth assessment report of the intergovernmental panel on climate change (p. 1—30). Cambridge University Press.

Jasechko, S., Sharp, Z. D., Gibson, J. J., Birks, S. J., Yi, Y., & Fawcett, P. J. (2013). Terrestrial water fluxes dominated by transpiration. *Nature*, *496*(7445), 347–351.

Javaux, M., Schröder, T., Vanderborght, J., & Vereecken, H. (2008). Use of a three-dimensional detailed modeling approach for predicting root water uptake. *Vadose Zone Journal*, *7*(3), 1079–1088.

Javot, H., & Maurel, C. (2002). The role of aquaporins in root water uptake. *Annals of Botany*, *90*(3), 301–313.

Jobbagy, E. G., & Jackson, R. B. (2004). Groundwater use and salinization with grassland afforestation. *Global Change Biology*, *10*(8), 1299–1312.

Kirkham, M. (2014). Chapter 10 - field capacity, wilting point, available water, and the nonlimiting water range. In M. Kirkham (Ed.), *Principles of soil and plant water relations (second edition)* (Second Edition ed., pp. 153–170). Boston: Academic Press.

Koeniger, P., Marshall, J. D., Link, T., & Mulch, A. (2011). An inexpensive, fast, and reliable method for vacuum extraction of soil and plant water for stable isotope analyses by mass spectrometry. *Rapid Communications in Mass Spectrometry*, *25*(20), 3041–3048.

Kulmatiski, A., Adler, P. B., Stark, J. M., & Tredennick, A. T. (2017). Water and nitrogen uptake are better associated with resource availability than root biomass. *Ecosphere*, *8*(3), e01738.

Kulmatiski, A., Beard, K. H., Verweij, R. J., & February, E. C. (2010). A depth-controlled tracer technique measures vertical, horizontal and temporal patterns of water use by trees and grasses in a subtropical savanna. *New Phytologist*, *188*(1), 199–209.

Lai, C.-T., Ehleringer, J. R., Bond, B. J., & Tha Paw U, K. (2006). Contributions of evaporation, isotopic non-steady state transpiration and atmospheric mixing on the δ18o of water vapour in pacific northwest coniferous forests. *Plant, Cell & Environment*, *29*(1), 77–94.

Limm, E. B., Simonin, K. A., Bothman, A. G., & Dawson, T. E. (2009). Foliar water uptake: a common water acquisition strategy for plants of the redwood forest.

Oecologia, *161*(3), 449–459.

Lobet, G., Couvreur, V., Meunier, F., Javaux, M., & Draye, X. (2014). Plant water uptake in drying soils. *Plant Physiology*, *164*(4), 1619–1627.

Majoube, M. (1971). Fractionnement en oxygene 18 et en deuterium entre l'eau et sa vapeur. *Journal de Chimie Physique*, *68*, 1423–1436.

Marshall, J. D., Brooks, J. R., & Lajtha, K. (2008). Sources of variation in the stable isotopic composition of plants. In *Stable isotopes in ecology and environmental science* (pp. 22–60). Blackwell Publishing Ltd.

McCutcheon, R. J., McNamara, J. P., Kohn, M. J., & Evans, S. L. (2017). An evaluation of the ecohydrological separation hypothesis in a semiarid catchment. *Hydrological Processes*, *31*(4), 783–799.

McDonnell, J. J. (2014). The two water worlds hypothesis: ecohydrological separation of water between streams and trees? *Wiley Interdisciplinary Reviews: Water*, *1*(4), 323–329.

McGuire, K., & McDonnell, J. (2008). Stable isotope tracers in watershed hydrology. In *Stable isotopes in ecology and environmental science* (pp. 334–374). Blackwell Publishing Ltd.

Meinzer, F. C., Andrade, J. L., Goldstein, G., Holbrook, N. M., Cavelier, J., & Wright, S. J. (1999). Partitioning of soil water among canopy trees in a seasonally dry tropical forest. *Oecologia*, *121*(3), 293–301.

Meißner, M., Köhler, M., Schwendenmann, L., Hölscher, D., & Dyckmans, J. (2014). Soil water uptake by trees using water stable isotopes (δ 2 h and δ 18 o)- a method test regarding soil moisture, texture and carbonate. *Plant and Soil*, *376*(1-2), 327–335.

Meunier, F., Rothfuss, Y., Bariac, T., Biron, P., Richard, P., Durand, J.-L., ... Javaux, M. (2017). Measuring and modeling hydraulic lift of lolium multiflorum using stable water isotopes. *Vadose Zone Journal*, *17*(1).

Moreira, M. Z., Sternberg, L. d. S. L., & Nepstad, D. C. (2000). Vertical patterns of soil water uptake by plants in a primary forest and an abandoned pasture in the eastern amazon: an isotopic approach. *Plant and Soil*, *222*(1), 95–107.

Murray, F. W. (1966). *On the computation of saturation vapor pressure.* (Tech. Rep.). The RAND Corporation, Santa Monica, Calif.

Niklas, K. J. (2004). Modelling below-and above-ground biomass for non-woody and woody plants. *Annals of Botany*, *95*(2), 315–321.

Orlowski, N., Breuer, L., Angeli, N., Boeckx, P., Brumbt, C., Cook, C., ... McDonnell, J. J. (2018). Inter-laboratory comparison of cryogenic water extraction systems for stable isotope analysis of soil water. *Hydrology and Earth System Sciences Discussions*, *2018*, 1–36.

Orlowski, N., Breuer, L., & McDonnell, J. J. (2016b). Critical issues with cryogenic extraction of soil water for stable isotope analysis. *Ecohydrology*, *9*(1), 1–5.

Orlowski, N., Frede, H.-G., Brüggemann, N., & Breuer, L. (2013). Validation and application of a cryogenic vacuum extraction system for soil and plant water extraction for isotope analysis. *Journal of Sensors and Sensor Systems*, *2*(2), 179–193.

Orlowski, N., Pratt, D. L., & McDonnell, J. J. (2016a). Intercomparison of soil pore water extraction methods for stable isotope analysis. *Hydrological Processes*, *30*(19), 3434–3449.

Parnell, A. C., Inger, R., Bearhop, S., & Jackson, A. L. (2010). Source partitioning using stable isotopes: coping with too much variation. *PloS one*, *5*(3), e9672.

Parnell, A. C., Phillips, D. L., Bearhop, S., Semmens, B. X., Ward, E. J., Moore, J. W., ... Inger, R. (2013). Bayesian stable isotope mixing models. *Environmetrics*, *24*(6), 387–399.

Pérez-Priego, O., López-Ballesteros, A., Sánchez-Cañete, E. P., Serrano-Ortiz, P., Kutzbach, L., Domingo, F., ... Kowalski, A. S. (2015). Analysing uncertainties in the calculation of fluxes using whole-plant chambers: random and systematic errors. *Plant and Soil*, *393*(1-2), 229–244.

PFAF. (2012). *Centaurea jacea*. `https://pfaf.org/User/Plant.aspx?LatinName=Centaurea+jacea`. Plants for a future. (Accessed: 2018-02-22)

Phillips, D. L., & Gregg, J. W. (2001). Uncertainty in source partitioning using stable isotopes. *Oecologia*, *127*(2), 171–179.

Phillips, D. L., & Gregg, J. W. (2003). Source partitioning using stable isotopes: coping with too many sources. *Oecologia*, *136*(2), 261–269.

Piayda, A., Dubbert, M., Siegwolf, R., Cuntz, M., & Werner, C. (2017). Quantification of dynamic soil–vegetation feedbacks following an isotopically labelled precipitation pulse. *Biogeosciences*, *14*(9), 2293-2306.

R Core Team. (2017). R: A language and environment for statistical computing [Computer software manual]. Vienna, Austria. Retrieved from `https://www.R-project.org/`

Raes, D., & Deproost, P. (2003). Model to assess water movement from a shallow water table to the root zone. *Agricultural Water Management*, *62*(2), 79–91.

Rothfuss, Y., & Javaux, M. (2017). Reviews and syntheses: Isotopic approaches to quantify root water uptake: a review and comparison of methods. *Biogeosciences*, *14*(8), 2199–2224.

Rothfuss, Y., Merz, S., Vanderborght, J., Hermes, N., Weuthen, A., Pohlmeier, A., ... Brüggemann, N. (2015). Long-term and high-frequency non-destructive monitoring of water stable isotope profiles in an evaporating soil column. *Hydrology and Earth System Sciences*, *19*(10), 4067–4080.

Rothfuss, Y., Vereecken, H., & Brüggemann, N. (2013). Monitoring water stable isotopic composition in soils using gas-permeable tubing and infrared laser absorption spectroscopy. *Water Resources Research*, *49*(6), 3747–3755.

Schindler, U., Durner, W., Von Unold, G., Mueller, L., & Wieland, R. (2010). The evaporation method: Extending the measurement range of soil hydraulic properties using the air-entry pressure of the ceramic cup. *Journal of Plant Nutrition and Soil Science*, *173*(4), 563–572.

Schlesinger, W. H., & Jasechko, S. (2014). Transpiration in the global water cycle. *Agricultural and Forest Meteorology*, *189–190*, 115–117.

Schmidt, M., Maseyk, K., Lett, C., Biron, P., Richard, P., Bariac, T., & Seibt, U. (2010). Concentration effects on laser-based δ18o and δ2h measurements and implications for the calibration of vapour measurements with liquid standards. *Rapid Communications in Mass Spectrometry*, *24*(24), 3553–3561.

Schmidt, M., Maseyk, K., Lett, C., Biron, P., Richard, P., Bariac, T., & Seibt, U. (2012). Reducing and correcting for contamination of ecosystem water stable isotopes measured by isotope ratio infrared spectroscopy. *Rapid Communications in Mass Spectrometry*, *26*(2), 141–153.

Schopfer, P., & Brennicke, A. (2016). *Pflanzenphysiologie*. Springer-Verlag.

Schymanski, S. J., Sivapalan, M., Roderick, M. L., Beringer, J., & Hutley, L. B. (2008). An optimality-based model of the coupled soil moisture and root dynamics. *Hydrology and Earth System Sciences*, *12*(3), 913–932.

Sheil, D. (2014). How plants water our planet: advances and imperatives. *Trends in Plant Science*, *19*(4), 209–211.

Simonin, K. A., Roddy, A. B., Link, P., Apodaca, R., Tu, K. P., Hu, J., ... Barbour, M. M. (2013). Isotopic composition of transpiration and rates of change in leaf water isotopologue storage in response to environmental variables. *Plant, Cell & Environment*, *36*(12), 2190–2206.

Sprenger, M., Leistert, H., Gimbel, K., & Weiler, M. (2016). Illuminating hydrological processes at the soil-vegetation-atmosphere interface with water stable isotopes. *Reviews of Geophysics*, *54*(3), 674–704.

Sprenger, M., Tetzlaff, D., & Soulsby, C. (2017). Stable isotopes reveal evaporation dynamics at the soil-plant-atmosphere interface of the critical zone. *Hydrology and Earth System Sciences Discussion (In review)*.

Stahl, C., Hérault, B., Rossi, V., Burban, B., Bréchet, C., & Bonal, D. (2013). Depth of soil water uptake by tropical rainforest trees during dry periods: does tree dimension matter? *Oecologia*, *173*(4), 1191–1201.

Steudle, E. (2001). The cohesion-tension mechanism and the acquisition of water by plant roots. *Annual Review of Plant Biology*, *52*(1), 847–875.

Sulzman, E. W. (2008). Stable isotope chemistry and measurement: A primer. In *Stable isotopes in ecology and environmental science* (pp. 1–21). Blackwell Publishing Ltd.

Sun, S.-J., Meng, P., Zhang, J.-S., & Wan, X. (2014). Hydraulic lift by juglans regia relates to nutrient status in the intercropped shallow-root crop plant. *Plant and Soil*, *374*(1), 629–641.

Sutanto, S., Wenninger, J., Coenders-Gerrits, A., & Uhlenbrook, S. (2012). Partitioning of evaporation into transpiration, soil evaporation and interception: a comparison between isotope measurements and a hydrus-1d model. *Hydrology and Earth System Sciences*, *16*(8), 2605–2616.

Thompson, S., Harman, C., Heine, P., & Katul, G. (2010). Vegetation-infiltration relationships across climatic and soil type gradients. *Journal of Geophysical Research: Biogeosciences*, *115*(G2).

Topp, C. N. (2016). Hope in change: The role of root plasticity in crop yield stability. *Plant Physiology*, *172*(1), 5–6.

Vaisala, O. (2013). Humidity conversion formulas [Computer software manual]. Re-

trieved from https://www.vaisala.com/sites/default/files/documents/Humidity_Conversion_Formulas_B210973EN-F.pdf (Accessed: 2018-05-03)

Varado, N., Braud, I., & Ross, P. (2006). Development and assessment of an efficient vadose zone module solving the 1d richards' equation and including root extraction by plants. *Journal of Hydrology*, *323*(1-4), 258–275.

Vereecken, H., Huisman, J.-A., Hendricks Franssen, H.-J., Brüggemann, N., Bogena, H. R., Kollet, S., ... Vanderborght, J. (2015). Soil hydrology: Recent methodological advances, challenges, and perspectives. *Water Resources Research*, *51*(4), 2616–2633.

Vetterlein, D., & Doussan, C. (2016). Root age distribution: how does it matter in plant processes? a focus on water uptake. *Plant and Soil*, *407*(1-2), 145–160.

Volkmann, T. H., Haberer, K., Gessler, A., & Weiler, M. (2016a). High-resolution isotope measurements resolve rapid ecohydrological dynamics at the soil–plant interface. *New Phytologist*, *210*(3), 839–849.

Volkmann, T. H., Kühnhammer, K., Herbstritt, B., Gessler, A., & Weiler, M. (2016b). A method for in situ monitoring of the isotope composition of tree xylem water using laser spectroscopy. *Plant, Cell & Environment*, *39*(9), 2055–2063.

Volkmann, T. H., & Weiler, M. (2014). Continual in situ monitoring of pore water stable isotopes in the subsurface. *Hydrology and Earth System Sciences*, *18*(5), 1819–1833.

Von Caemmerer, S. v., & Farquhar, G. D. (1981). Some relationships between the biochemistry of photosynthesis and the gas exchange of leaves. *Planta*, *153*(4), 376–387.

Wahl, M. H., & Urey, H. C. (1935). The vapor pressures of the isotopic forms of water. *The Journal of Chemical Physics*, *3*(7), 411–414. doi: 10.1063/1.1749690

Wang, L., Good, S. P., Caylor, K. K., & Cernusak, L. A. (2012). Direct quantification of leaf transpiration isotopic composition. *Agricultural and Forest Meteorology*, *154*, 127–135.

Wang, X.-F., & Yakir, D. (2000). Using stable isotopes of water in evapotranspiration studies. *Hydrological Processes*, *14*(8), 1407–1421.

Wassenaar, L., Hendry, M., Chostner, V., & Lis, G. (2008). High resolution pore water δ2h and δ18o measurements by h2o (liquid)- h2o (vapor) equilibration laser spectroscopy. *Environmental Science & Technology*, *42*(24), 9262–9267.

Werner, C., Correia, O., & Beyschlag, W. (2002). Characteristic patterns of chronic and dynamic photoinhibition of different functional groups in a mediterranean ecosystem. *Functional Plant Biology*, *29*(8), 999–1011.

Werner, C., & Dubbert, M. (2016). Resolving rapid dynamics of soil–plant–atmosphere interactions. *New Phytologist*, *210*(3), 767–769.

Werner, C., Schnyder, H., Cuntz, M., Keitel, C., Zeeman, M. J., Dawson, T. E., ... Gessler, A. (2012). Progress and challenges in using stable isotopes to trace plant carbon and water relations across scales. *Biogeosciences*, *9*(8), 3083–3111.

Wershaw, R., Friedman, I., Heller, S., & Frank, P. (1966). Hydrogen isotopic fractionation of water passing through trees. *Advances in Organic Geochemistry*, 55–67.

West, A. G., Goldsmith, G. R., Brooks, P. D., & Dawson, T. E. (2010). Discrepancies between isotope ratio infrared spectroscopy and isotope ratio mass spectrometry for the stable isotope analysis of plant and soil waters. *Rapid Communications in Mass Spectrometry*, *24*(14), 1948–1954.

White, J. W., Cook, E. R., Lawrence, J. R., & Broecker, W. S. (1985). The dh ratios of sap in trees: Implications for water sources and tree ring dh ratios. *Geochimica et Cosmochimica Acta*, *49*(1), 237–246.

Working Group WRB, I. (2015). *World reference base for soil resources 2014, update 2015 international soil classification system for naming soils and creating legends for soil maps. world soil resources reports no. 106.* FAO Rome.

Zimmermann, U., Münnich, K., Roether, W., Kreutz, W., Schubach, K., & Siegel, O. (1966). Tracers determine movement of soil moisture and evapotranspiration. *Science*, *152*(3720), 346–347.

A Appendix

A.1 List of Symbols

^1H, ^2H	stable isotopes of hydrogen
^{16}O, ^{17}O, ^{18}O	stable isotopes of oxygen
α	fractionation factor
α_{eq}	equilibrium fractionation factor
a, b, c	coefficients for the calculation of equilibrium fractionation during phase change from liquid to vapor form
δ	isotope ratio in deviation from a standard [‰]
δ_{water}, δ_{vapor}	isotopic composition of liquid water and sampled water vapor [‰]
δ^2H	hydrogen stable isotope composition [‰]
$\delta^{18}O$	oxygen stable isotope composition [‰]
δ_{in}, δ_{out}	isotopic composition in plant chamber in- and outflow [‰]
δ_E	calculated isotopic composition in plant transpiration [‰]
$\delta^{18}O_{eve}$, $\delta^{18}O_{pre}$, $\delta^{18}O_{act}$	oxygen isotopic composition of event water, in soil water the day before the event and at a certain time after the event [‰]
ϵ_{eq}	enrichment factor for equilibrium fractionation [‰]
ϵ_{kin}	enrichment factor for kinetic fractionation [‰]
f_{eve}	recovered fractions of event water in different soil depths
R	ratio of heavy to light isotope
R_{sample}, $R_{standard}$	ratio of heavy to light isotope in sample and standard
A	column cross-section area [$0.0095\,m^2$]
E	transpiration rate, standardized to column cross-section area [$mmol\,sec^{-1}\,m^{-2}$]
e_s	saturation vapor pressure [kPa]
K_s	saturated hydraulic conductivity [$cm\,day^{-1}$]
m_{dry}, m_{water}	weight of dry soil and water added to the column
mfv	most frequent value of 1 % increments of modelled water uptake fractions for each soil depth

n	shape parameter of water retention curve, measure for pore-size distribution [-]
pF	common logarithm of the absolute value of matric potential in soil water [-log hPa]
R^2	coefficient of determination for linear regressions
rh	relative humidity [%]
sd	standard deviation
St_{heavy}, St_{light}	standards with heavy and light isotopic composition used in data processing
T	temperature [°C]
T_K	temperature [K]
u	air flux provided to the plant chamber [$mol\, sec^{-1}$]
vpd	vapor pressure deficit [kPa]
w_{in}, w_{out}	mole fraction [$mole_{water}\, mole_{air}^{-1}$]
$wvmr$	water vapor mixing ratio [ppmV]
α_{vG}	shape parameter of water retention curve, related to the inverse of the air entry suction [$1\, cm^{-1}$]
ρ_{soil}	soil bulk density [$1.11\ g\, cm^{-3}$]
ρ_{water}	density of water [$1\ g\, cm^{-3}$]
θ	volumetric soil moisture content [$cm^3\, cm^{-3}$]
θ_r, θ_s	residual and saturated volumetric soil moisture content (0.017 and 0.52 respectively)[$cm^3\, cm^{-3}$]

A.2 List of Abbreviations

CO_2	Carbon Dioxide
CRDS	Cavity Ring Down Spectroscopy
DFG	Deutsche Forschungsgemeinschaft
DoE	Day of Experiment
GMWL	Global Meteoric Water Line
LMWL	Local Meteoric Water Line
MFC	Mass Flow Controler
MRI	Magnetic Resonance Imaging
PTFE	Polytetrafluorethylen
pwp	Permanent wilting point, defined at a water potential of -1.5 MPa
R-SWMS	Root-Soil Water Movement and Solute Transport, model developed by Javaux et al. (2008)
RWU	Root Water Uptake
SIAR	Stable Isotope Analysis in R, statistical mixing model developed by Parnell et al. (2010)
SiSPAT-Isotope	Simple Soil Plant Atmosphere Transfer, model developed by Braud et al. (2005)
SVAT	model describing soil-vegetation-atmosphere transfer
VSMOW	Vienna Standard Mean Ocean Water
WRB	World Reference Base for Soil Resources

A.3 Calibration of soil moisture sensors

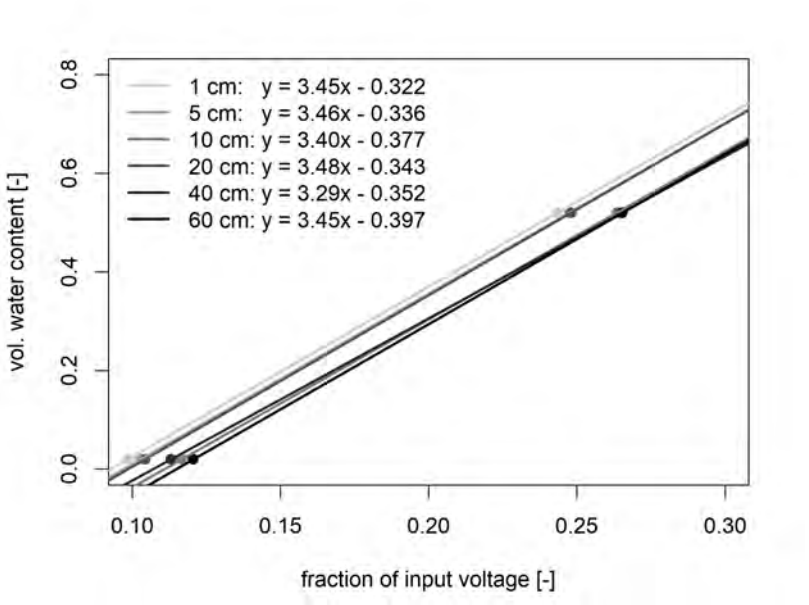

Figure A.1: Linear regressions between input voltage fraction and volumetric soil moisture content for the calibration of all six soil moisture sensors installed in column I.

A.4 CRDS - dependency between $wvmr$ and isotopic composition

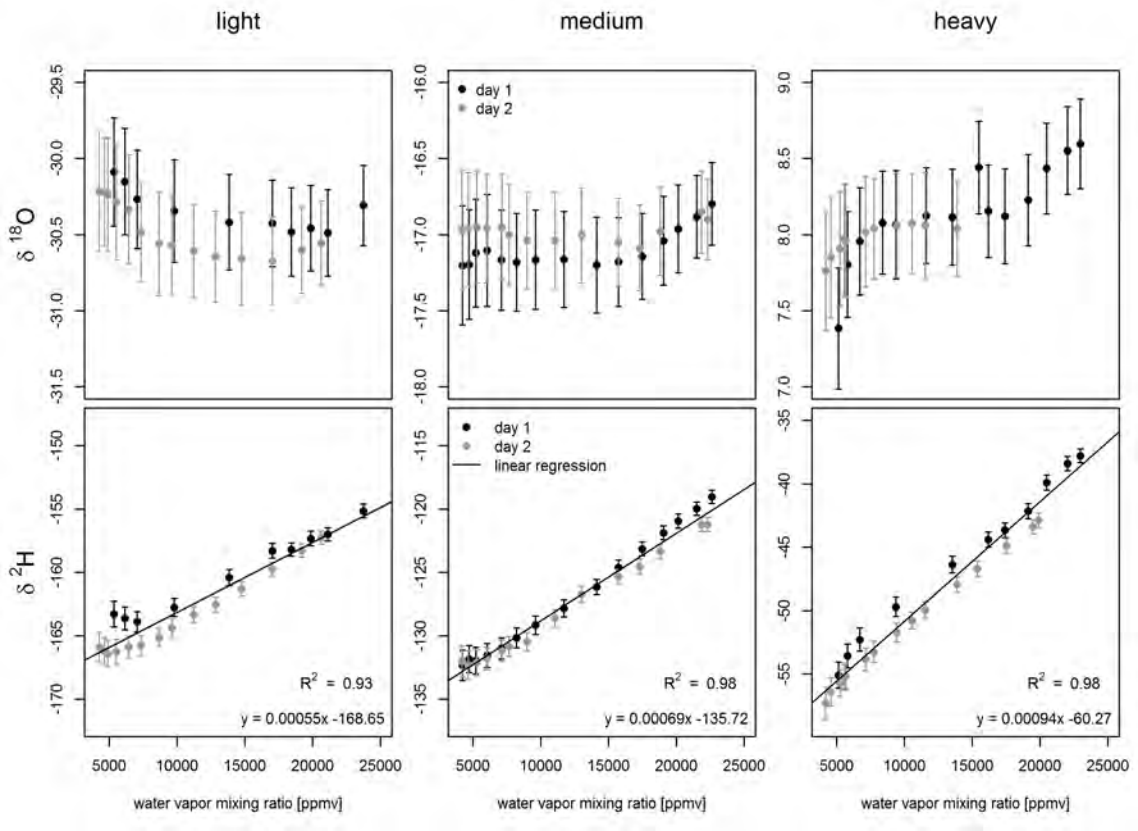

Figure A.2: Instrument specific dependency between isotope ratios and water vapor mixing ratio of the sample gas. Linear regressions used for correcting measurements of $\delta^2 H$ are also plotted with their equation and R^2.

A.5 Data processing - formulas and error propagation

Step 1: $wvmr$ correction

$$\delta_{vap\,corr} = \delta_{raw} + m\,(15000 - wvmr_{raw}) \tag{A.1}$$

$$\sigma^2_{vap\,corr} = \left(\frac{\partial\,\delta_{vap\,corr}}{\partial\,\delta_{raw}}\right)^2 \sigma^2_{\delta\,raw} + \left(\frac{\partial\,\delta_{vap\,corr}}{\partial\,wvmr_{raw}}\right)^2 \sigma^2_{wvmr\,raw}$$

$$\frac{\partial\,\delta_{vap\,corr}}{\partial\,\delta_{raw}} = 1$$

$$\frac{\partial\,\delta_{vap\,corr}}{\partial\,wvmr_{raw}} = -m$$

Step 2: equilibrium fractionation - vapor to liquid

$$\delta_{water} = \alpha_{eq}\,(1000 + \delta_{vap}) - 1000 \tag{A.2}$$

$$\alpha_{eq} = e^{\frac{a\,\frac{10^6}{T_K^2} + b\,\frac{10^3}{T_K} + c}{1000}}$$

$$\sigma^2_{\delta\,water} = \left(\frac{\partial\,\delta_{water}}{\partial\,\delta_{vap}}\right)^2 \sigma^2_{\delta\,vap} + \left(\frac{\partial\,\delta_{water}}{\partial\,T_K}\right)^2 \sigma^2_{T_K}$$

$$\frac{\partial\,\delta_{water}}{\partial\,\delta_{vap}} = e^{\frac{a\,\frac{10^6}{T_K^2} + b\,\frac{10^3}{T_K} + c}{1000}}$$

$$\frac{\partial\,\delta_{water}}{\partial\,T_K} = \frac{e^{\frac{a\,\frac{10^6}{T_K^2} + b\,\frac{10^3}{T_K} + c}{1000}} \left(-\frac{2\,10^6\,a}{T_K^3} - \frac{10^3\,b}{T_K^2}\right)\,(1000 + \delta_{vap})}{1000}$$

Step 3: standardization

$$\delta_{cal} = \delta_{soll\,light} + \frac{\delta_{soll\,heavy} - \delta_{soll\,light}}{\delta_{ist\,heavy} - \delta_{ist\,light}}(\delta_{liq} - \delta_{ist\,light}) \tag{A.3}$$

$$\sigma_{cal}^2 = \left(\frac{\partial\,\delta_{cal}}{\partial\,\delta_{soll\,light}}\right)^2 \sigma_{soll\,light}^2 + \left(\frac{\partial\,\delta_{cal}}{\partial\,\delta_{soll\,heavy}}\right)^2 \sigma_{soll\,heavy}^2 + \left(\frac{\partial\,\delta_{cal}}{\partial\,\delta_{ist\,light}}\right)^2 \sigma_{ist\,light}^2 + \left(\frac{\partial\,\delta_{cal}}{\partial\,\delta_{ist\,heavy}}\right)^2 \sigma_{ist\,heavy}^2 + \left(\frac{\partial\,\delta_{cal}}{\partial\,\delta_{liq}}\right)^2 \sigma_{lig}^2$$

$$\frac{\partial\,\delta_{cal}}{\partial\,\delta_{soll\,light}} = 1 - \frac{1}{\delta_{ist,heavy} - \delta_{ist,light}}(\delta_{liq} - \delta_{ist\,light})$$

$$\frac{\partial\,\delta_{cal}}{\partial\,\delta_{soll\,heavy}} = \frac{1}{\delta_{ist,heavy} - \delta_{ist,light}}(\delta_{liq} - \delta_{ist\,light})$$

$$\frac{\partial\,\delta_{cal}}{\partial\,\delta_{ist\,light}} = \frac{\delta_{soll\,heavy} - \delta_{soll\,light}}{(\delta_{ist\,heavy} - \delta_{ist\,light})^2}(\delta_{liq} - \delta_{ist\,light}) - \frac{\delta_{soll\,heavy} - \delta_{soll\,light}}{(\delta_{ist\,heavy} - \delta_{ist\,light})}$$

$$\frac{\partial\,\delta_{cal}}{\partial\,\delta_{ist\,heavy}} = -\frac{\delta_{soll\,heavy} - \delta_{soll\,light}}{(\delta_{ist\,heavy} - \delta_{ist\,light})^2}(\delta_{liq} - \delta_{ist\,light})$$

$$\frac{\partial\,\delta_{cal}}{\partial\,\delta_{liq}} = \frac{\delta_{soll\,heavy} - \delta_{soll\,light}}{\delta_{ist\,heavy} - \delta_{ist\,light}}$$

Step 4: isotopic composition of transpiration

$$\delta_E = \frac{w_{out}\,\delta_{out} - w_{in}\,\delta_{in}}{w_{out} - w_{in}} - \frac{w_{in}\,w_{out}\,(\delta_{out} - \delta_{in})}{w_{out} - w_{in}} \tag{A.4}$$

$$\sigma_{\delta E}^2 = \left(\frac{\partial \delta_E}{\partial w_{in}}\right)^2 \sigma_{w\,in}^2 + \left(\frac{\partial \delta_E}{\partial w_{out}}\right)^2 \sigma_{w\,out}^2 + \left(\frac{\partial \delta_E}{\partial \delta_{in}}\right)^2 \sigma_{\delta\,in}^2 + \left(\frac{\partial \delta_E}{\partial \delta_{out}}\right)^2 \sigma_{\delta\,out}^2$$

$$\frac{\partial \delta_E}{\partial w_{in}} = -\frac{\delta_{in}}{w_{out} - w_{in}} - \frac{w_{out}\,\delta_{out} - w_{in}\delta_{in}}{(w_{out} - w_{in})^2} + \frac{w_{out}(\delta_{out} - \delta_{in})}{w_{out} - w_{in}} - \frac{w_{in}\,w_{out}\,(\delta_{out} + \delta_{in})}{(w_{out} - w_{in})^2}$$

$$\frac{\partial \delta_E}{\partial w_{out}} = \frac{\delta_{out}}{w_{out} - w_{in}} - \frac{w_{out}\,\delta_{out} - w_{in}\delta_{in}}{(w_{out} - w_{in})^2} - \frac{w_{in}(\delta_{out} - \delta_{in})}{w_{out} - w_{in}} - \frac{w_{in}\,w_{out}\,(\delta_{out} - \delta_{in})}{(w_{out} - w_{in})^2}$$

$$\frac{\partial \delta_E}{\partial \delta_{in}} = \frac{w_{in}\,w_{out}}{w_{out} - w_{in}} - \frac{w_{out}}{w_{out} - w_{in}}$$

$$\frac{\partial \delta_E}{\partial \delta_{out}} = \frac{w_{out}}{w_{out} - w_{in}} - \frac{w_{in}\,w_{out}}{w_{out} - w_{in}}$$

A.6 Ambient air and soil temperature during section 2

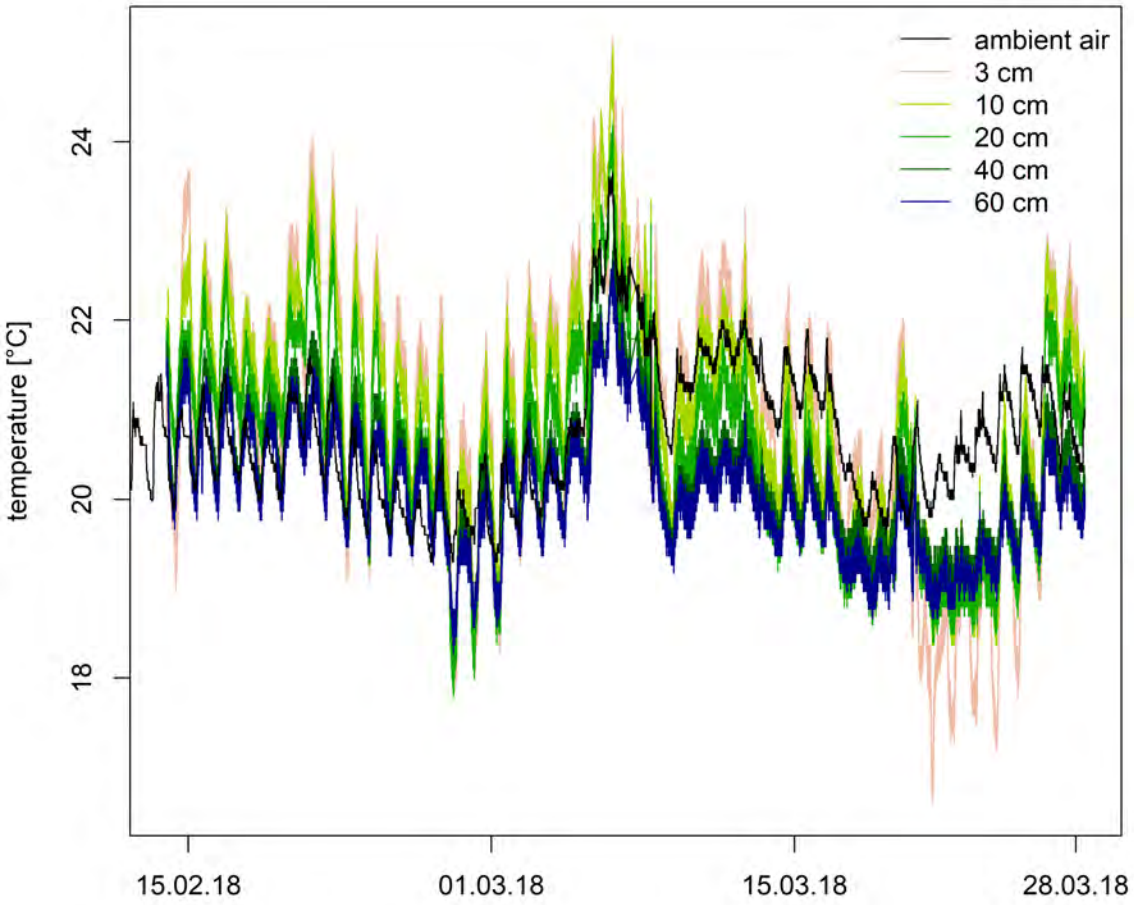

Figure A.3: Ambient air and soil temperature for column I in section 2.

A.7 Wvmr inside the plant chamber - comparison of measured and calculated values

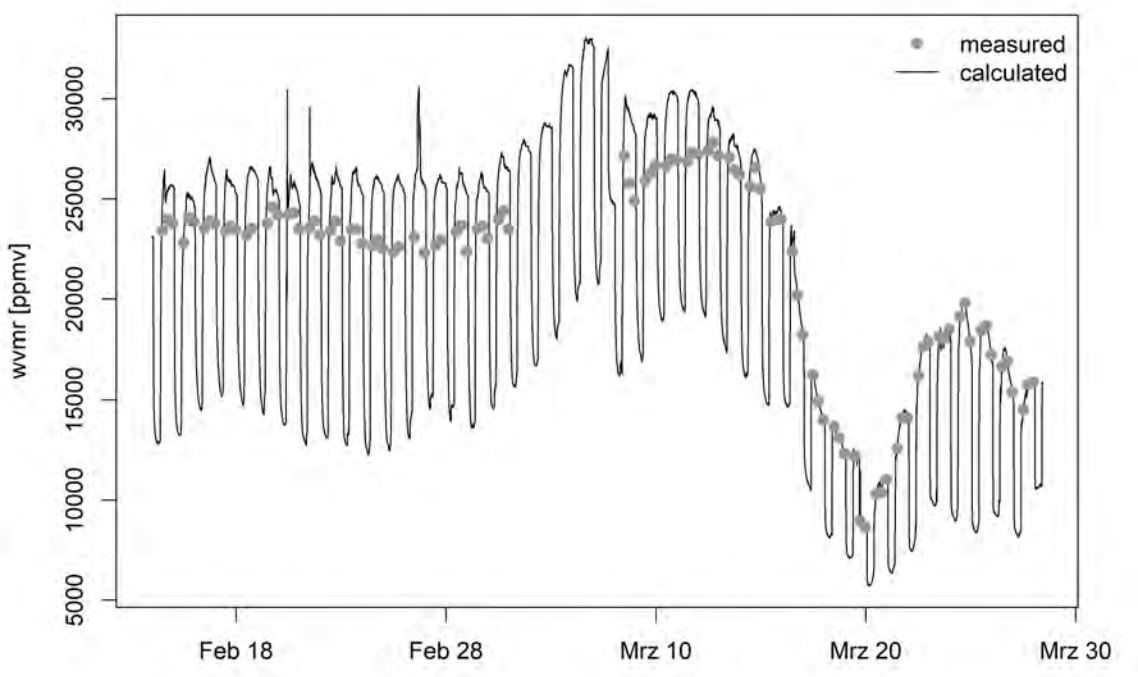

Figure A.4: Measured *wvmr* of chamber air outflow in comparison to values calculated with T and rh inside the plant chamber.

A.8 Water balance - section 2

To restrict evaporative water losses, the soil column was covered during section 2. Therefore the daily decrease in soil moisture content integrated over the column can be can be used to verify daily sums of transpired water. Results on days, when no water was added to the column, are shown in figure A.5. In general, the calculated transpiration rate underestimates water loss calculated with soil moisture sensors. On average daily water loss was $34\,ml \pm 7.3$ and $44\,ml \pm 9.8$ in transpiration and soil moisture values for all days displayed. Uncertainties are associated with both data sets. Transpiration rate could be underestimated, e.g. due to incomplete mixing of chamber air and integration over the day. In the soil moisture water balance, errors could e.g. arise from measurement uncertainty, especially because daily variations in moisture contents are small, and horizontal as well as vertical heterogenity of soil moisture content in the column.

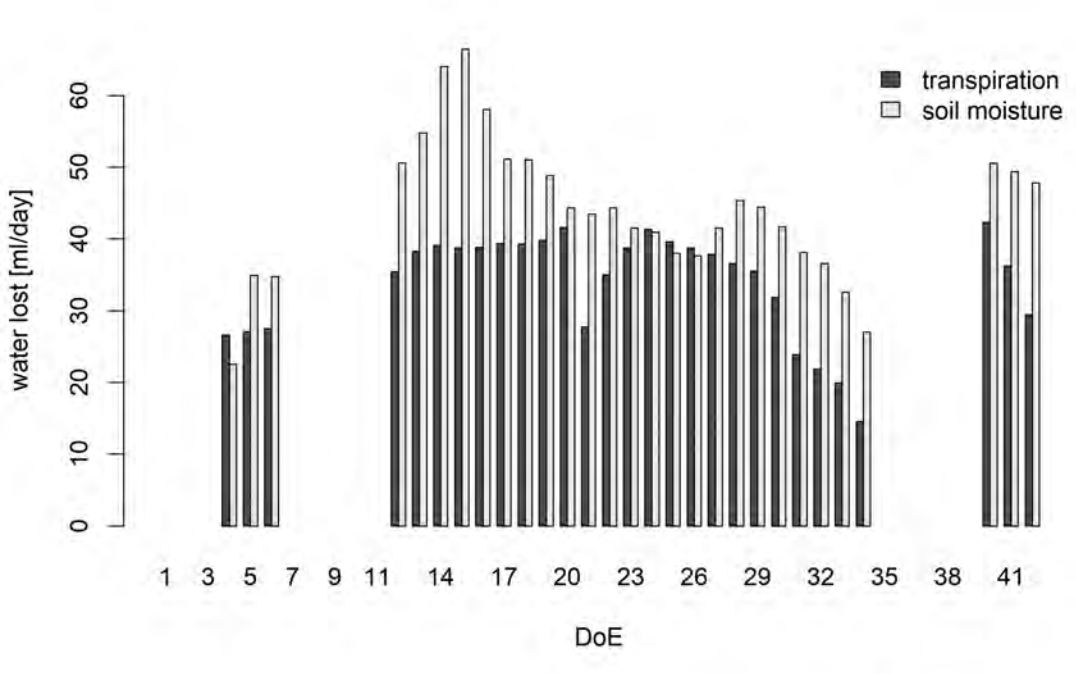

Figure A.5: Comparison of daily sums of transpired water to water loss calculated with the variations in soil moisture content. Time spans when water was added to the column were excluded.

A.9 Diurnal variations in plant chamber conditions

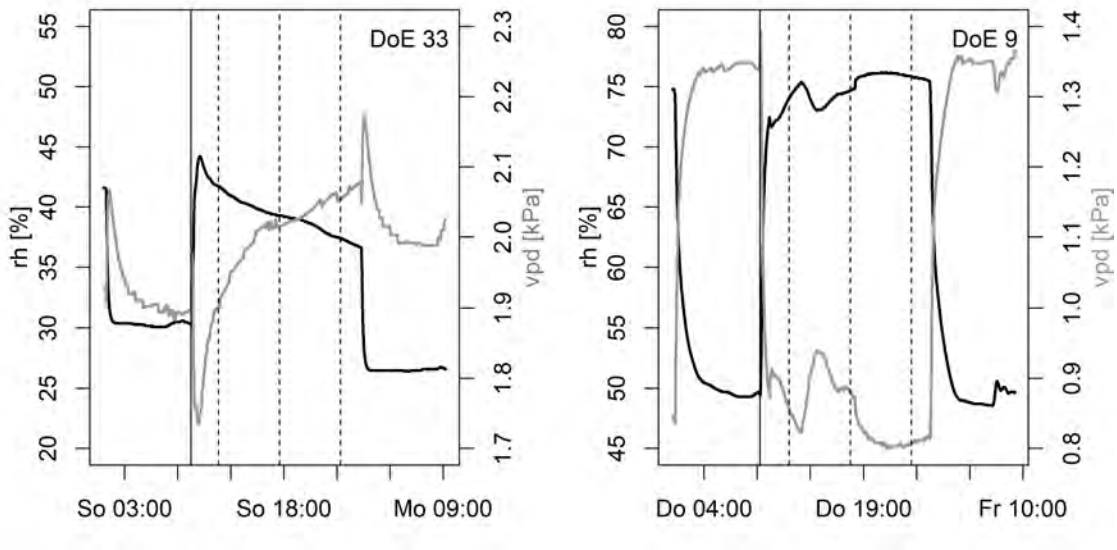

Figure A.6: Diurnal cycle of ambient conditions (rh und vpd) inside the plant chamber for DoE 9 and 33. These days were selected, because they exhibited the highest and lowest deviation in isotopic composition of transpiration. The solid line shows the time when LED lights were switched on. Dashed lines indicate the centres of time spans over which chamber outflow measurements were averaged.

A.10 Boxplots of RWU fractions

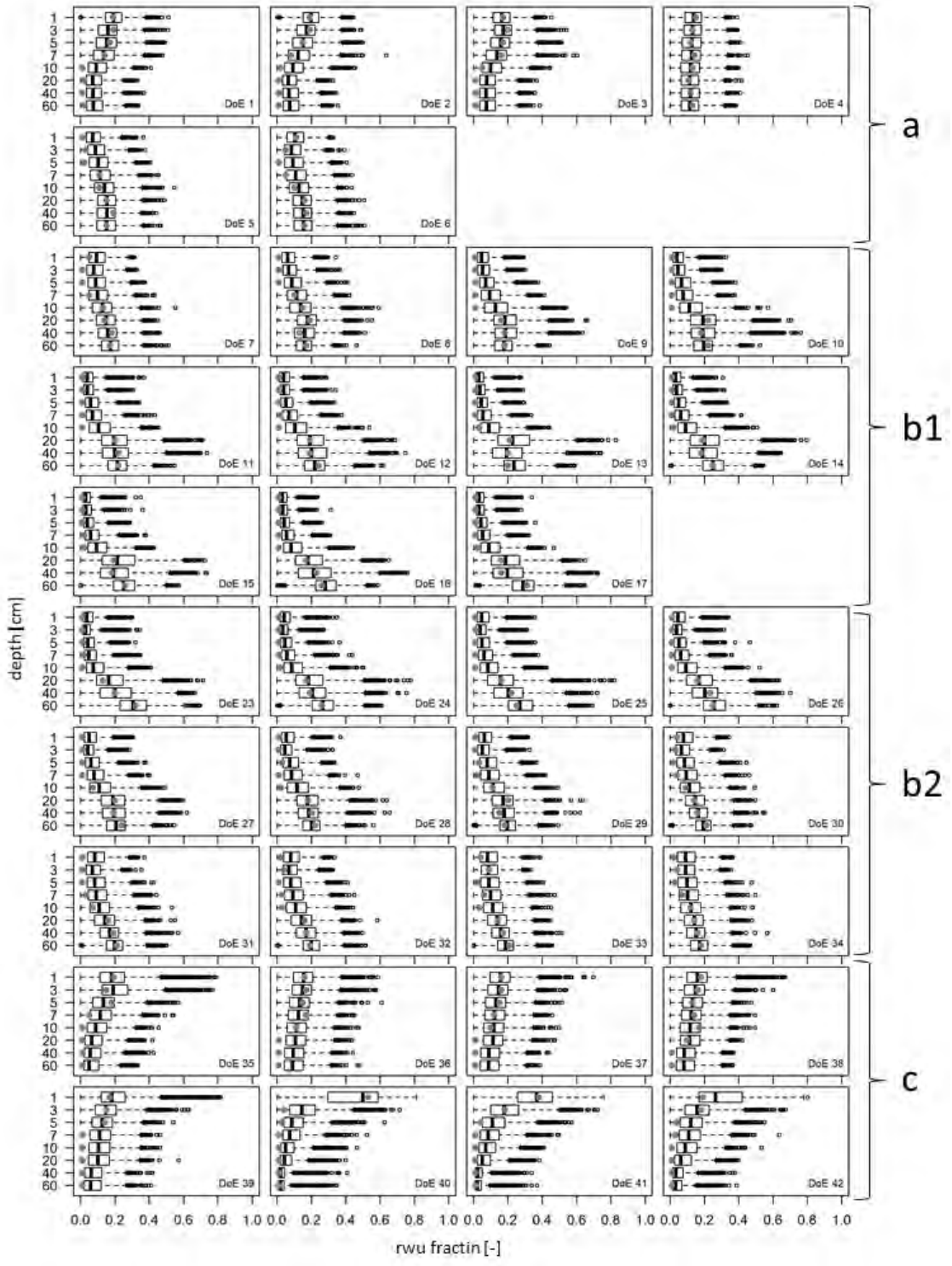

Figure A.7: Boxplots showing RWU fractions for all valid transpiration measurements in daily resolution. The statistical mixing model SIAR was used for calculation. The borders of the box and the band inside represent quartiles and the median of the data set respectively. Whiskers extend to one and a half times of the box width. Provided as well is the mfv for each depth.

Ehrenwörtliche Erklärung

Hiermit erkläre ich, dass die Arbeit selbstständig und nur unter Verwendung der angegebenen Hilfsmittel angefertigt wurde.

Freiburg i.Br., 22.05.2018